Development of anisotropic Nd-Fe-B powders from sintered magnets by Hydrogen Decrepitation/Desorption process

Jianjun Luo

Joseph Fourier University – Grenoble

Northwestern Polytechnical University – Xi'an

PhD Thesis

To obtain the grades of

Doctor of the Joseph Fourier University, Spécialité Physique des Matériaux
Doctor of the Northwestern Polytechnical University

Presented by

LUO Jianjun

Development of anisotropic Nd-Fe-B powders from sintered magnets by Hydrogen Decrepitation / Desorption process

November 20th 2009

Jury :

HU Rui	Professor NPU	Rapporteur
MORALES Magali	Professor ENSICAEN	Rapporteur
JIE Wangi	Professor NPU	Examinator
LI Yulong	Professor, dean of Graduate School at NPU	Examinator
SULPICE André	Research Director at Néel Institut	Examinator
ZHOU Lian	Professor NPU, Doctor Honoris Causa UJF	Supervisor
FRUCHART Daniel	Research Director at Néel Institut	Supervisor
DE RANGO Patricia	Researcher at Néel Institut	Supervisor

PhD thesis prepared at the Institut Néel and the CRETA, CNRS Grenoble, France
and at the Northwestern Institut for Non-ferrous Metal Research, Xi'an, China
in the framework of the French-Chinese International Associated Laboratory LAS2M.

Table of Content

PART 1

GENERAL INTRODUCTION

Significantly increased efficiency opportunities of replacing standard magnets and electrically-generated magnetic fields with high energy rare earth magnets in motors and actuators, is envisaged as being one of the major enablers for reduced energy and improved environmental conditions.

The magnetic Nd–Fe–B alloys have become of much importance since the first permanent magnets were manufactured of them in 1984 [CRO1984], [SA1984]. These magnets were continuously improved and became a significant part of the permanent magnets market due to their advantageous magnetic properties and relatively low costs of manufacturing.

Neodymium-iron-boron materials having excellent magnetic properties and potential economic advantages have instituted a new era in permanent magnet technology.

Resin-bonded Nd–Fe–B magnets have been used in a wide and growing range of computer peripheral, office automation, consumer electronic applications and electric vehicles, constitute the fastest growing segment of the permanent magnet market [FAS1996], [CRO1997]. Worldwide output of bonded Nd-Fe-B magnets is increased very fast every year, and this increase is even faster in recent years since 2005, as shown in Fig.1-1, [LUOY2007]. Bonded Nd-Fe-B permanent magnets have significant market potential; the main growth is expected in current mainstream applications.

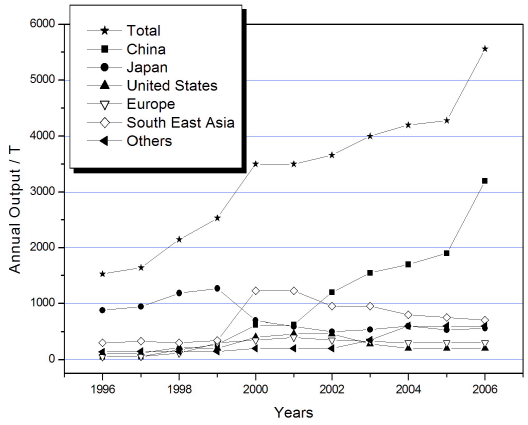

Fig.1-1 Annual production output of bonded Nd-Fe-B magnets in the world [LUOY2007].

However, the rare earth materials used for fabricating Nd-Fe-B magnets are becoming increasingly scarce and expensive. With the rapid growth in the use of NdFeB-type magnets and with the growing environmental need to conserve both energy and raw materials, the recycling of these magnets is becoming an ever important issue, It will even be of growing importance with the expected growth in

electric vehicles and with increasing emphasis on energy conservation. This is likely to demand greater degrees of energy efficiency and materials recycling, particularly in the case of automotive applications, where "end of life" rules are already being implemented. Such measures can be justified in terms of environmental impact (metal contamination of land-fill sites), energy saving (CO_2 reductions) and resource depletion (particularly for the rarer elements such as Dy).

With the development of bonded magnets, impulses are done to optimise powders with high level extrinsic properties. In these powders, the coercive force is not an intrinsic property. It is directly related to the microstructure. To avoid the propagation of the domain walls, the size of the elementary crystallites must be controlled as well as the distribution of the minor intergranular Nd-rich phase. Furthermore, if the grains are textured, i.e. with crystallites oriented along a common direction, the inductive force of the resulting magnet can be magnified up to 2.

Non-melt processes have shown most attractive methods to recycle Nd-Fe-B magnets, because their less energy consume characteristic. Among these processes, two processes involving hydrogenation of bulk Nd-Fe-B alloys have been developed to produce highly coercive and anisotropic powders. The Hydrogen Decrepitation (HD), a low temperature process, applies on starting anisotropic and coercive bulk materials [FRU1984, FRU1990]. On the contrary, the Hydrogen Disproportionation Desorption Recombination (HDDR) process, first reported by Takeshita et al. [TAK1989], applies directly on a standard alloy. It consists in the disproportionation of the starting alloy under a hydrogen atmosphere above 600 °C, followed by a recombination reaction to form an improved microstructure after desorption using a vacuum heat treatment typically around 850 °C. The transformation of the initial coarse grains into very fine grains is responsible for the high coercivity, but the resulting powders are isotropic.

1.1 The application of bonded Nd-Fe-B magnets

Trends in the application areas of Nd-Fe-B, bonded magnets are presented with the focus on miniaturization [FAS1996], [CRO1997]. Bonded Nd-Fe-B magnets can provide significant size and weight reduction and/or performance enhancement over sintered and, particularly, bonded ferrite permanent magnets. Moreover, they provide these benefits at reasonable cost [CRO1997]. The main motivation for using Nd-Fe-B magnets is weight and volume reduction. This restricts its high volume use to high specific price products, such as HDD and CD-ROM, where miniaturization is a key driving factor [FAS1996], [CRO1997].

1.1.1 Miniaturization of the magnetic device

In order to cope with the trend of miniaturization in the main application area, there remains a strong need for higher energy product material, which is made with a low cost process for small and accurate shapes [FAS1996], [CRO1997]. Rapidly

solidified isotropic powders offer a combination of low cost and good thermal aging characteristics [CRO1988]. However, the maximum energy products (BH)max of bonded Nd-Fe-B magnets made from rapidly solidified magnet powders are about 13MGOe (103.5kJ/m^3) at the most [TAK1996] [MA2002], because they are magnetically isotropic.

One concern in using rapidly solidified anisotropic powders for bonded magnets is the difficulty in aligning the powders. It is believed to be due to the shape of the particles which are "flakelike" in geometry [ESH1988]. Analysis of these flakes shows that the magnetization can be at an angle to the surface making alignment more difficult [DOS1991].

The development of anisotropic bonded magnets possessing a larger maximum energy product than the isotropic magnets are therefore greatly expected in the Nd-Fe-B magnets system.

1.1.2 High precision and shaping processes for bonded Nd-Fe-B magnets

Despite the importance of improving magnetic properties, material developers should be aware of a potential competitive advantage of their material in magnetizability, mechanical properties or high temperature irreversible losses. Furthermore, there is a demand for low cost, high precision, shaping processes [FAS1996].

1.1.3 Anisotropic Nd-Fe-B powders

Hydrogen decrepitation has been advantageously used to prepare anisotropic powders from magnetically textured materials, such as bulk Nd-Fe-B sintered magnets[FRU1990], [RIV2000], [NAM2004], [KWO2006], die-upset MQ3 material [DOS1991], [DOS1991B], hot-rolled Nd-Fe-B ingots [HIN1994], hot-forged Nd-Fe-B-Cu ingots [RIV2000] and from sintered Nd-Dy-Fe-Nb-Al-B bulk magnets obtained from the voice coil motors of hard disk drivers [ZAK2006],[ZAK2008].

1.1.4 Recycle Nd-Fe-B magnets by HD process

Nd-Fe-B magnets have been rapidly applied in many fields in recent years. However, an environmental problem has been aroused from increasing wastes of Nd-Fe-B magnet products. On the other hand, there exists a strong demand for high-energy anisotropic Nd-Fe-B powders for bonded magnets, therefore, it is most attractive to fabricate coercive and anisotropic powders using waste sintered Nd-Fe-B magnets [FRU1990], [FRU1997].

The Hydrogen Decrepitation (HD) process could be used at large scale in order to recycling of $SmCo_5$, $Sm_2(Co,FeCu,Zr)_{17}$ [KIA1985] and NdFeB-type magnets [FRU1984],[FRU1990]. Hydrogen insertion in $Nd_2Fe_{14}B$ compounds leads to a decrepitation of the alloys. This phenomenon is used to obtain very fine powders used

both for sintered or bonded magnets [FRU1984], [HAR1985], [RIV2000], [ZAK2008]. Another most important method, the so-called "hydrogen desorption decomposition recombination (HDDR)", is also used to manufacture Nd-Fe-B anisotropic magnets powders [TAK1989], [NAK1993].

$Nd_2Fe_{14}B$-hydrogen systems have been extensively studied for their fundamental aspects as well as for their applications. Many studies have also been devoted to the analysis of the $R_2Fe_{14}B$-hydrogen systems some of which were focused on the thermodynamical aspects [HER1991]**.** Since hydrogen can easily be accommodated in the $R_2Fe_{14}B$ structure, it has also been introduced as an interstitial element to modify the physical properties of the $R_2Fe_{14}B$ type of compounds.

The HD-process converts Nd-Fe-B magnets to powders due to the expansion of the material on hydrogen absorption. Recycling of Nd-Fe-B magnets by this means has been proposed by Fruchart et al. [FRU1990], [FRU1992], [FRU1997], [FRU2003], [FRU2004], Rivoirard et al. [RIV2000] and by Zakotnik et al. [ZAK2008] and these workers reported very encouraging results on production of anisotropic powders from degassed HD powders obtained from sintered Nd-Fe-B magnets.

The HD-process is a well-established stage of manufacturing technologies of sintered [MCG1986], [MCG1989] and bonded [DOS1991B] Nd-Fe-B magnets.

However, the interstitial hydrogen in the ferromagnetic $Nd_2Fe_{14}B$ phase reduces significantly its anisotropy field H_A [FRU2004] and reduces the intrinsic coercivity [ZAK2008]. Hence the material can not be directly usable as a permanent magnet, *e.g.* by resin bonding. That is why desorption of hydrogen is necessary in order to recover the high values of the intrinsic magnetic coercivity of the magnets.

Possible routes to recycle the powders into permanent magnets are:

· Vacuum degassing to remove the hydrogen followed by coating, alignment and bonding.

· Vacuum degassing, pre-aligning and hot pressing into fully dense magnets.

· Hydrogenation Disproportionation Desorption Recombination (HDDR) processing to give high coercivity powder for bonding or hot pressing.

· Milling, alignment / pressing and vacuum sintering into fully dense magnets.

· The powder could be blended with fresh powder and processed in one of the ways above.

Other studies have also looked to process the powder by surface treatment [HOR2004] or to remove carbon and free carbides at grain boundaries [SUZ2001] or oxygen removal by using calcium vapor [SAG2006]. Some recycling processes simply look to recover the rare earth elements for subsequent reuse [TAK2006].

1.2 The fundamental for hydrogen in the field of Nd-Fe-B magnets

Just after the discovery and the crystal structure determination of the new $R_2Fe_{14}B$ hard magnetic materials in 1984 [SAG1984], [CRO1984], it is proven that these materials actively react with hydrogen thus forming stable quaternary hydrides [FRU1984], [HAR1985]. To better understand all the effects of hydrogen on the physical and magnetic properties of $R_2Fe_{14}B$, a better knowledge of the crystal structure is required.

A successful model for interstitial site occupation of hydrogen is built which allowed understanding the changes observed with structural parameters and magnetic parameters as well. And it is shown that the effect of the hydrogen uptake after substitution of Fe by other elements can also be described using a multi-site occupation scheme owing to the bonding characteristics, e.g. of *p*-type elements.

1.2.1 The structure of $Nd_2Fe_{14}B$ hydride

The structure of the $Nd_2Fe_{14}B$ hydride is complex [DAL1987], [ISN1995], [FRU2004] :

- The structure of the $Nd_2Fe_{14}B$ contains 68 atoms per unit cell (Fig.1-2a). It can take up to five hydrogen atoms per formula unit, leading to 88 atoms per unit cell in $Nd_2Fe_{14}B$ hydride. This makes the structure of $Nd_2Fe_{14}B$ hydride complex.
- The magnetic moment carried by the Nd atoms is of the same order of magnitude of that of the iron atoms.
- $Nd_2Fe_{14}B$ hydrides are only obtained as powder samples due to the decrepitation of the alloy upon insertion of hydrogen.
- The magnetic structure of $Nd_2Fe_{14}B$ is known to exhibit a spin reorientation phenomenon in the (110) plane and a non-collinear alignment of the magnetic moment at low temperature [FRU1992].

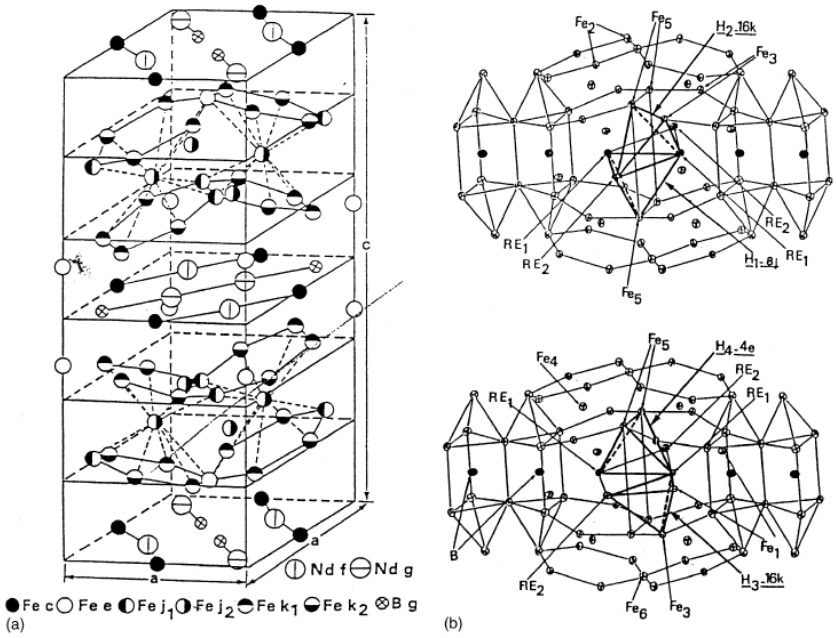

Fig.1-2. Crystal structure of $Nd_2Fe_{14}B$ showing the interstitial sites occupied by hydrogen [ISN1995], [FRU2004].

For all these reasons, resolution of the crystal and magnetic structure of $Nd_2Fe_{14}BH_x$ compounds required high-resolution neutron-diffraction data. According to both x-ray diffraction and neutron diffraction experiments performed at room temperature, insertion of hydrogen in the $Nd_2Fe_{14}B$ crystal structure does not change the lattice symmetry whose space group remains *P42/mnm*. A preliminary remark is that this system behaves as a solid solution without any plateau pressure (no defined intermediate phases).

Table 1-1 Lattice parameters and Curie temperature of the $Nd_2Fe_{14}BH_x$ compounds

	a (Å)	*c* (Å)	*V*(Å3)	*Tc* (Å)	$\Delta V/H$ (Å^3/at.)
$Nd_2Fe_{14}B$	8.805	12.206	946	588	···
$Nd_2Fe_{14}BH$	8.841	12.242	957	628	2.7
$Nd_2Fe_{14}BH_2$	8.869	12.294	967	654	2.6
$Nd_2Fe_{14}BH_3$	8.906	12.327	978	662	2.7
$Nd_2Fe_{14}BH_4$	8.917	12.344	982	665	2.3
$Nd_2Fe_{14}BH_{4.5}$	8.926	12.366	985	670	2.1

Once more the Pressure-Composition-Temperature (PCT) measurements reveal a solid solution like behaviour, neutron diffraction investigations (R=Y, Ce, Nd, Ho, Er) indicated a coherent scheme of occupancy for the four sites involved in the hydrogen absorption [FRU1984], [DAL1987] (Fig.1-2b), depending on the alloyed R-element (light and large to heavy and small rare earth atom). The relative occupancy of the most attractive types of sites (R2Fe and R2Fe2) reveals differences during the first

step of hydrogenation. A clear anisotropic cell expansion (Table 1-1) results from the selectivity of the site under filling with the hydrogen content.

1.2.1.1 Hydrogen interstitial sites

The interest reveals to be double :

• First, hydrogen modifies the metal lattice (via elastic constants, electric charges, electron transfers) and it is interesting to use it as a perturbating probe,

• Second, the relatively large expansion in lattice parameters induces a decrepitation process and consequently offers the technical interests of easily produce very fine magnetic particles.

However, the cell parameters do not vary linearly with H concentration (Fig.1-3, Table1-1). The maximum uptake is 5.5 H/f.u. and is reached via a two-step process as deduced from the *c* versus *a* curves plotted for the $R_2Fe_{14}BH_{max}$ series (Fig. 1-4). It can be seen that the curves are shifted towards larger *c* and *a* values, but they are largely similar to that of the pure $R_2Fe_{14}B$ compounds.

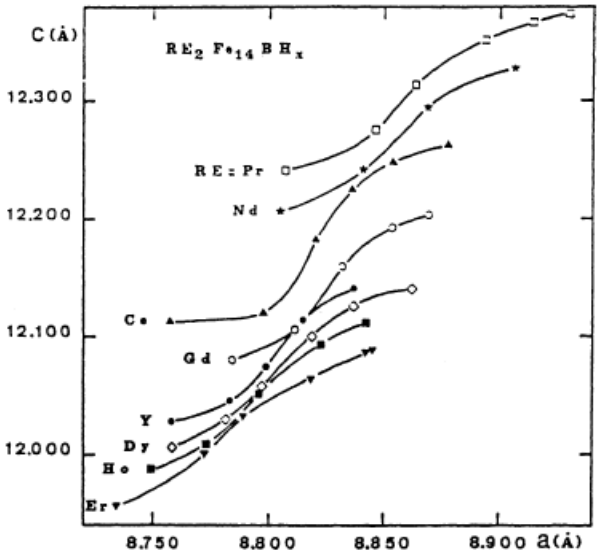

Fig. 1-3. The *c*(*a*) variation in $R_2Fe_{14}BH_x$ series at selected hydrogen concentrations [FRU2004].

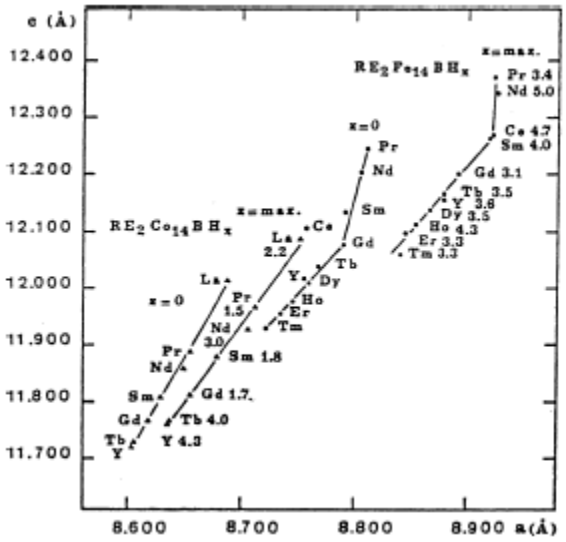

Fig.1-4 The *c* parameter variation as a function of the *a* parameter in $R_2Co_{14}BH_x$ (x=0 and maximum content) and $R_2Fe_{14}BH_x$ (x=0 and maximum content).

Table 1-2 Site occupancy in percentage of the different interstitial sites by hydrogen atoms for the different $Nd_2Fe_{14}BH_x$ compounds x = 1, 2, 3, 4

Site	Position	Hydrogen near neighbors	x=1	x=2	x=3	x=4
H(1)	8*j*	2xNd(2), Nd(1), Fe(5)	50	41	39	24
H(2)	16k_1	Nd(2), Nd(1), Fe(3), Fe(5)	1	26	38	48
H(3)	16k_2	Nd(2), Nd(1), Fe(3), Fe(1)	0	0	23	49
H(4)	4*e*	2x Nd(2), 2x Fe(5)	0	0	9	37

It was first reported in 1984 that $Nd_2Fe_{14}B$ is able to absorb significant amount of hydrogen at room temperature and reasonable pressure [FRU1984]. The effects of hydrogenation on the structural, chemical, physical and mechanical properties have been well established [FRU1997], [ISN1995], [WOL2001], [YAR1997], [FRU2004]. Interstitial sites occupied by hydrogen in crystal structure of the $Nd_2Fe_{14}B$ are shown in Fig.1-2b, Table 1-2. In $R_2Fe_{14}BH_x$ lattice, hydrogen insertion involves four types of R-rich tetrahedral interstitial sites in the lattice of tetragonal (Φ) phase, among which two are mostly active for hydrogen absorption. The first site (8*j*) is the largest one (r_i = 0.45 *Å*) and the most attractive (3R–1Fe) and should be filled first giving way to a larger cell expansion in the basal plane (Table 1-1). With the filling of the next smaller site (16*k*) (r_i = 0.4 *Å*, 2R–2Fe) a larger increase of the *c* parameter is observed (Table 1-1). The relatively large expansion in lattice parameters induces a hydrogen decrepitation process and very fine magnetic particles can be produced easily [FRU1990], [FRU2004].

A comparison of Nd-H interatomic distances encountered in the $Nd_2Fe_{14}BH_x$ (2.2-2.4 *Å*) series with those observed in the $Nd_2Fe_{17}H_x$ (2.32-2.52 *Å*) reveals that

shortest distances are found for the $Nd_2Fe_{14}BH_x$ series and denotes a strong Nd-H bond in that structure. The Nd-H bonds are even shorter than those observed for the pure NdH_2 compounds.

It is also interesting to notice that depending on the size of the rare-earth element the relative occupancy of the most attractive sites reveals differences during the first step of hydrogenation. For the light R elements, the (16*k*) site is favored, whereas for the heavier R elements a saturation of the (8*j*) site is observed with a moderate occupancy of the (16*k*) site. This filling scheme can be accounted for by considering the relative size of the light and heavy R elements. The (16*k*) site appears indeed to be sensitive to the size of the R element. [ISN1995], [FRU2004]

1.2.1.2 Chemical environment

The second major criterion for hydrogen accommodation in interstitial sites is related to the chemical environment. H location in the $R_2Fe_{14}BH_x$ series and in Si to Fe substituted compounds supports the fact that in hydrogen-absorbing compounds containing *p*-electron elements (B, Si, Al), the *s*-like character atoms do not bond directly with the former elements. This point of view was first developed by [RUN1984].

1.2.2 Effects on the magnetic properties due to the hydrogen filling

The effects of hydrogenation on magnetic properties have been described by several autors [FRU2004], [CAD1986]. These effects are :

(i) an increase in the lattice parameters by 1-2 %,

(ii) a minimal increase in the average iron moment of no more than 2%,

(iii) a significant increase in Curie temperature.

The effects of the structural modifications on the magnetic properties may be spectacular. These effects concern the Curie temperature, the magnetocrystalline anisotropy and the magnetisation.

Insertion of hydrogen in the $Nd_2Fe_{14}B$ structure leads to an increase of the magnetic moment observed at room temperature, on both Fe and Nd atomic sites[ISN1995]. This is not particular to Nd compounds and it has been observed for many other $R_2Fe_{14}B$ compounds [DAL1987]. The higher magnetization observed at room-temperature on the hydride compared to the pure alloy must be related to the higher Curie temperature of the H-containing material.

1.2.2.1 Curie Temperature

Since Fe neighbours are at some very short Fe-Fe distances (Fe3-Fe5, Fe5-Fe5), once more a large increase in Curie temperature results in the increase of these critical

distances (Fig.1-4). However, the Tc increase is markedly dependant on the filling scheme of the sites (depending on the size of the rare earth atom).

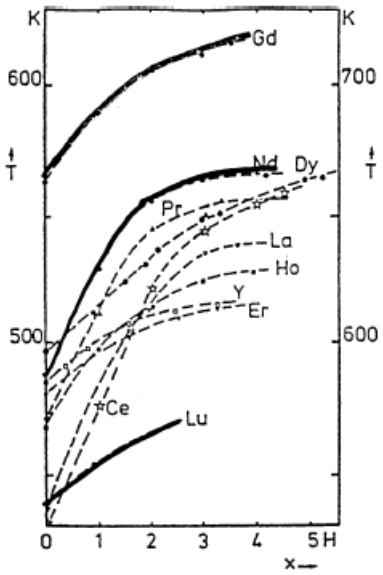

Fig. 1-5. Evolution of the Curie temperature as a function of H concentration in the $R_2Fe_{14}BH_x$ series [FRU2004] (Note that a dual scale is used).

However, the observed *T*c increase is more pronounced at the beginning of hydrogen absorption. Filling of these sites leads to an increase of the Fe2–Fe5 and Fe5–Fe5 distances, which are known to be anomalously short and responsible for the low Curie temperature in the series due to the local negative exchange coupling. The relative *c* versus *a* cell expansion (Fig.1-3) during the progressive filling of the interstitial sites reflects the two-step process of hydrogen absorption via a change in the 2D corrugation of the Kagomé nets.

1.2.2.2 Magnetization

A systematic increase in magnetization is observed upon hydrogenation, presumably associated with a narrowing of the Fe bandwidth upon volume increase and relevant with the weak ferromagnetic character of this element [FRU2004]. A review paper on the relationship between the Wigner-Seitz volume and the local moment of Fe in intermetallics experimentally supports this point of view [ISN1994].

An almost systematic effect of hydrogen absorption is the decrease of the anisotropy field. It is however rather difficult to give a general trend since:

• Anisotropy in this system results from two distinct (and competing) contributions namely the transition metal (M) anisotropy and the rare-earth element (R) anisotropy;

• The effect of hydrogenation on the rare earth anisotropy is subtle and related to

modifications of the crystalline electric field on one hand and of the exchange energy on the other hand.

Generally speaking the anisotropy constants K_1(M) and K_1(R) related to the transition metal and the rare-earth sub lattice, respectively, decrease with H concentration. K_1(R) decreases more severely for R elements with negative αj, whereas, it can be rather insensitive to H absorption in the case of R elements with positive αj. The changes of the crystal field parameters upon hydrogen absorption can be understood in terms of contributions to crystalline electric field of the valence electron distribution [FRU2004]. Higher orders in the expansion of the crystal field parameters involve the Stevens operators (used in the expansion of the exchange interactions) which are also sensitive to hydrogen insertion (modulation of the molecular field upon hydrogenation).

In this respect the relevant parameters to be investigated are the spin reorientation temperatures (SRT) as a function of the hydrogen concentration. These SRT phenomena have been extensively studied throughout the entire $R_2Fe_{14}BH_x$ series and it has been shown that they can be more or less monitored by the hydrogen concentration (Fig. 1-5) [FRU1991],[BUS1988],[OHA1988],[BRA1993].

1.2.2.3 Magnetic anisotropy

A dramatic decrease of the magnetic anisotropy parameters is observed upon hydrogenation. As for the exchange forces, the decrease is faster when the most attractive tetrahedral sites are filled, which are also the R-richest ones. The CEF parameters are concerned in such a way that existing SRT (e.g. R=Nd, Ho, Er, Tm) are changed continuously, monitored by the hydrogen uptake. A unique set of critical exponents well applies to the variations of the CEF upon H insertion. These changes of the parameters can be understood in terms of the contribution to CEF of the valence electron distribution.

1.3 Hydrogen absorption and desorption processes

Nd-Fe-B permanent magnets exhibit a complex multiphase microstructure. According to the ternary phase diagram, at least three phases occur : the ferromagnetic phase $Nd_2Fe_{14}B$ (Φ), the boride phase $Nd_{1+\varepsilon}Fe_4B_4$ (η) and the low melting Nd-rich phase (n) [FID1995]. Standard $Nd_{16}Fe_{78}B_8$ magnets comprise 85 vol%, 3 vol%, 12 vol% of $Nd_2Fe_{14}B$ (Φ), $Nd_{1+\varepsilon}Fe_4B_4$ (η) and Nd-rich phase, respectively [YAN1999]. Two phases, the Φ phase and Nd-rich phase, play most important roles in view of the magnetic properties of Nd-Fe-B magnets. The Φ phase is the carrier of the high saturation magnetization of the materials. The Nd-rich phase not only plays a dominant role in the densification during the sintering process, but is

also reported to be crucial in the improvement of the magnetic properties, though the exact mechanism is still not clearly understood [SAG1984]. During absorption process and desorption process, the reaction between Nd-Fe-B materials and hydrogen is combined with its interaction between these two phases.

When Nd-Fe-B material is exposed to hydrogen, initially the Nd-rich phase absorbs hydrogen. The exothermic nature of the Nd-rich reaction then initiates the absorption of hydrogen by the Φ phase, whereas, under these conditions, the η phase remains inert [HAR1985]. Due to hydrogenation, Nd hydride is produced from the Nd-rich phase and hydrogen atoms penetrate into the interstitial sites of the Φ lattice. The materials become brittle and are decrepitated into powders, as a result of the large volume expansion of the lattice of both the Nd-rich phase and the matrix Φ phase.

1.3.1 Reactions between Nd-Fe-B materials and hydrogen

Hydrogen atoms reacted with two of the phases, the Φ phase and the Nd-rich phase, in Nd-Fe-B materials as following:

1.3.1.1 Reaction between hydrogen and Nd-rich phase

The reaction between hydrogen and Nd-rich phase has been described by McGuiness et al. [MCG1988], [MCG1990] :

$Nd + H_2 \rightarrow NdH_2$ (Temperature range: room temperature) (1)

$NdH_2 + 1/2H_2 \rightarrow NdH_3$ (Temperature range : 200 – 300 ℃) (2)

1.3.1.2 Reaction between hydrogen and $Nd_2Fe_{14}B$ phase

The reaction between hydrogen and $Nd_2Fe_{14}B$ has been described by [LHE1984], [HAR1985], [CAD1986].

$Nd_2Fe_{14}B + H_2 \longleftrightarrow Nd_2Fe_{14}BH_x$ (Temperature range: 150 – 200 ℃) (3)

$Nd_2Fe_{14}B + (2\pm x)H_2 \longleftrightarrow 2NdH_{2\pm x} + \alpha\text{-}Fe + Fe_2B$ (above 650 ℃) (4)

Equations (3) can not happen at room temperature even up to hydrogen pressures of 25 bar [HAR1985]. The $Nd_2Fe_{14}B$ phase has to be heated to around 160 ℃ in a hydrogen pressure of 1 bar in order to achieve the hydrogen absorption [MCG1988], [TAK1995].

Equation (4) can be reversed by heating the disproportionated mixture under vacuum, thus producing the recrystallization of the $Nd_2Fe_{14}B$ phase. If the experimental conditions are well controlled, a fine-grained microstructure can be obtained by this process. The combination of these two reactions is called as Hydrogenation, Disproportionation, Desorption, Recombination (HDDR) process

[TAK1989], [MCG1990B], [MCG1990C].

1.3.2 Effect of the Nd-rich phase on the kinetics of hydrogen absorption and desorption

Nd-rich phase plays a great important role in the reaction between hydrogen and Nd-Fe-B materials [ZHO1999]. The hydrogen absorption by Nd-Fe-B materials takes place firstly by the Nd-rich phase on the grain boundaries, and secondly this reaction leads to hydrogenation of the $Nd_2Fe_{14}B$ phase [MOO1988], [FRU2004].

The Nd-rich phase affects the whole reaction between Nd-Fe-B materials in the following ways:

1.3.2.1 Reduction of the absorption temperature of Nd-Fe-B materials

The hydrogen absorbing properties of Nd-Fe-B materials have confirmed that Nd-rich phase reacts first with hydrogen, and this reaction is necessary if room-temperature activation of the whole alloy is to be achieved [HAR1987]. The hydrogen absorption behavior of the freshly crushed $Nd_{16}Fe_{76}B_8$ alloy has emphasized the importance of Nd-rich grain-boundary phase in achieving room-temperature absorption [MCG1988]. The presence of Nd-rich phase activates hydrogen absorption by the $Nd_2Fe_{14}B$ matrix phase, markedly reducing the hydrogenation temperature from about 160 °C for single-phase $Nd_2Fe_{l4}B$ ($Nd_{11.8}Fe_{82.3}B_{5.9}$) to room temperature for $Nd_{16}Fe_{76}B_8$ [HAR1987], [WIl1991].

The reason is that the strongly exothermic behavior of the neodymium hydride formation causes a pronounced temperature increase accompanying hydrogenation (e.g. ΔT=65 ℃ in the case of Nd to $NdH_{\sim 3}$) [YAR1997], which leads to the hydrogen absorption reaction of ferromagnetic Φ phase at a lower apparent temperature.

1.3.2.2 Amount of hydrogen absorbed in Nd-Fe-B materials

Despite accounting for only 15 vol % of the alloy, Nd-rich phase absorbs as much amount of hydrogen as Φ phase [MCG1988]. The amount of Nd-rich phase contains in Nd-Fe-B alloy affects greatly the amount of hydrogen absorbed. The hydrogen content of a range of Nd-Fe-B alloys was found to increase in value with increasing Nd content, as shown in Fig. 1-6 [BOO1995].

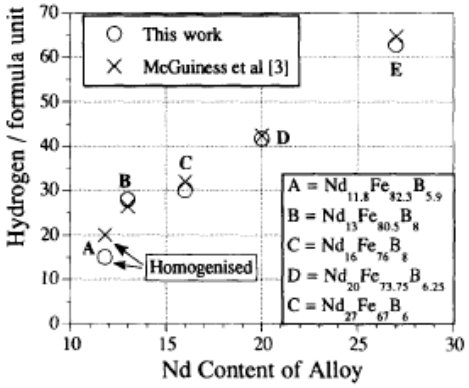

Fig. 2. Hydrogen content of Nd–Fe–B alloys against Nd content. The values obtained by McGuiness et al. [3] are shown for comparison.

Fig. 1-6. Hydrogen content of Nd-Fe-B alloys against Nd content. The values obtained by McGuiness et al. are shown for comparison.

1.3.2.3 Effect on HDDR process

The HDDR behaviors for $Nd_{16}Fe_{76}B_8$ and $Nd_2Fe_{14}B$ alloys are very different. The disproportionation of Φ phase in $Nd_{16}Fe_{76}B_8$ alloy begins at the Nd-rich grain boundary [BOO1995], which suggests that Nd-rich phase on the grain boundary acts as hydrogen diffusion paths during the disproportionation reaction.

This effect of Nd-rich phase comes from two factors as following:

(i) The temperature range of the disproportionation reaction decreases with increasing proportion of Nd-rich phase;

(ii) In disproportionated Nd-Fe-B, the hydrogen desorption kinetics for $NdH_{\sim 2.7}$ and the dihydride were different for Nd in the Nd-rich grain boundary and Nd in the disproportionated matrix.

1.3.2.4 Oxidation of Nd-rich phase

Because that Nd-rich phase has played a great important role in hydrogen treatment in Nd-Fe-B materials, the oxidation degree of Nd-rich phase also affects the hydrogen absorption of Nd-Fe-B materials. In this case, the sample begins to absorb hydrogen at higher temperature than room temperature depending on the oxidation extent of Nd-rich phase [BOO1995].

Both the cast and homogenized $Nd_{16}Fe_{76}B_8$ alloys ingots are significantly more active with respect to hydrogen than the magnets [MCG1990], and it is most likely that it is the change in the Nd-rich material, due to the pickup of oxygen during the sintering process which causes the increased activation time when the material is exposed to hydrogen [WIE1988].

1.3.3 Hydrogen absorption characteristics

A typical ternary Nd-Fe-B ingot or magnet absorbs hydrogen at three steps. Firstly, hydrogen is absorbed by Nd-rich phase on grain boundary to form NdH_2 ; secondly, hydrogen is combined with NdH_2 to form NdH_3; thirdly, hydrogen is absorbed by Φ phase.

The hydrogenation in Nd-Fe-B magnets can be controlled by two parameters [TUR2000], [TUR2001], [LIS2000]: the amount of hydrogen and the rate of feeding with hydrogen at low pressure. By proper combination of these parameters, selective or full hydrogenation of Nd-rich phase and $Nd_2Fe_{14}B$ phase can be obtained. Expansion of specific surface resulting from decrepitation of Nd-Fe-B materials accelerates the diffusion rate by five orders of magnitude for a bulk Nd-Fe-B materials [LIS2000].

Anyway, different Nd-Fe-B materials show different hydrogenation characteristics, especially the $Nd_2Fe_{14}B$ alloys between the other Nd-Fe-B alloys, such as $Nd_{16}Fe_{76}B_8$ as reported by [MCG1990]. Also, different forms of Nd-Fe-B materials, such as ingots, annealed ingots, and magnets, show different hydrogenation characteristics. These differences are shown in the following.

When exposed to hydrogen atmosphere, sintered Nd-Fe-B magnets exhibit different hydrogen reaction behaviors as that of cast Nd-Fe-B ingots, and that of single $Nd_2Fe_{14}B$ alloy as shown in Fig.1-7.

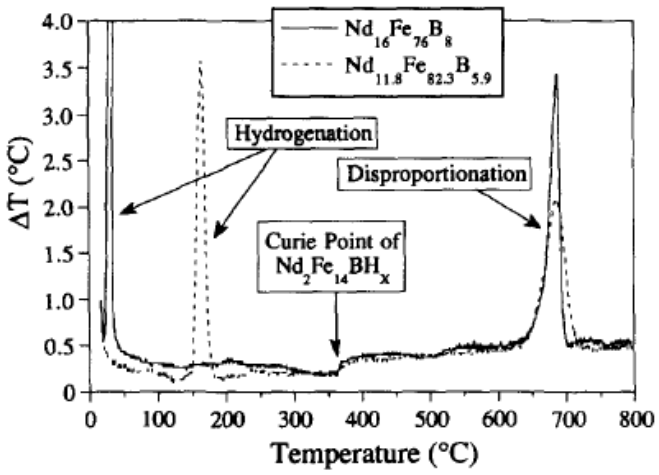

Fig. 1-7. DTA measurements performed on $Nd_{16}Fe_{76}B_8$ and $Nd_{11.8}Fe_{82.3}B_{5.9}$ ($Nd_2Fe_{14}B$), heated in 100 kPa of hydrogen pressure 5 °C min^{-1} [BOO1995].

3.1.3.1 The different decrepitation morphologies

Sintered $Nd_{16}Fe_{76}B_8$ magnets show a striking feature, resulting in finer particle

size of the resulting powder, which is connected with fine microstructure of the magnets. The high-magnification photographs revealed that the failure is predominantly intergranular in nature (Fig.1-8). Individual crystals can be seen, with the hydride-induced cracks propagating around the ~10 µm grains.

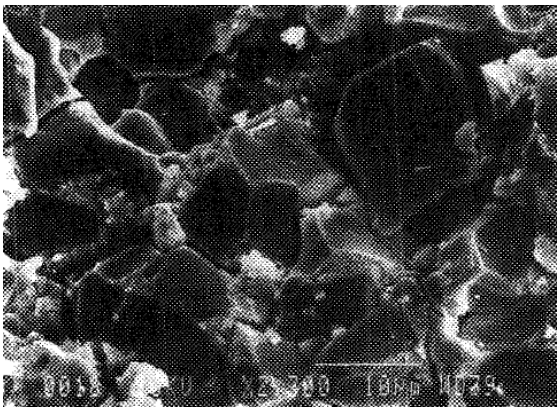

Fig.1-8 Decrepitated $Nd_{16}Fe_{76}B_8$ magnets [MCG1990]

When exposed to hydrogen atmosphere, cast $Nd_{16}Fe_{76}B_8$ alloy shows "onion skin" morphology (Fig.1-9) [MCG1986]. Flakes of material ~20µm thick appear to be peeling away from the outside of the sample in layers.

However, the annealed $Nd_{16}Fe_{76}B_8$ alloy does not exhibit the same effect. The cracks in the sample are more random (Fig.1-10), exhibiting a block like morphology typical of fractured grains [MCG1990].

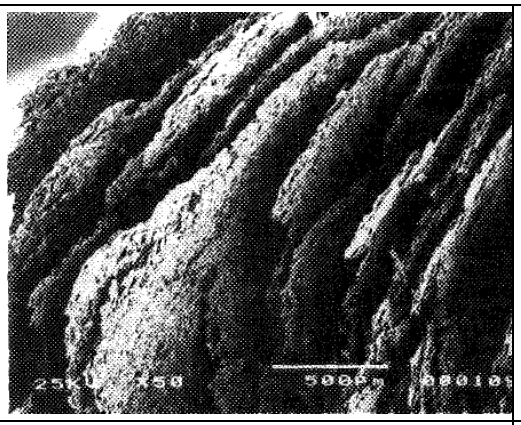

Fig.1-9 Decrepitated cast $Nd_{16}Fe_{76}B_8$

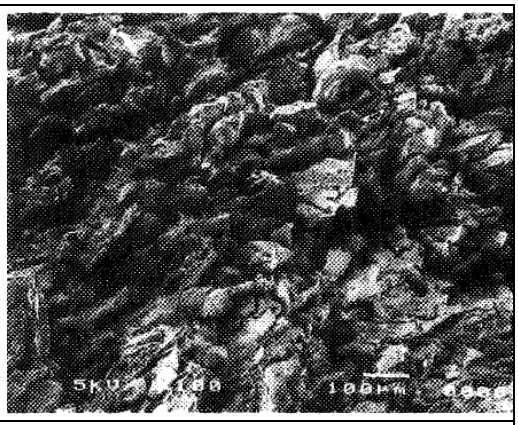

Fig.1-10 Decrepitated $Nd_{16}Fe_{76}B_8$ (homogenized) [MCG1990]

1.3.3.2 Anisotropic hydrogen decrepitation characteristics of sintered Nd-Fe-B magnets

When exposed to a flow of hydrogen gas at room temperature, aligned sintered rod of $Nd_{16}Fe_{76}B_8$ sample show a clear anisotropic hydrogen decrepitation characteristic [YAR1996]. Two distinct stages of decrepitation can be observed : The

first stage is an explosive-like fracture resulting in plates of the material being ejected from the end of the sample. In this stage the $Nd_2Fe_{14}B$ phase in this material remains non-hydrogenated, the decrepitation is a result of the selective hydrogenation of Nd-rich intergranular phase; the second stage is a continuous flaking away of layers of the magnet, hydrogenation is both for $Nd_2Fe_{14}B$ phase as well as Nd-rich intergranular phase.

Easy hydrogenation at the ends of the aligned sintered magnets compared with its sides appears to be a result of their differing activation properties with regard to molecular hydrogen.

However, why the ends of the aligned samples are so much more active than their sides is not very clear. The increased activity seems be related to the following factors:

(a) The distribution of the grain boundary material,

(b) Magnetic fields at the surface,

(c) The nature of the oxide layer,

(d) The intrinsic activity of the atomic configuration of the basal planes of the $Nd_2Fe_{14}B$ phase, or a combination of some or all of these factors.

Factor (d) seems unlikely since it is very difficult to activate single-phase, bulk material of stoichiometric composition [HAR1985], [HAR1987] and X-ray diffraction studies showed that the initial decrepitation of the aligned material did not involve hydrogenation of the $Nd_2Fe_{14}B$ phase [YAR1996].

1.3.3.3 The difference on reaction kinetics

Figure 1-11 shows the important differences in the reactions with hydrogen among Nd-Fe-B materials in different condition.

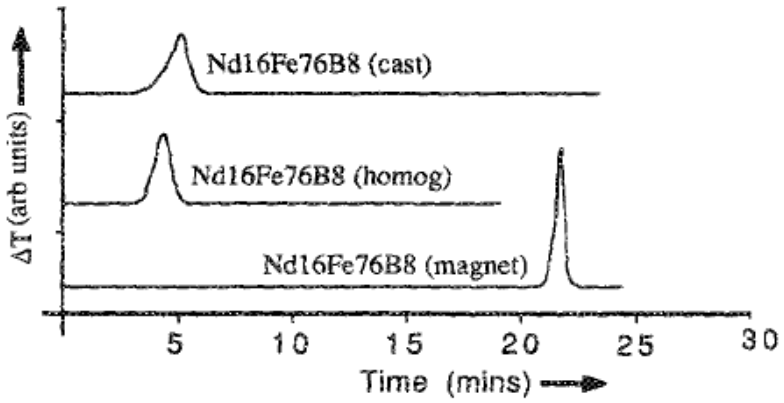

Fig.1-11. DTA Traces of $Nd_{16}Fe_{76}B_8$ (cast, homogenized, and magnet) [MCG1990].

1.3.3.3.1 Reaction time

According to the width of the exothermic peaks, Fig.1-11 shows that the reaction time for cast $Nd_{16}Fe_{76}B_8$ alloy is 3.7 times longer than that of $Nd_{16}Fe_{76}B_8$ magnet, while annealed $Nd_{16}Fe_{76}B_8$ alloy require 2.8 times than that of $Nd_{16}Fe_{76}B_8$ magnet.

The shorter reaction time for $Nd_{16}Fe_{76}B_8$ magnet (which has a grain size smaller than that of the alloy) and annealed $Nd_{16}Fe_{76}B_8$ alloy, indicates that an increased reaction rate takes place in the materials which do not contain iron and do not, as a consequence, exhibit the "onion skin" effect.

The decrepitation of $Nd_{16}Fe_{76}B_8$ magnets by intergranular and intragranular failures accounts for the faster reaction kinetics. The fastest HD kinetics, observed for the magnet, can be attributed to the finer grain size and the more brittle nature of the grain boundary (in comparison with the cast and annealed $Nd_{16}Fe_{76}B_8$ materials) due to its increased oxygen content.

1.3.3.3.2 Activation time

The activation time for freshly broken samples of $Nd_{16}Fe_{76}B_8$ magnets is found to be 20-27 min, significantly longer than the 2-4 min required for the activation of similarly prepared samples of $Nd_{16}Fe_{76}B_8$ (cast) $Nd_{16}Fe_{76}B_8$ (homogenized) alloys, as shown in Fig.2-6.

The longer activation for $Nd_{16}Fe_{76}B_8$ magnets than that for cast and annealed $Nd_{16}Fe_{76}B_8$ material is also due to the finer grain size and the increased oxygen content of Nd-rich phase on the grain boundary.

1.3.4 The hydrogen desorption characteristics

When Nd-Fe-B materials are heated in vacuum, the hydrogen can be desorbed from the materials. A detail hydrogen desorption behavior has been investigated on decrepited $Nd_{16}Fe_{76}B_8$ and $Nd_{11.8}Fe_{82.3}B_{5.9}$ ($Nd_2Fe_{14}B$) materials as shown in Fig.1-12.

The hydrogen desorption behavior in vacuum is consistent with a three-stage desorption process [MCG1988]:

- Firstly, from the matrix $Nd_2Fe_{14}B$ phase,
- Secondly, from tri-hydride of Nd-rich phase,
- And then, from the di-hydride of Nd-rich phase.

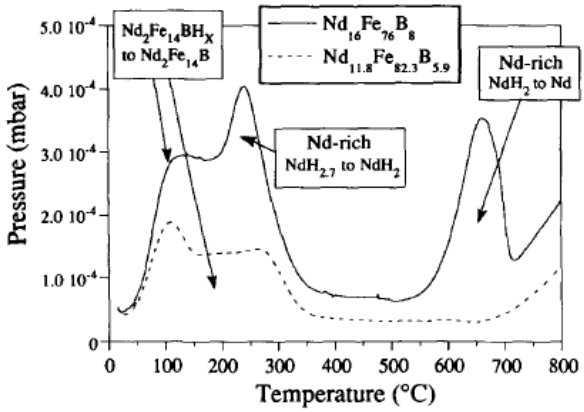

Fig. 1-12. Desorption pressure recorded for $Nd_{16}Fe_{76}B_8$ and $Nd_{11.8}Fe_{82.3}B_{5.9}$ ($Nd_2Fe_{14}B$) hydrides, heated under vacuum at 5 °C/min [BOO1995].

1.3.4.1 Hydrogen desorption from $Nd_2Fe_{14}B$ phase

Hydrogen desorption from the hydrided $Nd_2Fe_{14}B$ materials shows only a single desorption peak over the same range of temperature. This peak occurred at the same temperature and is of the same shape as the first desorption peak in the degassing of the $Nd_{16}Fe_{76}B_8$ alloy (Fig. 1-12) [MCG1988].

Moreover, hydrogen desorption from $Nd_2Fe_{14}B$ hydride occurs at lower temperature also shows a broad shoulder after a peak at about 100 °C (Fig. 1-12) [HAR1987], [BOO1995]. This desorption profile is similar to those for plateauless multisite hydrides [RUP1988], that means hydrogen is being desorbed from the four different sites within the $Nd_2Fe_{14}B$ phase [DAL1987], [ISN1995].

1.3.4.2 Hydrogen desorption from Nd-rich phase

Hydrogen desorption from Nd-rich phase hydride at high-temperature [HAR1987], [HAR1985], [RUP1988], [WIL1990]. The measurements on rare earth elements hydride desorption show the existence of two separated events of hydrogen desorption for all the hydrides. These events are associated with the low temperature desorption $RH_3 \rightarrow RH_2$ and the high temperature desorption $RH_2 \rightarrow R$. [YAR1997]

Desorption measurements of $Nd_{16}Fe_{76}B_8$ hydride show that hydrogen desorbs from the Nd-rich phase from $NdH_{\sim 2.7}$ to NdH_2 and then from Nd di-hydride to Nd metal (Fig.2-7) , as shown as equation 5 and equation 6 in following [WIL1991], [BOO1995].

$NdH_{\sim 2.7} \rightarrow NdH_2 + 1/2H_2$ (Temperature range: 150 - 350°C) (5)

$NdH_2 \rightarrow Nd + H_2$ (Temperature range: 500 - 660°C) (6)

Especially, when Nd-rich phase is alloyed with other elements, such as Co, Cu,

the hydride is much stable, hydrogen desorption can only be completed at much high temperature than 1000 °C [RIV2000].

1.4 The practice of preparing anisotropic Nd-Fe-B powders from textured precursor magnets

The challenge of anisotropic and coercive powders of high performance materials corresponds to the larger and larger needs in bonded magnets [LUOY2007]. The preparation of permanent magnet powders with anisotropic behaviour is very important for the production of bonded magnets with a high maximum energy product. A lot of efforts have made to prepare anisotropic powders from magnetically textured material, mechanically alloyed and hot deformed $Nd_{14.8}Fe_{79.1}Al_{0.3}B_{5.8}$ and $Nd_{16}Fe_{72}Co_5Ga_{0.5}B_{6.5}$ magnets [HAN1996], hot-forged Nd-Fe-B-Cu ingots [RIV2000] and from sintered Nd-Dy-Fe-Nb-Al-B bulk magnets obtained from the voice coil motors of hard disk drivers [ZAK2007]. S. Rivorard etc. [RIV2000] had successfully obtained the anisotropic and coercive powders with the same level of magnetic properties of the bulk precursors, in the method of applying the Hydrogen Decrepitation (HD) process to both bulk of sintered Nd-Fe-B magnets and the high-speed bulk forging bulk magnet. Aichi Steel Comp. [HON2004] discovered a *d*-HDDR phenomenon which results in anisotropy under limited condition, based on the reaction kinetics between Nd-Fe-B and hydrogen without the addition of Co in 1996. Under optimum conditions, a (BH)max of 343 kJ/m^3 was obtained in the alloy $Nd_{12.5}Fe_{bal}B_{6.4}Ga_{0.3}Nb_{0.2}$, and it is possible to obtain a fine recombined grain structure and a high coercivity by the d-HDDR reaction.

The best way to obtain anisotropic powders seems from textured Nd-Fe-B magnets which are already anisotropic [FRU1990], [RIV2000], [ZAK2006]. However, some powdering processes, such as mechanical grinding, inert gas atomization or spark erosion methods, are not suitable routes to develop or to preserve these optimized qualities of a coercive and anisotropic microstructure.

There are several methods to prepare Nd-Fe-B magnets with textured microstructure, such as powder metallurgy [SAG1984], die-upsetting of rapidly quenched materials, hot forming of melt-spun ribbon material, forging. Among these, the sintered Nd-Fe-B bulk magnets, which are prepared by powder metallurgy process, usually exhibit high coercivity due to their anisotropic microstructure, and hold the largest industrial applications in the field of Nd-Fe-B magnets.

1.4.1 Powders from crushing of sintered Nd-Fe-B magnets

1.4.1.1 Crushing magnets into powders directly

Sintered Nd-Fe-B bulk magnets can crush directly into powders through mechanical crushing, however, it looses its magnetic properties dramatically, especially of H_{cj} [STA1986], [NAM2004]. Severe mechanical damage that reduces the effectiveness of the grain boundary phases in stopping reverse magnetization in the crushed material is mostly responsible for such coercivity drop [STA1986].

To crush sintered Nd-Fe-B magnets at high temperature (500 - 700 ℃) [JIA2003] can result in better grain boundary phase distribution in the crushed Nd-Fe-B powders due to inter-granular fracture behaviour of samples other than intra-granular as that crushed at room temperature, leading to modifying magnetic properties of the powders,

1.4.1.2 Crushed powders treated with mixing with DyF_3

Magnetic property of crushed Nd-Fe-B powders can be partly recovered by a heat-treatment due to the healing of micro-structural damages [KWO2004], [KWO2006], especially H_{cj} of the powders.

Furthermore, H_{cj} of crushed Nd-Fe-B powders could be fully restored by heat-treatment with a surface modifier such as DyF_3. In this technique, crushed powders were mixed with some amount of surface modifiers like DyF_3 and subsequently annealed. Surface-morphology change and micro-structural uniformity lower nucleation sites of reversed domains, which are responsible for recovery of demagnetization loop squareness and an increase in H_{cj} [JAN2004], [KWO2004]. Anisotropic powders obtained from sintered $Nd_{14}Fe_{80}B_6$ magnet scrap by this type of treatment exhibits magnetic properties of B_r=11.6 kGs (1.16 T), H_{cj}=13.3 kOe (1058.7 kA/m), and $(BH)_{max}$=31.1 MGOe (247.6 kJ/m^3) [KIM2004].

1.4.2 Powders from hot-forming or die-upset magnets of melt-spun ribbon materials

Anisotropic Nd-Fe-B powders have been obtained from kinds of anisotropic Nd-Fe-B magnets, such as magnets prepared by hot deformation of rapidly solidified materials, by using a different pulverizing method [ESH1988], [NOZ1988]. These Nd-Fe-B powders can be more stable than those prepared by mechanically pulverizing conventional sintered Nd-Fe-B magnets; This is attributed to the much smaller crystallite size of the rapidly solidified materials [ESH1988].

Anisotropic powders are prepared by pulverizing die-upset $Nd_{14}Fe_{79.25}B_6Ga_{0.75}$ magnets, which show typical magnetic properties as: B*r* = 12.4 kGs (1.24 T), H*cj* = 19 kOe (1512.4 kA/m), (BH)*max* = 36 MGOe (286.56 kJ/m^3) [NOZ1988]. H*cj* of the powders is nearly independent of particle size; this is associated with finer grain size (submicron) and pinning mechanism.

Anisotropic bonded magnets, which are made from rapidly solidified powders, have the magnetic properties of B*r* = 8.4 kGs (0.84 T), H*cj* = 14.75 kOe (1174.1 kA/m), (BH)*max* = 15.8 MGOe (125.8 kJ/m^3) [DOS1991]. A select range of particle sizes are desirable to achieve the best potential magnetic and thermal stability from anisotropic powders.

Anisotropic MQ-powders have been also obtained by milling of MQ3-magnets [VON1996-2], which show a much smaller dependence on particle size. The properties of this type of anisotropic powder are with the energy products of 15-17 MGOe (119.4 – 135.3 kA/m) [ESH1988].

D. Hinz et al [HIN1994] had employed the Hot Rolling of cast $Nd_{16.5}Fe_{77.5}B_6$ ingots wrapped in iron to produce anisotropic magnets as starting material for anisotropic powder. After application of the HD process, predominantly needle- and shell-shaped Nd-Fe-B powders with medium particle sizes of about 160 µm were formed with their magnetically easy axis perpendicular to the great half axis. But the magnetic performance of such powders have not mentioned in his paper.

1.4.3 Hydrogen treatment to prepare anisotropic powders from anisotropic Nd-Fe-B magnets

Hydrogen treatment of Nd-Fe-B material at low temperatures and moderate to high hydrogen pressures causes brittlement and fracture resulting in spontaneous HD and the material is more easily crushed into a fine powder [FRU1984], [HAR1985]. Positive volume changes of hydrogenated Nd-rich phase cause cracks between the grains of the matrix phase. Hydrogen easily penetrates through these cracks into the alloy and the hydrogenation of the matrix phase is followed by transgranular fracture. The microstructure characteristics of textured Nd-Fe-B magnets have been restored at a high level in free powders after dehydrogenation and subsequent heat treatments [FRU1997], [FRU2004]. A process which allows restoring the main characteristics of coercive and textured precursors is opened. [FRU1990]

In the case of sintered Nd-Fe-B magnets, hydrogen treatment has proved to be very suitable to prepare anisotropic powders needed both for sintered magnets [HAR1985], [MCG1988] and bonded magnets. [FRU1984], [FRU1997], [FRU2004].

The two possible hydrogen treatment routes to recycle the powders from textured Nd-Fe-B magnets are:

- Hydrogen decrepitation (HD), and then vacuum degassing to remove the hydrogen to obtain anisotropic powders. [FRU1990], [RIV2000], [ZAK2008].
- Hydrogenation, disproportionation, desorption, recombination (HDDR) processing to give high coercivity powders. [TAK1989], [TAK1995], [TAK1996], [LIE1996].

1.4.3.1 Hydrogen decrepitation (HD) route

HD can be advantageously used to prepare anisotropic powders from magnetically textured material, as has been done from die-upset MQ3 material [DOS1991], from hot-rolled Nd-Fe-B ingots [HIN1994], from mechanically alloyed and hot deformed magnets using HD process [HAN1996], [BUR2000]. It has also been accepted to supersede the mechanical crushing required in the powder metallurgy process for making sintered magnets [MCG1989], [MCG1990]. Since, from coercive and textured massive precursors, these main characteristics have been restored at a high level in free powders after dehydrogenation and subsequent heat treatments [FRU1990], [FRU1997], [FRU2004].

Recycling sintered NdFeB-type magnets by HD process has been proposed by Fruchart *et al*. [FRU1990], [FRU1997], [RIV2000], [FRU2004] and by Zakotnik *et al*. [ZAK2008]. These works have reported very encouraging results on the production of anisotropic powders from degassed HD powders obtained from sintered NdFeB-type magnets. Such an application will be of growing importance with the expected growth of electric vehicles and with increasing environmental legislation which is likely to demand even greater degrees of energy efficiency and materials recycling, particularly in the case of automotive applications where "end of life" rules are already being implemented. Such measures can be justified in terms of environmental impact (metal contamination of land-fill sites), energy saving (CO_2 reductions) and resource depletion (particularly for the rarer elements such as Dy).

Powders prepared from fully dense sintered NdFeB-type magnets by HD process have been subsequently processed in one of two ways in order to produce permanent magnets: [FRU1990], [RIV2000], [ZAK2008]

- Firstly, the powders have been subjected to a vacuum degassing treatment over a range of temperatures up to 1000□ in order to produce powders that would be suitable for the production of anisotropic bonded or hot pressed magnets.

- Secondly, the powders have been used to produce fully dense sintered magnets. The optimum degassing temperature for coercive powder was found to be 700□, giving powders with a remanence B*r* of 1.35T and an intrinsic coercivity H*cj* of 750 kA/m. [ZAK2006]. The best sintered magnet has produced by very lightly milling the powder (30 min, roller ball mill), aligning, pressing and vacuum sintering at 1080□ for 1 h. The magnetic properties of this magnet are: (BH)*max* = 290 kJ/m^3, B*r* = 1.24T and H*cj* = 830 kA/m; representing decreases of 15%, 10% and 20%, respectively, from the properties of the initial magnet.

In the case of HD process, it is possible to recover hard magnetic powders from a particular device (e.g. hard disk drive or electric motor) by simply exposing the

complete system to a hydrogen atmosphere in a specially designed chamber. A major advantage of using HD process is the ability to avoid a further buildup of the oxygen content in the powders during recycling. Such a build-up will inhibit subsequent processing of the powders such as sintering, hot pressing or blending with freshly milled material.

However, as mentioned above in the sections dealing with fundamental properties, hydrogen drastically reduces the intrinsic anisotropy of the $Nd_2Fe_{14}B$-type phase and thereby substantially lowers the magnetic coercivity, hence the hydrogen decrepitated material is not directly usable as a permanent magnet, e.g. by resin bonding.

1.4.3.2 Hydrogen–decrepitation–desorption–recombination (HDDR) route

When heat-treated under hydrogen to above 650 ℃, the $Nd_2Fe_{14}B$ phase disproportionates into neodymium hydride, iron and ferroboron [LHE1984]. Subsequently it was proposed that it should be possible to produce a fine-grained microstructure by recombining the disproportionated mixture. [TAK1989], [LIE1996], [LIE1997].

HDDR was first reported by Takeshita *et al*. and a scheme of principle of the operating conditions is given in [TAK1989], chemical equation is then given in [LIE1996].

Starting from non-stoichiometric Nd-Fe-B material (without initial coercivity or anisotropy), Large coercive forces have been obtained from well controlled homogeneous microstructures developed after dehydrogenation and recombination. Typically the resulting magnets are isotropic, but an oriented growth of the elementary crystallites from textured precursors or via epitaxy mechanisms due to elemental additives (Zr, Nb…) can induce a certain level of texture, similarly texture can be developed during recrystallisation under high magnetic fields [LIE1996].

A torsion pendulum magnetometer [VON1995] is used to investigate Nd-Fe-B powders prepared by a standard HDDR-process, mainly to distinguish the magnetization reversal mechanisms, namely a pinning controlled or a nucleation controlled magnetization reversal. It suggested that in the HDDR-powders the magnetization reversal mechanism is a pinning controlled mechanism. [VON1996]

The particle diameter of the powders obtained by the HDDR-process varies between 40 and 400 μm. Vibrating sample magnetometer measurements show a dependence of the coercive force H*cj* of the anisotropic HDDR-powder samples on the mean particle diameter [VON1996]. The degree of alignment of the individual Nd-Fe-B grains within each powder particle is a function of the particle size [VON1996-2]. However, the magnetization processes of the HDDR-powders are

independent on the particle size.

As the non-aligned samples exhibit practically the same remanent polarization for different values of $\bar{d}$, the different values of J_r in the aligned samples must be caused by a different degree of alignment of the nanocrystalline $Nd_2Fe_{14}B$-grains within each powder particle. [VON1996-2]

For anisotropic, aligned HDDR-powders the remanent magnetization depends on the mean particle size $\bar{d}$. A slight decrease of the coercive force with decreasing particle size for $\bar{d} \leq 100\mu m$, was found for HDDR-powders, may be explained with increasing oxygen content [VON1996-2].

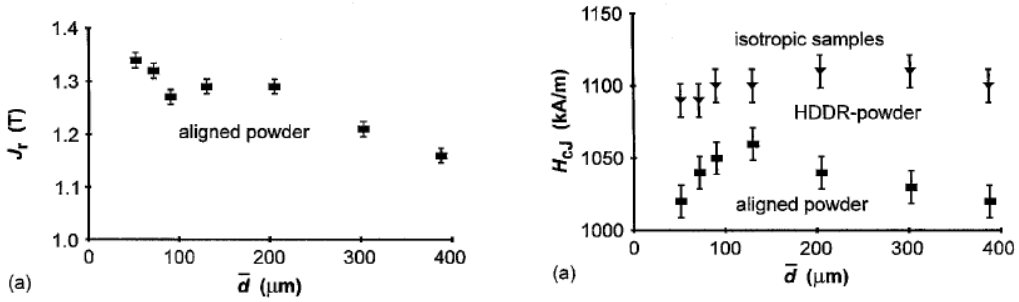

Fig.1-12. The J_r (a) and H_{cj} (b) of the HDDR powders changed with the size of the powders [VON1996-2]

The increase of H*cj* in the range of 400 to 100 *μm* for the HDDR-powders may be explained by an increasing degree of magnetic alignment of the grains within each of the powder particles, as indicated in Fig. 3-lb.Taking into account the well known influence of interactions between neighboring, misaligned grains on H_{cj}, a lower portion of misaligned grains should give a larger value of H_{cj} for a pinning dominated coercive mechanism [VON1996-2].

1.4.4 Other studies on preparing Nd-Fe-B powders from the wastes magnets

Carbon and oxygen contamination damage the magnetic properties in the field of Nd-Fe-B magnets production. In the recycling of the permanent Nd-Fe-B magnet, the carbon such as free carbon and carbides at the grain boundary segregation in the magnet scrap are elements that are harmful and which obstruct the magnet performance. By surface treatment [HOR2004], [ASA2001], carbon and free carbides at grain boundaries can be removed; by using calcium vapour [SUZ2001], oxygen can be removed.

The carbon content can be also decreased less than 0.001% by heating waster magnets scraps in air [SAG2006]. The two stage de-oxidation is applied, iron oxides are reduced by heating in hydrogen thereafter rare earth oxides are removed by Ca-reduction and leaching [SAG2006]. The heating pattern in Ca-reduction and the

leaching condition for the mixture composed of Ca compounds and Nd-Fe-B alloy powders greatly affects the oxygen content of recycled material. By this technique, the decarburized and deoxidized Nd-Fe-B magnet scraps can be recycled as alloying elements by melting, can not used directly as powders for bonded magnets.

1.4.4.1 Surface treatment [HOR2004]

Fine powders by grinding Nd-Fe-B sintered magnet bulks (particle size is 46-125μm in diameter) were coated and alloyed with Zn, Mg or Yb metal by sorbing them, for which the boiling points were low.

Among these volatile metals, Yb showed a good ability to recover the decreased magnetic property of as-ground Nd-Fe-B powders, viz. 0.95 T for remanence (B_r), 227 kA/m for coercivity (H_{cj}) and 48.8 kJ/m^3 for maximum energy product ((BH)$_{max}$), by sorbing (coating and alloying) its vapor at 550–850□under an evacuated condition (10^{-6} Torr). The poor B_r, H_{cj} and (BH)$_{max}$ values were increased to be 0.98 T, 712 kA/m and 173 kJ/m^3, respectively. It was found on the basis of the microstructural characterizations that the sorbed Yb metal uniformly covered the surface and penetrated to the grain boundary to form a (Nd,Yb)Fe_2 phase for the fine powders of Nd-Fe-B sintered magnet bulks.

For the sorption of Zn or Mg metal vapor, no effective improvement of the magnetic properties was observed for the ground Nd-Fe-B powders: The Zn metal vapor sorption resulted in the formation of α-Fe lowering considerably the magnetic properties. For the sample powders sorbed with Mg metal vapor, since Mg mainly reacted with the boundary phase of Nd-Fe-B sintered magnet powders to form a Mg-Nd phase, the coercivity was still more decreased although the B_r value was not changed.

Remelting of scraps could make the carbon content lower to an appropriate level [ASA2001]. Decarburization via oxidation in air allowed the removal of not only free carbon but also grain boundary carbides at temperatures higher than 1000 □ down to 300 %wt. However, an increase in the oxygen content is inevitable with the high temperature oxidation. The powders are then heated in a hydrogen atmosphere at 1000 □ to reduce the iron oxide [ASA2001]; and to eliminate the oxygen combined with the rare-earth constituent, the calcium, which has a strong affinity with oxygen, is used [ASA2001],[SUZ2001]. Three type of calcium, calcium vapor, liquid or $CaCl_2$ melt, can be used to deoxidize of powder scraps of Nd-Fe-B permanent magnet.

1.4.4.2 Nanocomposite powders by disproportionation for wave absorption applications

Nanocomposite magnetic powders of α-Fe/Nd_2O_3 have been effectively recovered from Nd-Fe-B sintered magnet scrap sludge [MAC2003-2], the resin-bonded sheets produced from these powders showed good microwave absorption properties over a

range of 4-8 GHz.

Furthermore, by disproportionation method, nanocomposite powders composed of α-Fe, Fe_xB and Nd_2O_3 can be recovered from Nd-Fe-B magnet scraps [MIU2006]. Resin-bonded discs prepared from these composites powders of α-Fe/Fe_xB/Nd_2O_3 (mean diameter ≅ 20 nm), Fe_xB (amorphous) and Nd_2O_3 particles showed the excellent electromagnetic wave absorption ability in a frequency range of 4.0–6.7GHz, which shifted to the high GHz region side compared with binary composite ones of α-Fe/rare earth oxide.

Nd-Fe-B sintered magnet scraps can also be melted and solidified with Si or Ti to produce Fe-based intermetallic compounds and coproducts of rare-earth-oxide slugs. [HOR2006]. About 60% of the rare earth components in the raw scrap powders can be collected as rare-earth-oxide slugs during the melting process. The epoxy resin composites with 80–83 wt% of these powders showed good microwave absorption properties at GHz range. For Fe–Si (18.5 at% Si) and heat-treated (250 ℃, 3 h) Laves phase Fe_2Ti intermetallic compound, the minimum reflection loss (RL) values of −38.8 and −39.4 dB were observed at 3.3 and 12.3 GHz, respectively.

1.4.4.3 Nd-Fe-B powders recovered from Nd-Fe-B Sludge

Nd-Fe-B sintered magnet scrap powders sludge, as produced in the sizing and polishing processes for well-shaped magnets of small-sized motors and other equipments have been effectively recovered as the raw powders for isotropic Nd–Fe–B bonded magnets (B_r = 0.66 T, H_{cj} = 920 kA/m, and $(BH)_{max}$ = 70 kJ/m^3) by means of Ca metal reduction and melt-spun.

1.4.4.4 Recover the rare earth elements from magnet scraps

There are still some recycling processes simply look to recover the rare earth elements directly from magnet scraps for subsequent reuse. A device has invented [TAK2006], which can simultaneously accomplish continuous extraction of Nd metal from scraps, re-extraction of magnesium (Mg) from Mg-Nd alloy, and finally, recovery of pure Mg. The Nd metal with purity of 98% can be achieved by this technique.

In summary, many efforts have done to prepare anisotropic Nd-Fe-B powders or to recover waster sintered Nd-Fe-B scraps. In the third part of this thesis, the investigation work is focus on preparing anisotropic Nd-Fe-B powders from sinter Nd-Fe-B magnets by hydrogen decrepitation, desorption and subsequent annealing treatment, in order to provide an effective way to reuse waster sintered Nd-Fe-B magnets as treasure.

PART 2

Hydrogen Decrepitation and Desorption Characteristics of Sintered Nd-Fe-B magnets

2.1 Experimental procedure

2.1.1 Start Materials

Nd-Dy-Fe-Co-Nb-Cu-B sintered magnets have good thermal stability due to relatively large amount of Dy, Co elements, and also Nb, Cu doping elements. In this part 2, some hydrogenation absorption and desorption characteristics of $(NdDy)_{15}(FeCoNbCu)_{79}B_6$ bulk magnets are presented, aiming to provide more information for preparing anisotropic powders from waster bulk magnets by hydrogen decrepitation technique in next step.

2.1.1.1 Magnetic properties

Sintering magnets of composition $(NdDy)_{15}(FeCoNbCu)_{79}B_6$ were manufactured by powder metallurgy process in Northwest Institute for Non-ferrous Metal Research (NIN) in Xi'an China, and characterized with high intrinsic coercivity and relative low remanence as showing in Fig.2-1 and table 2-1.

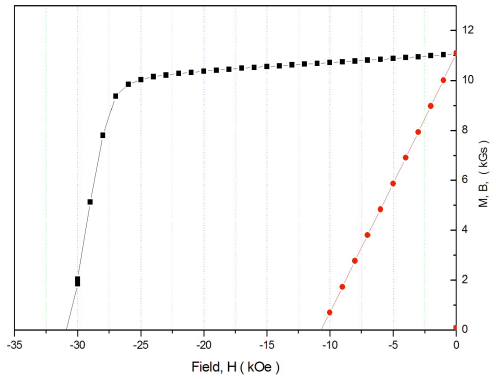

Fig.2-1. The de-magnetization curves of sintered $(NdDy)_{15}(FeCoNbCu)_{79}B_6$ magnets

Table 2-1 The magnetic properties of bulk sintered $(NdDy)_{15}(FeCoNbCu)_{79}B_6$ magnets

Remanence (Br)	11.1 kGs / 1.11 T
Intrinsic coercivity (Hcj)	30.9 kOe / 2459.64 kA/m
Maximum Energy Product (BHmax)	29.4 MGOe / 234.02 kJ/m^3

2.1.1.2 Microstructure

Scanning electron microscopy (SEM) observations performed on polished surfaces of the magnets are shown in Fig.2-2. Therein, a main phase appears in gray and a intergranular phase in white. The black parts in Fig. 2-2 are holes on the surface of the sample, resulted from losing of the main phase grains during the sample polishing procedure.

Energy dispersive X-ray (EDX) analyses are reported in Table 2-2. Because it isn't possible to quantify the boron element by this technique, the following analyses do not take it into account. The main phase corresponds to the Φ phase $(NdDy)_2(FeCo)_{14}B$ with a mean grain size

of about 12 μm. The intergranular phase is the Nd-rich phase (NdDy)(FeCoCuNb) as shown in table 2-3.

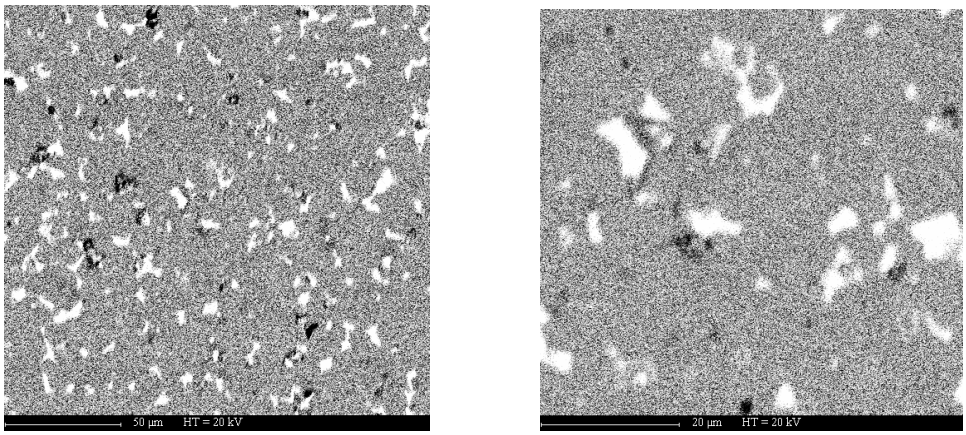

Fig.2-2 SEM figures of sintered $(NdDy)_{15}(FeCoNbCu)_{79}B_6$ magnets

Table 2-2 EDX analysis (at %) of sintered $(NdDy)_{15}(FeCoNbCu)_{79}B_6$ magnets as shown in Fig.2-2

Elements	Nd	Dy	Fe	Co	Cu	Nb
Main-phase	10.3	1.7	81.7	5.8	0.3	0.2
Nd-rich phase	66.9	1.4	6.2	12	13.4	0.1

X-ray diffraction patterns (XRD) analysis performed on these magnets are shown in Table 2-3. The main phase structure is as that of $Nd_2Fe_{12.8}Co_{1.2}B$, which belongs to the space group *P*42/*mnm* with a unit cell of a=0.87926 nm and c= 1.21707 nm.

However, X-ray diffraction (XRD) patterns present extra peaks belonging to several hexagonal phases. Due to the large amount of alloy elements, the grain boundary phases constituent in the magnets are complex.

As for the structure of Nd-rich phase, most of the literature showed that it assumes a structure based on the face-centered cubic (*fcc*) lattice with the unit cell parameter of $a \approx 0.52$ nm [GOO1986], [RAM1987]. Since the metallic Nd phase does not exist in *fcc* forms, Nd-rich phase that appears in sintered magnets is thought to arise from oxidation of the metallic Nd. Namely, it has been suggested that, Nd with a double hexagonal close packed (*dhcp*) structure transforms to an *fcc* based structure, which is stabilized by the introduction of oxygen during annealing [GOO1986]. The presence of oxygen has been confirmed by several independent techniques, including energy dispersive spectroscopy (EDS) and Auger electron spectroscopy [KNO1989], [YIN1993], [SHI2004], [SHI2005]. In this investigation, Nd-rich phase is assumed to be constituted of Nd_4Co_3 and Nd_2O_3, both being in hexagonal structure (Table 2-3).

Table 2-3 XRD results of sintered $(NdDy)_{15}(FeCoNbCu)_{79}B_6$ magnets

Formula	System	a	b	c	Bravais L.	Space Group
$Nd_2Fe_{12.8}Co_{1.2}B$	Tetragonal	8.7926	8.7926	12.1707	Primitive	P42/mnm (136)
Nd_4Co_3	Hexagonal	5.853	5.853	9.58	Primitive	P (0)
NbFeB	Hexagonal	6.015	6.015	3.222	Primitive	P-62m (189)
Nd_2O_3	Hexagonal	3.8297	3.8297	5.9987	Primitive	P-3m1 (164)

2.1.2 Measurement methods

Two types of investigating measurements were employed in this part to study the hydrogen absorption and desorption characteristics of $(NdDy)_{15}(FeCoNbCu)_{79}B_6$ sintered magnets.

During the process of both measurements, before the subsequent measurement, the bulk sintered $(NdDy)_{15}(FeCoNbCu)_{79}B_6$ magnets are crushed to scraps by hand, and weighted to certain mass according to the needs.

2.1.2.1 Differential scanning calorimetry (DSC)

Differential scanning calorimetry (DSC) measurements were performed with NETZSCH DSC404S in MCMF/ Neel Institut, CNRS in Grenoble, France.

The measurements are performed under a flowing Ar_2 + H_2 mixing gases with a flow rate of 100 ml/min, therein the H_2 gas flowing rate was 10 ml/min, at the temperature range from room temperature to 1000℃, the heating rate was 30K/min. The mass of the sample used in this test was about 110mg.

2.1.2.2 Hydrogenation kinetics measurements

Hydrogenation kinetics measurements were performed in hydrogen titration system GenⅢ (Base B) in MCMF/ Neel Institute as shown in Fig.2-3, CNRS in Grenoble, France. The hydrogen mass gain of the sample during the reaction was estimated from the hydrogen pressure changes.

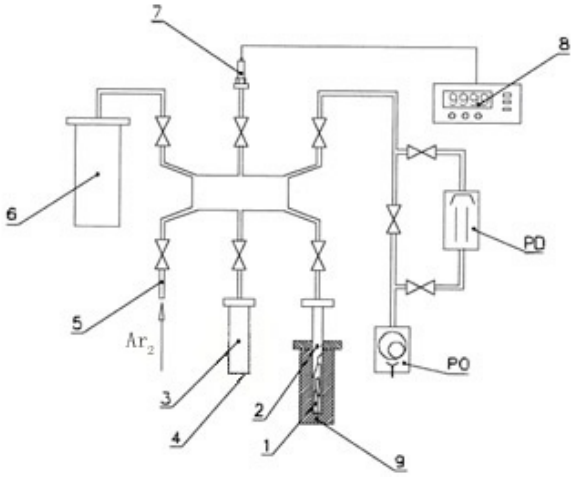

Fig. 2-3. Principle sketch for hydrogen titration system GenIII (Base B) Tensometric analyser

for the investigations of the hydrogenation kinetics.
(1) Sample, (2) reaction chamber, (3) hydrogen source — high purity bottle with high pressure, (4) supporter to hold the bottle, (5) inlet to fill chamber 3 with argon, (6) introductory chamber, (7) tensometric pressure transducer, (8) display, (9) furnace to heat the sample; PO, rotary pump; PD, diffusion pump.

The impact of several experimental factors on the hydrogenation of sintered $(NdDy)_{15}(FeCoNbCu)_{79}B_6$ magnets are investigated in this part. The samples hydrogenated at 50, 100, 150°C were respectively marked as HA50, HA 100 and HA150. The samples submitted to a further dehydrogenation step were marked HA50D, and HA150D. The test conditions are shown in Table 2-4. Hydrogen absorption of the samples were performed at the pressure of 70 kPa. The effect of sample weight on the hydrogenation kinetics measurement is also investigated in this test.

Table 2-4. The test conditions for hydrogenation kinetics measurement

Sample Name	Hydrogen absorption	hydrogen pressure	Hydrogen desorption
HA50	50℃	70 kPa	-
HA100	100℃	70 kPa	-
HA150	150℃	70 kPa	-
HA50D	50℃		300℃， in vaccum
HA150D	150℃		300℃， in vaccum

The microstructure of these samples was analyzed by SEM and EDX on JEOL SEM JSM5600LV in MCMF/ Neel Institute, CNRS in Grenoble, France.

The phase analysis XRD of samples was performed at PHILIPS PW 3830 X-Ray Generator in CRETA/CNRS in Grenoble, France.

2.2 Hydrogen absorption and desorption characteristics of sintered $(NdDy)_{15}(FeCoNbCu)_{79}B_6$ magnets

2.2.1 DSC measurements

Fig.2-4 shows the DSC trace pattern for the hydrogenation of bulk sintered $(NdDy)_{15}(FeCoNbCu)_{79}B_6$ magnets. Two large and one small exothermic peaks can be observed on this DSC curve. Fig.2-5 shows the XRD patterns of the samples at the different stages during the hydrogenation procedure.

The first exothermic peak, rather broad, appeared between 40°C and 185℃. It corresponds mainly to the hydrogenation of Nd-rich phase, as confirmed by X-Ray diffraction (Fig. 2-5b) which showed that the Nd-rich phase was almost fully hydrogenated. but the tetragonal phase (Φ phase) remained mostly unreacted with hydrogen. Moreover, the sample was not broken after this first step.

The second exothermic peak was recorded in the range 185℃ to 220℃. It corresponds mainly to the hydrogenation of $(NdDy)_2(FeCo)_{14}B$ phase. No $Nd_2Fe_{14}B$ phase peak was identified on the XRD pattern (Fig. 2-5c), indicated that the Φ phase had completely hydrogenated.

A small transition occurs around 360℃. It corresponds to the Curie temperature of the $(NdDy)_2(FeCo)_{14}BH_x$ phase.

A third exothermic peak that correspond to the decomposition reaction (disproportionation) of $R_2M_{14}BH_x$, presents a broad and flat profile in the wide range of 450°C to 800°C as displayed in Fig.2-4. This exothermal peak looks rather different to that evidenced by Book et al. [BOO1995] who recorded a sharp and narrow peak at disproportionation during DTA measurements under 1 bar H_2 pressure. In our case, the flat signal can be correlated to the limited hydrogen partial pressure applied during the measurement leading to a softer process according to the as monitored penetration and diffusion process in the Φ phase particles [TUR2000]. Indeed, after the experiment the sample was found fully disproportionated as shown on Fig. 2-5d.

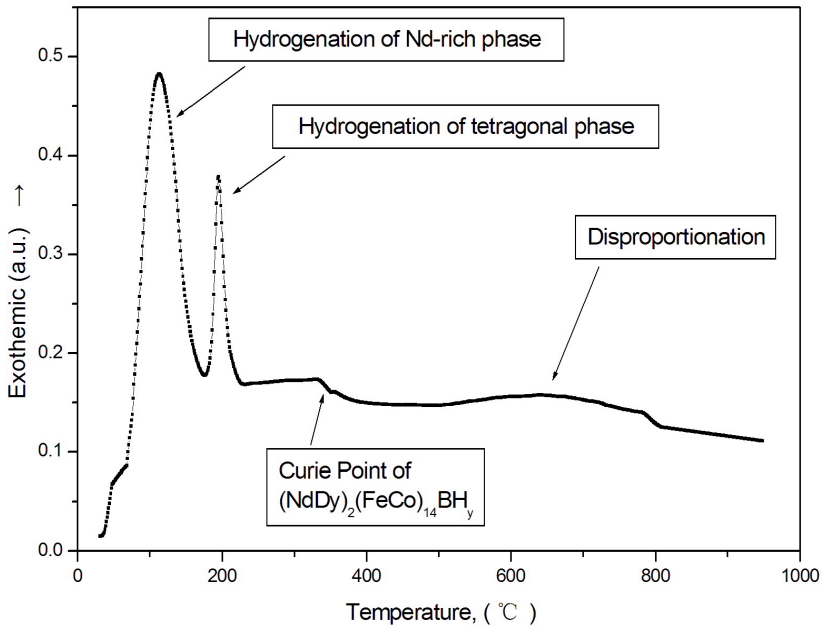

Fig. 2-4. The hydrogenation DSC curve for sintered $(NdDy)_{15}(FeCoNbCu)_{79}B_6$ magnets

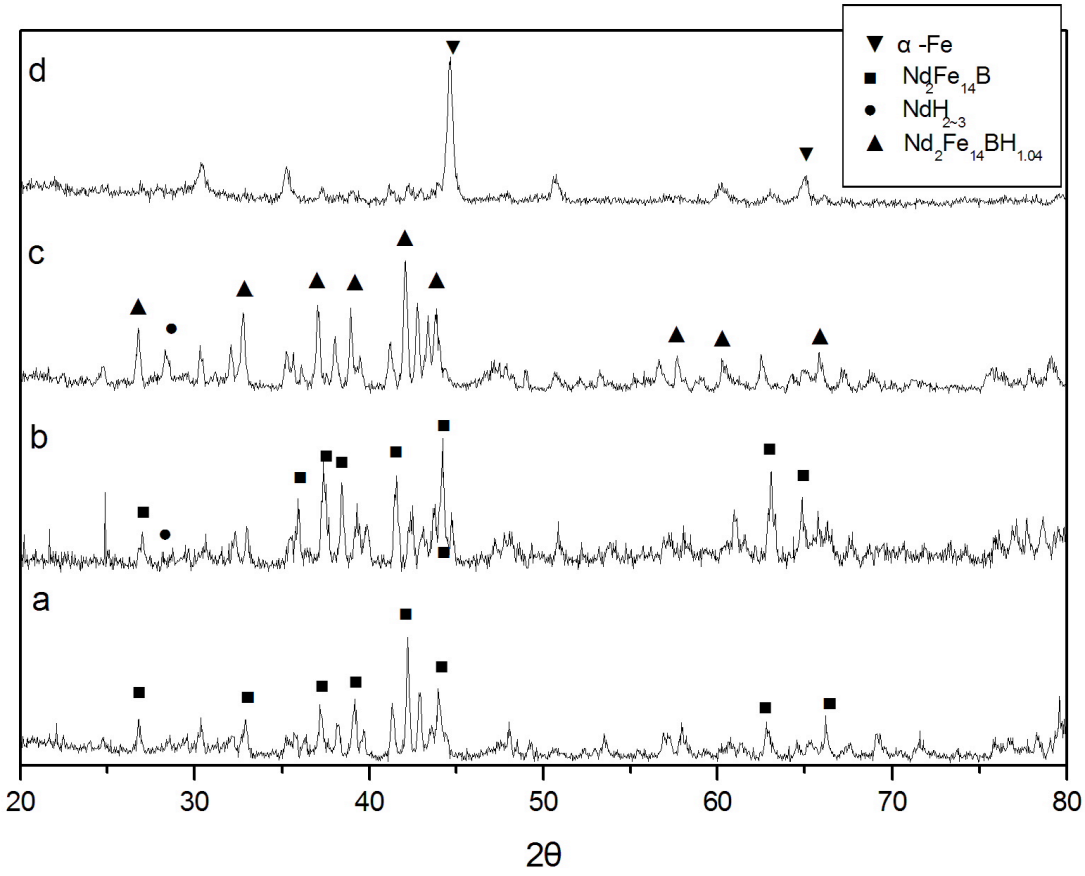

Fig. 2-5. X-Ray diffraction patterns for the DSC measurement
(a), bulk magnet ; (b), after the first DSC peak; (c), after the second DSC peak; (d), at the end of DSC measurement

2.2.2 Hydrogenation kinetics measurement

2.2.2.1 Effect of temperature

2.2.2.1.1 Hydrogen absorption at room temperature

Several tests have been performed in order to hydrogenate sintered $(NdDy)_{15}(FeCoNbCu)_{79}B_6$ magnets scraps at room temperature, but it appears impossible to hydrogenated these compounds at room temperature. However, we will shown that these magnets can be hydrogenated at room temperature when these scraps are submitted to a previous heat-treatement under high vacuum (5×10^{-3} Pa) above 150℃. The heat-treatment conditions are shown in Table 2-5, and the treatment processes are illustrated in Fig.2-6.

Table 2-5 The heat-treatment conditions applied to the sintered $(NdDy)_{15}(FeCoNbCu)_{79}B_6$ magnets scraps before hydrogenation at room temperature

Sample Name	Sample Weight	Heat-treatment Temperature	Vacuum Condition	Dwell time at Temperature
PHT100	61.65 mg	100℃	5×10^{-5} mbar	1h

PHT150	61.99 mg	150℃		1h
PHT200	60.49 mg	200℃		1h

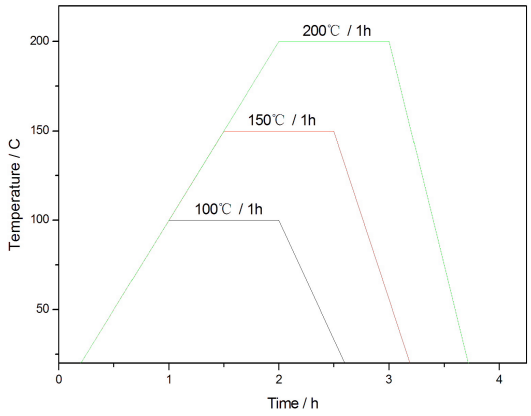

Fig. 2-6 The pre heat-treatment processes applied to sintered $(NdDy)_{15}(FeCoNbCu)_{79}B_6$ magnets under vacuum

The magnets scraps show different hydrogenation ability at room temperature when they are previously heat treated at different temperatures in vacuum as describe above (Table 2-5 and Fig.2-6).

1/ Heat treatment in vacuum at 100℃

After heat treated at 100℃ for 1h in vacuum, the sample PHT100 is cooled down to room temperature. When the sample is completely cold, hydrogen gas with high purity is introduced into the furnace chamber, up to 70 kPa. Then hydrogen pressure and sample temperature are recorded, as reported on Fig.2-7.

Standing at room temperature, it appears difficult to initiate the hydrogenation of these sintered $(NdDy)_{15}(FeCoNbCu)_{79}B_6$ magnets scraps, as observed during the first stage in Fig.2-7. However, when PHT100 is heated, then, the increase of temperature immediately induces a rapid hydrogen absorption coming with an exothermic peak in the temperature range from about 20°C to 60℃ as shown as the second stage in Fig.2-7. The fact that the hydrogenation seems to start simultaneously with the beginning of the heating comes from the temperature measurement the sample which is detected behind the hydrogen absorption reaction due to heat insulation of the ceramic sample holder used in this test.

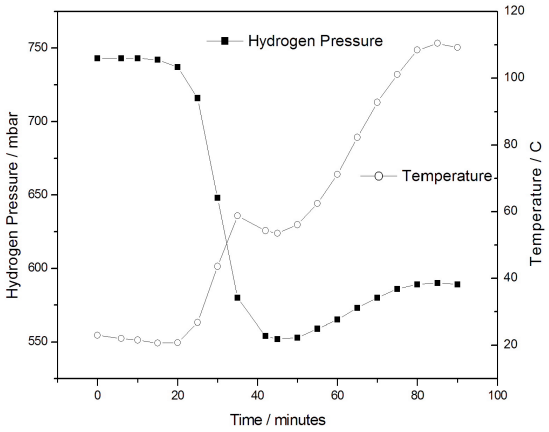

Fig.2-7 Hydrogen pressure and temperature recorded during absorption for sintered $(NdDy)_{15}(FeCoNbCu)_{79}B_6$ magnets treated at 100℃ under vacuum

2/ Heat-treatment in vacuum at 150°C at 200°C

After the heat treatement under vacuum at 150°C and 200°C respectivly, samples PHT150 and PHT200 have been submitted to the same hydrogen pressure of 70 kPa, but without any heating. Fig.2-8 shows the corresponding hydrogen pressure and temperature rising curves. Both of these samples absorb hydrogen at room temperature with shorter incubation time of about 10 minutes.

Iin both cases, the temperature rising are of the same order, respectively 24℃ and 19°C for PHT150 and PHT200.

Then, it has been shown that a previous heat-treatment under vacuum at the temperature above 150 ℃ is effective to promote hydrogen absorption of sintered $(NdDy)_{15}(FeCoNbCu)_{79}B_6$ magnets scraps at room temperature.

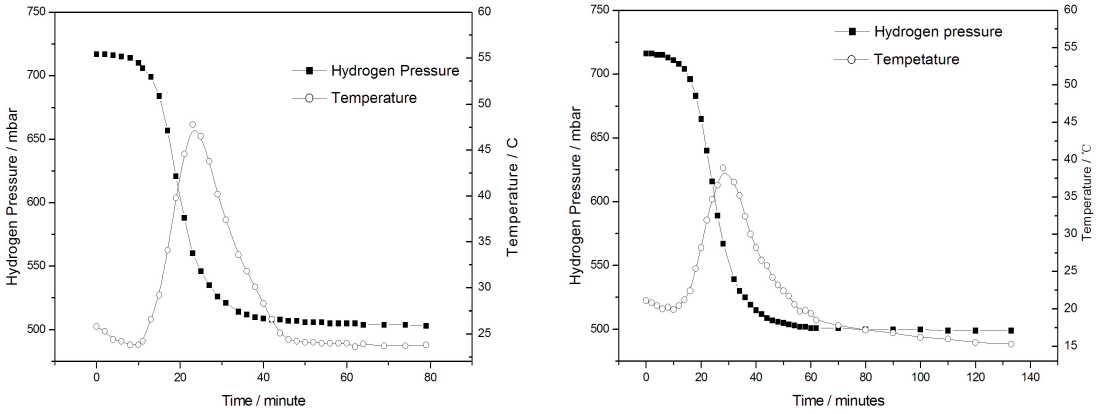

Fig. 2-8 Hydrogenation pressure and temperature recorded for the samples treated under vacuum (a) at 150°C and (b) at 200°C

2.2.2.1.2 Hydrogen absorption and desorption at moderate temperatures

Hydrogen absorption and desorption characteristics are followed recording the hydrogen up-take (expressed in weight %) versus time (kinetics measurements).

Fig. 2-9 shows the hydrogen absorption kinetics performed at 50℃ and 150℃ and the

hydrogen desorption kinetics performed during a following desorption at 300°C, on sintered $(NdDy)_{15}(FeCoNbCu)_{79}B_6$ magnets. XRD patterns have been recorded after hydrogen absorption and desorption steps. Fig. 2-10 shows the containing phases of each sample. The main results concerning the absorption (incubation time, reaction time,…) are reported in table 2-6.

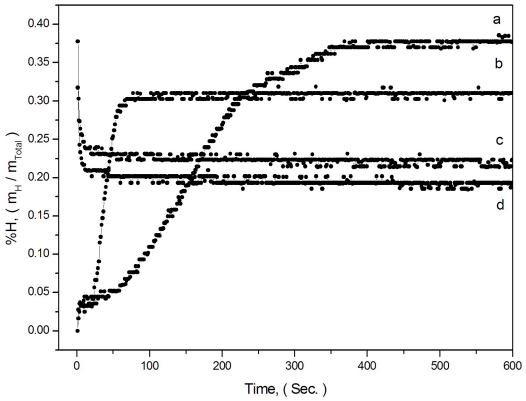

Fig.2-9 Hydrogen absorption and desorption kinetics (hydrogen up-take, in weight %) recorded at different temperatures

(a), absorption at 50℃ (HDT050);
(b), absorption at 150℃ (HDT150);
(c), desorption at 300℃, after absorption at 50℃, (HDT050D);
(d), desorption at 300℃, after absorption at 150℃, (HDT150D)

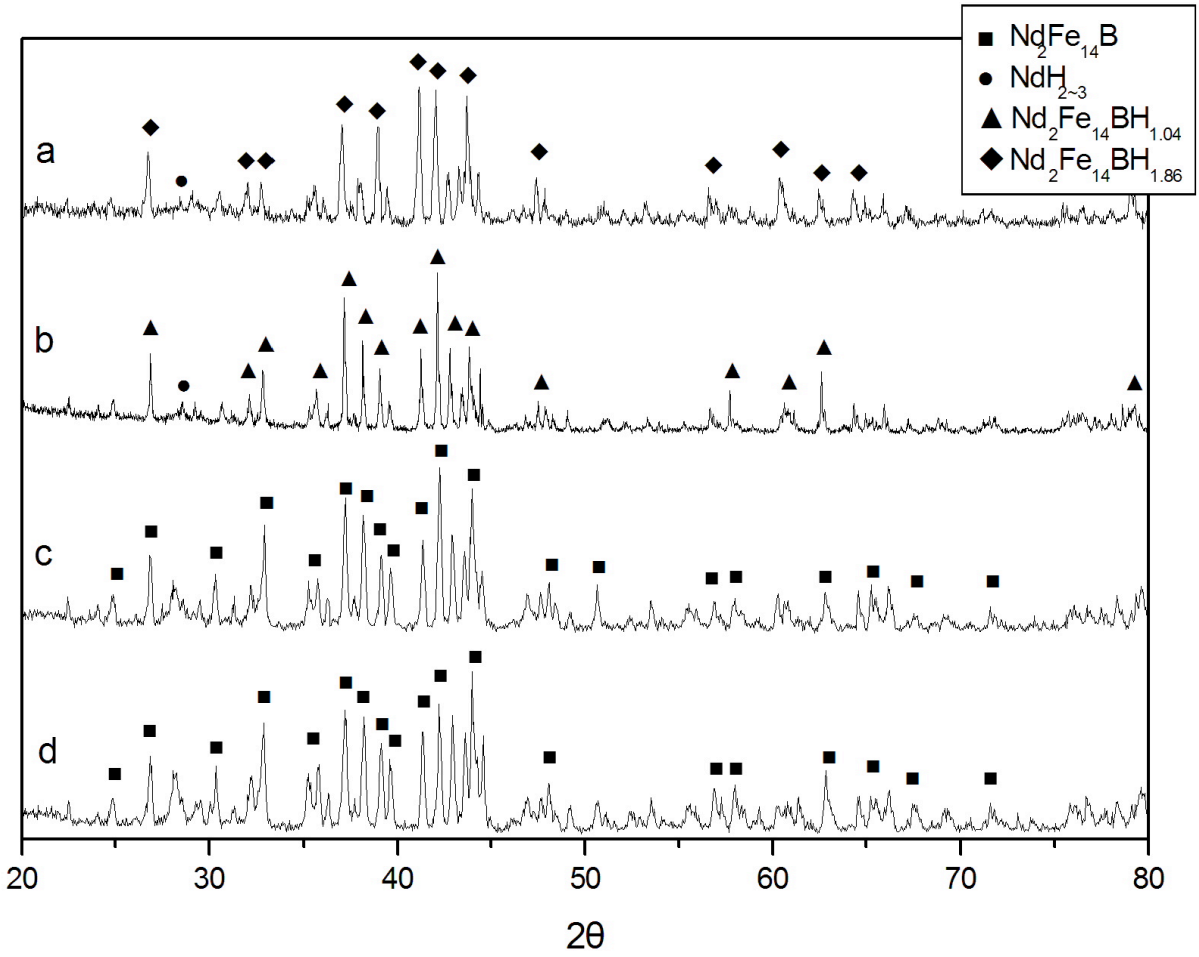

Fig. 2-10 X-ray diffraction patterns recorded after different hydrogen absorption and desorption kinetics measurements

(a), absorption at 50℃ (HDT050);

(b), absorption at 150℃ (HDT150);

(c), desorption at 300℃, after absorption at 50℃ (HDT050D);

(d), desorption at 300℃, after absorption at 150℃ (HDT150D)

Table 2-6 Main hydrogenation characteristics

Sample Name	Hydrogenation Temperature (℃)	Hydrogen Pressure (kPa)	Incubation Time (s)	Hydrogenation Time (s)	Saturated Value (% wt)	Average Hydrogenation Rate (% wt/s)
HDT050	50	200	50	350	0.38	0.0019
HDT150	150	200	10	60	0.31	0.0052

The hydrogenation behavior of sintered $(NdDy)_{15}(FeCoNbCu)_{79}B_6$ magnets is dependant from the hydrogenation temperature.

As shown on Fig.2-9, relatively slow hydrogen absorption occurs after a short incubation period when temperature of the sample was initially stabilized at 50°C. During the process, the

exothermal reaction leads the sample to a moderate increase of temperature of $\Delta T \sim 12.5°C$. Completing the experiment, the overall hydrogen absorption reaches the saturation value of 0.38 ± 0.02 wt% (realized after ~ 360 min), thus corresponding to the overall formula $(Nd,Dy)_{15}(Fe,Co,Nb,Cu)_{79}B_6H_x$ with $x = 25.5 \pm 0.2$.

Conversely and as reported also on Fig.2-9, fast hydrogen absorption occurs at 150°C after a shorter incubation period leading to a hydrogenation saturation value of 0.31 ± 0.02 wt% realized after ~ 80 sec. It corresponds to the overall formula $(Nd,Dy)_{15}(Fe,Co,Nb,Cu)_{79}B_6H_x$ with $x = 21 \pm 0.2$. Correspondingly, the exothermal rise of temperature of the sample is of $\Delta T \sim 46.5°C$.

The temperature rise of the sample during the hydrogen absorption at 150°C is ~ 4 times higher than that recorded at 50°C, meaning that the hydrogenation reaction is much vigorous when activated at 150°C than at 50°C. Unexpectedly, the overall hydrogen uptake is more marked when processed at 50°C than at 150°C. In fact this can be related to the rate of heat extraction from the present sample. The temperature of 150°C is quite close to the equilibrium temperature at normal H_2 pressure leading to the reaction $R_2Fe_{14}B \leftrightarrow R_2Fe_{14}BH_{xmax}$ ($x_{max} = 5.5$ [52]). Then a less efficient extraction of heat developed in the $R_2M_{14}B$ sample due to exothermal reaction according to the rate of supplying H_2 gas leads to reduce the hydrogen uptake when occurring in the range of transition temperature. As prove, such a limiting phenomenon has been observed to occur when hydrogenating different types of metal hydrides, e.g. when forming MgH_2 [53].

These results fairly agree with those obtained using XRD analysis of the hydrogenated samples. As shown on Fig.2-10a and b, the hydride of tetragonal Φ phase holds a nominal formula of $R_2M_{14}BH_{1.85}$ when the sample was hydrogenated at 50°C while the resulting formula is $R_2M_{14}BH_{1.05}$ when it was hydrogenated at 150°C.

Simultaneously, the R-rich phase always exhibits the same hydrogen content for both processing temperatures, corresponding well to the nominal formula $RH_{2.4}$ as deduced from Fig.2-10c and d.. Thereby, the larger amount of absorbed hydrogen in the sample when realized in moderate conditions contributes to the hydrogenation of tetragonal phase. Also the samples reveal homogeneously H-treated. For each case Fig.2-10 indicates the presence of unique hydrogenated phases, then hydrogen is quite homogeneously distributed in the main Φ and the minor R-rich phases.

Rescaling versus time and versus amplitude the two absorption traces displayed on Figure 3 does now allow considering a unique absorption process whatever is temperature. If both traces reveal an early incubation process that can be attributed to a similar nucleation-propagation mechanism, the trace recorded at 50°C evolves more complicatedly than that recorded at 150°C. A two steps absorption phenomenon takes a sigmoid type progression for ~ 2/3 of elapsed time and ~ 3/4 of the absorbed hydrogen, and an almost linear absorption progression for the remaining time and ~1/6 of the total amount of absorbed hydrogen. This behavior should be correlated to the evidence of 2 absorption peaks as observed on DSC analysis (Fig.2-4).

The decrepitated mechanism exhibits difference between 50°C and 150°C. As shown in Fig.2-11, HDT050 shows both intra-granular and inter-granular fractures, while in Fig.2-12, HDT150 shows only inter-granular fractures. This should be due to the larger hydrogen up-take

of HDT050 as compare to HDT150, which results in a larger volume expand of the tetragonal phase in HDT050 than in HDT150.

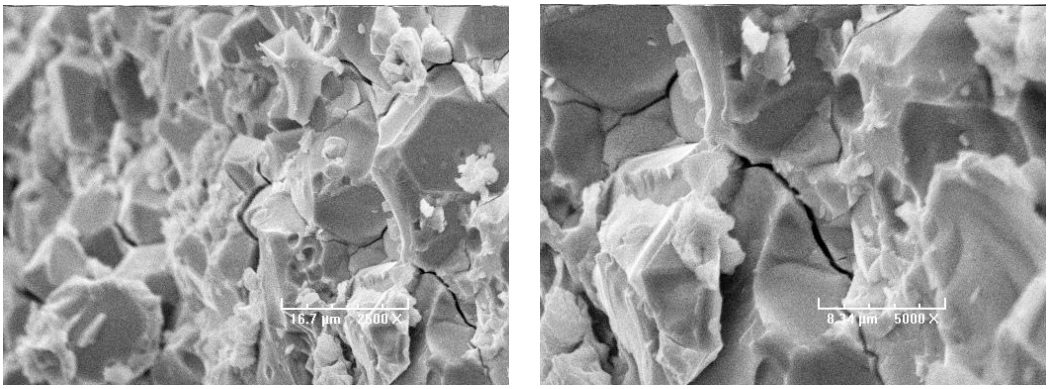

a b

Fig.2-11. SEM pictures for the decrepitated powder of HDT050. (a) x 2500; (b) x 5000

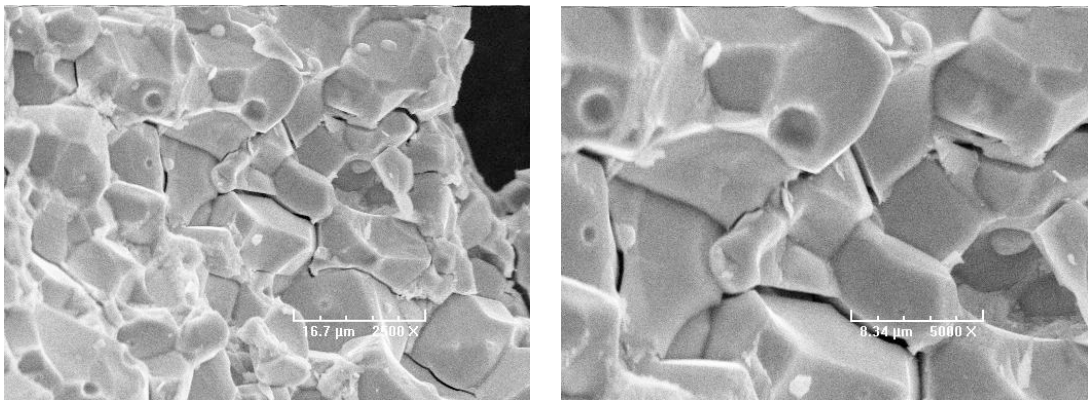

a b

Fig.2-12. SEM pictures for the decrepitated powder of HDT150 (a) x 2500; (b) x 5000

The hydrogen desorption of both HDT050D and HDT150D occurred very rapidly at 300℃ without any incubation period (Fig. 2-9). The released amounts of hydrogen are respectively 0.12 % wt. and 0.15 % wt. for HDT150D and HDT050D which is in rather good agreement with the amount of hydrogen contained in the hydride Φ phases (0.096 and 0.17 % wt. respectively). Accordingly, the hydrogen desorbed from hydride magnet $(NdDy)_{15}(FeCoNbCu)_{79}B_6H_x$ at 300℃ has been attributed to the hydrogen contained in the $(NdDy)_2(FeCo)_{14}BH_x$ phase. This is also confirmed from XRD patterns recorded after desorption : there were no $Nd_2Fe_{14}BH_x$ peaks, and only $Nd_2Fe_{14}B$ phase peaks were detected for both HDT150D and HDT050D (Fig. 2-10).

As shown in Fig.2-13 and Fig.2-14, the surface topography of desorbed powders have not change when compared with that of the hydrogenated decrepitated powders. The intra-granular (for HDT050D) and inter-granular cracks (for both samples) can still be clearly observed.

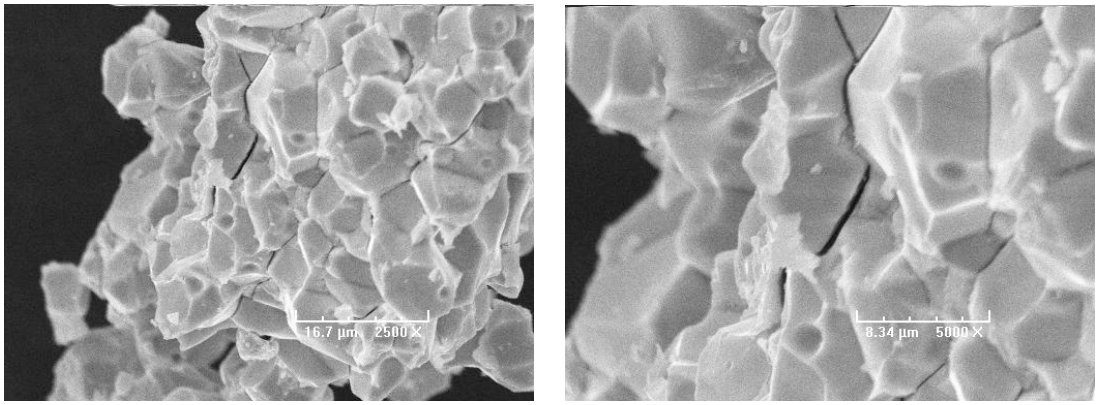

a b

Fig.2-13. SEM figures for the desorbed powder of HDT050. (a) x 2500 ; (b) x 5000

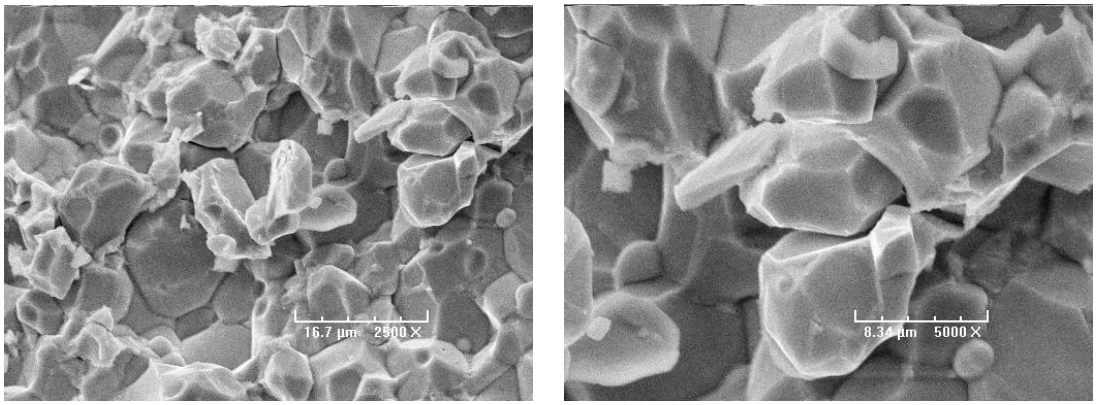

a b

Fig.2-14 SEM figures for the desorbed powder of HDT150 (a) x 2500 ; (b) x 5000

Fig.2-15 shows the powder size distribution of the decrepitated powders when the sintered $(NdDy)_{15}(FeCoNbCu)_{79}B_6$ magnets scraps were decrepitated in hydrogen at the temperature of RT, 150℃ and 200℃, respectively. Decrepitation at higher temperature, such as 150℃ and 200℃, results in a slightly larger amount of smaller particles than at RT. This should be due to the fact that the reaction between $(NdDy)_{15}(FeCoNbCu)_{79}B_6$ alloy and hydrogen is stronger at 150℃ and 200℃ than at RT.

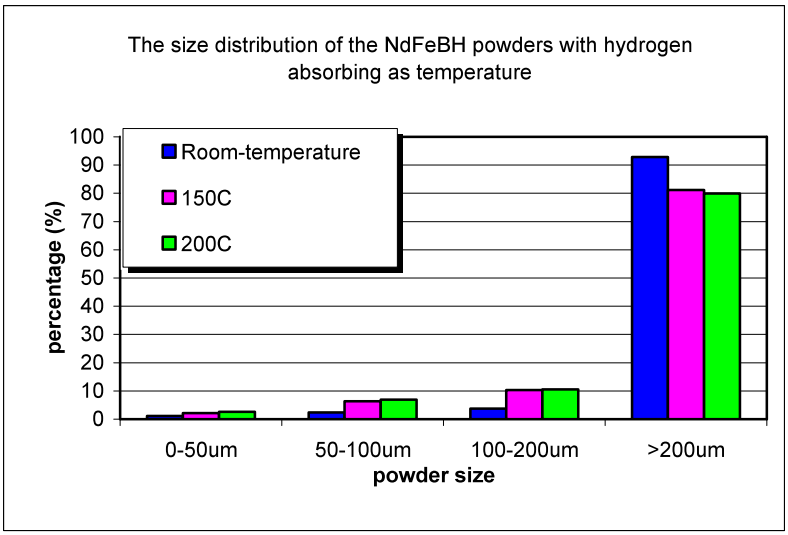

Fig. 2-15 Powder size distribution of the decrepitated $(NdDy)_{15}(FeCoNbCu)_{79}B_6$ magnets scraps, for different decrepitation temperatures.

2.2.2.1.3 Hydrogen desorption at high temperature

$(NdDy)_{15}(FeCoNbCu)_{79}B_6$ powders decrepited under 70 kPa of hydrogen pressure have been submitted to higher desorption temperatures. Fig.2-16, Fig.2-17, and Fig.2-18 show surface topographies of powders which have been desorbed at 300℃, 500 ℃, and 820℃, respectively. Great differences of morphology are observed depending on the corresponding desorption temperature.

When the powders are desorbed at 300°C (Fig.2-16), the morphology is similar to the one observed previously for lower desorption temperatures. On the contrary, for the decrepitated powders desorbed above 500°C, the surface of the powders is covered with the melted Nd-rich phase Fig.2-17, and Fig.2-18. This results from the presence of copper in this (NdDy)(FeCoCuNb) composition, which is known to reduce the melting point of the Nd-rich phase down to about 525°C [RIV2000].

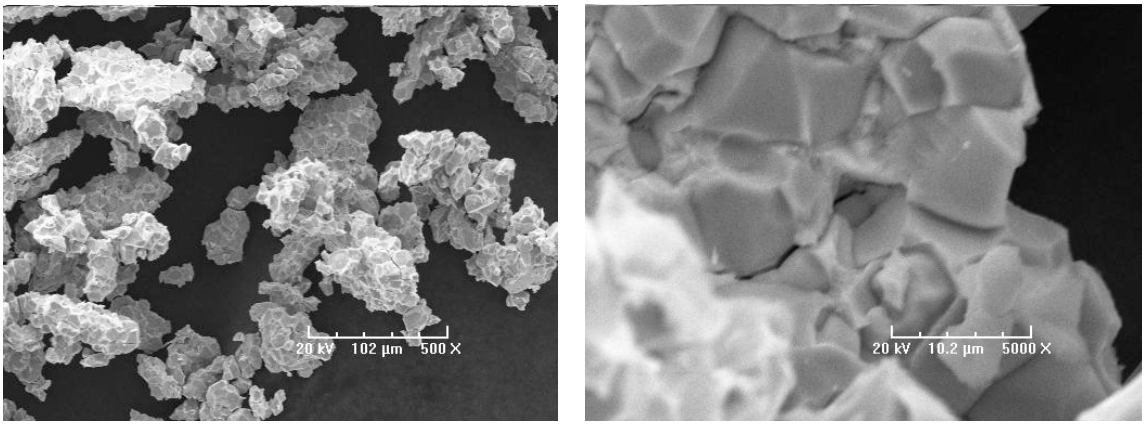

a b

Fig.2-16 SEM pictures of the surface of $(NdDy)_{15}(FeCoNbCu)_{79}B_6$ powders desorbed at 300°C (a) x 500 ; (b) x 5000

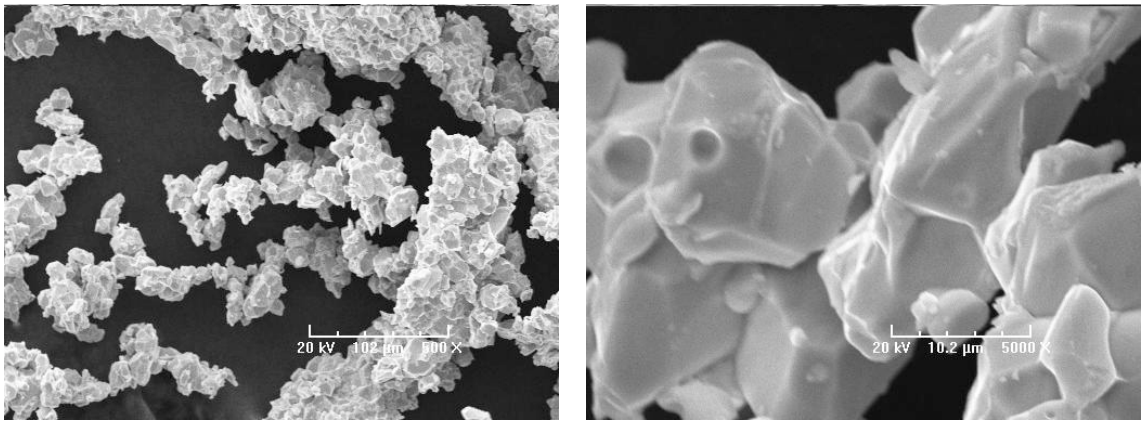

a b

Fig.2-17 SEM pictures of the surface of $(NdDy)_{15}(FeCoNbCu)_{79}B_6$ powders desorbed hydrogen at 500°C (a) x 500 ; (b) x 5000

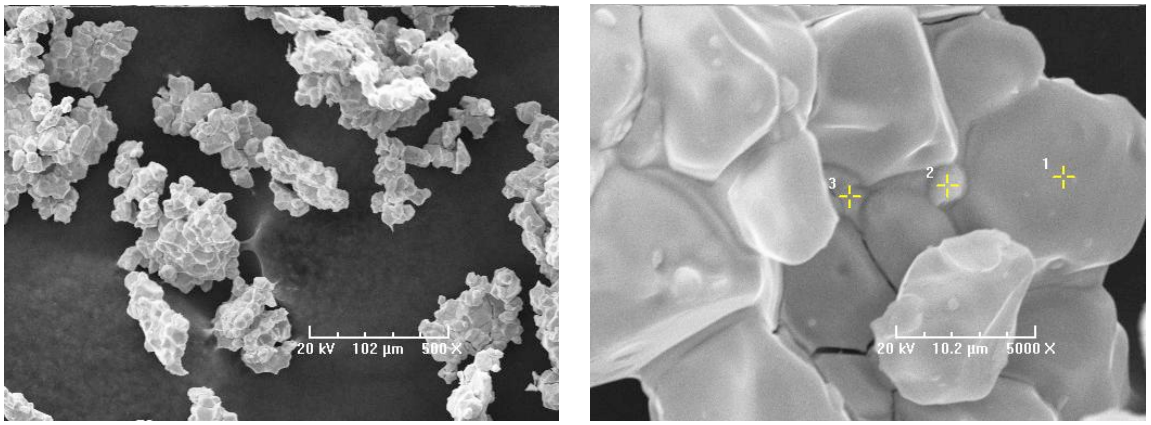

a b

Fig.2-18 SEM pictures of the surface of desorbed $(NdDy)_{15}(FeCoNbCu)_{79}B_6$ powders desorbed at 800°C (a) x 500; (b) x 5000

2.2.2.2 Effect of hydrogen pressure

In order to evaluate the impact of the hydrogen pressure during the decrepitation process, several experiments have been performed on $(NdDy)_{15}(FeCoNbCu)_{79}B_6$ magnets scraps at the same temperature (150°C) and for increasing hydrogen pressures ranging from 80 to 200 kPa. The sample references and the corresponding experimental conditions are reported in Table 2-7.

Fig.2-19 shows the hydrogen absorption and desorption kinetics measured on the samples HDP80, HDP160, and HDP200. Two typical times are considered, the first corresponding to incubation time of the reaction, the second to the faster absorption period. It is clear that both these characteristics decrease with the applied pressure. Besides, the total amount of absorbed hydrogen increases smoothly and linearly upon increasing the applied pressure.

After hydrogen desorption at 300℃, the samples hydrogenated at different hydrogen pressures release different amount of hydrogen, thus maintaining almost the same residual amount of hydrogen.

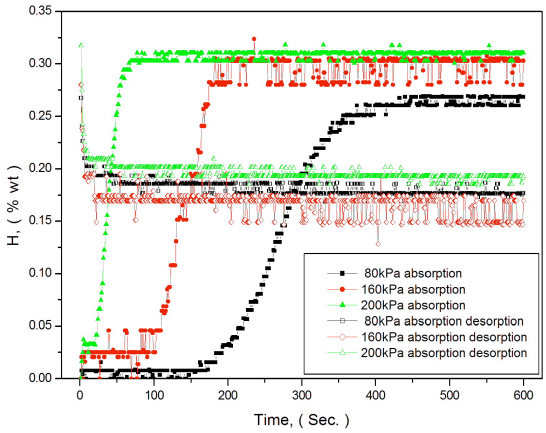

Fig. 2-19. Hydrogen absorption curves recorded at 150℃ for different hydrogen pressures and hydrogen desorption curves recorded at 300°C under vacuum.

Table 2-7 Experimental conditions and results of the samples hydrogenated at different absorption pressures

Sample Name	Absorption Temperature	Desorption Condition	Hydrogen Pressure	Incubation Time before Hydrogenation	Absorption period	Saturation Hydrogen Content	Desorption Hydrogen Content
	℃		kPa	Sec	Sec	wt%	wt%
HDP200	150	300℃ in vacuum	200	20	60	0.31	0.12
HDP160	150		160	95	80	0.29	0.11
HDP080	150		80	170	280	0.27	0.09

2.2.2.3 Effect of sample mass

Fig.2-20 shows the hydrogenation kinetics measurement of 2 samples weighted 655.8 mg and 256.3 mg respectively. Decrepitation was performed at 150℃ under 120 kPa of hydrogen pressure, while desorption was performed at 300℃ under vacuum. A shorter incubation period, as well as a shorter absorption period are observed for the heaviest sample. This is correlated with the increase of temperature due to the exothermic reaction, which is more important when the sample mass increases. However, the hydrogen up-takes remain equivalent in both cases.

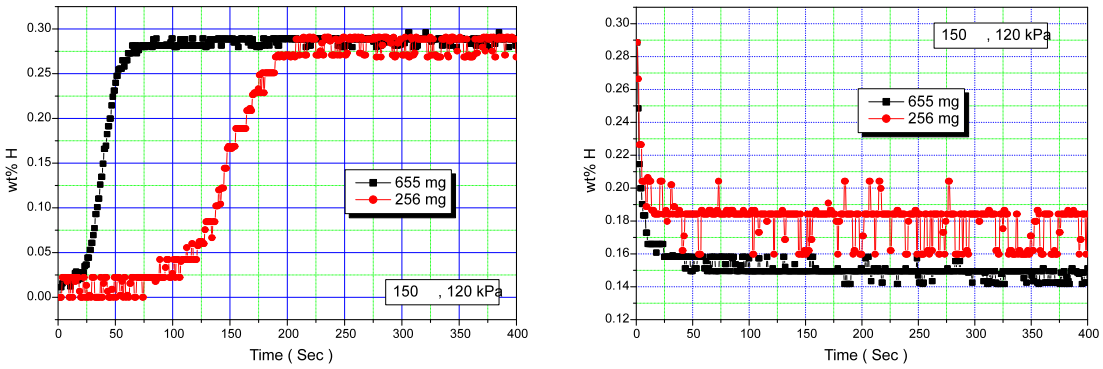

Fig.2-20 Hydrogen absorption and desorption kinetics measurements performed at 150°C under 120kPa of hydrogen pressure, on samples of different weights (655 mg in black and 256 mg in red).

Similar measurements have been performed applying 200 kPa of hydrogen pressure during the absorption, and using heaviest samples (806mg and 655.8mg) Fig.2-21.

As expected, for the sample weighted 655.8mg, both the incubation time and the absorption time are shorter at 200 kPa than at 120 kPa (20 sec. instead of 150 sec.). For the heaviest sample (806mg), the absorption starts immediately, without incubation time. Again, this behavior is correlated with the increase of temperature due to the exothermic reaction, which appears to be very fast when the sample mass increases, as observed on Fig 2-22 where the oven temperature has been recorded during this hydrogenation.

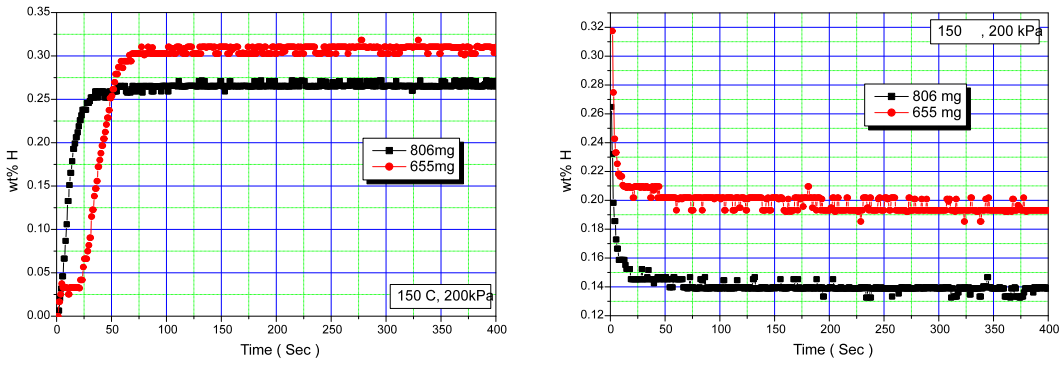

Fig.2-21 Hydrogen absorption and desorption kinetics measurements performed (a) at 150°C under 200kPa of hydrogen pressure, (b) at 300°C under vacuum, on samples of different weights (806mg in black and 655mg in red).

The increase of temperature observed on Fig.2-22 is rather low (less than 2°C). However, it has to be notice that the recorded temperature is measured in the furnace, and not directly into the sample. Then, the real increase of temperature into the sample is expected to be much more important.

As observed on Fig 2-21, the hydrogen up-take remains lower for the heaviest sample, probably because the equilibrium temperature corresponding to the applied pressure has been achieved, then stopping the hydrogenation reaction.

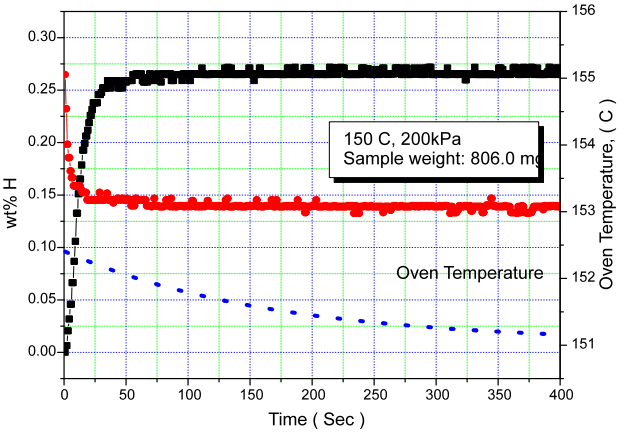

Fig.2-22 Temperature change of the sample weighted 806mg during the hydrogenation at 150℃ at the hydrogen pressure of 200 kPa

All these results are in agreement with a highest heat release for larger mass. Since the hydrogenation is a thermally activated process, it becomes faster, but the absorption reaction stops before the end if the equilibrium temperature is reached. All these parameters are of importance if a production in large bathes is expected.

2.2.2.4 Impact of sample oxidation

The characteristics of Nd-Fe-B magnets are known to be very sensitive both to oxidation and to moisture. In order to appreciate the impact of these parameters on the decrepitation process, a sample under the form of scraps was exposed outdoor for 3 days. Then, the absorption and desorption characteristics have been recorded and compare to the original sample, with "fresh" fracture surfaces (Fig.2-23).

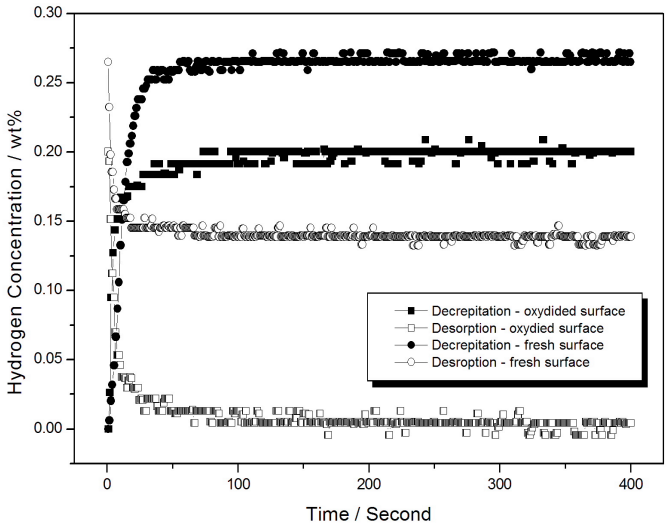

Fig.2-23 Decrepitation and desorption curves for the samples with fresh surface and oxidized surface

As shown in Fig.2-23, the hydrogenation process is greatly affected by the oxidation. Firstly, the oxidized sample absorbed less hydrogen than the sample not oxidized. Secondly, during desorption at 300℃, the oxidized sample give out all the hydrogen it has absorbed.

As shown before, only tetragonal phase desorbed hydrogen at this temperature. The sample begins to be oxidized from the phase on surface, mainly from Nd-rich phase in the case of Nd-Fe-B materials. Then, on the surface, hydrogen is absorbed only by tetragonal phase. Anyway, Nd-rich phase in the center of the sample should maintain the condition of no oxidized. However, the sample has not shown to absorb hydrogen by any Nd-rich phase in this oxidized sample, which is disclosed by the fact that the sample give out all of the absorbed hydrogen at 300℃(Fig.2-23).

2.2.2.5 Impact of hydrogenation cycles

When $(NdDy)_{15}(FeCoNbCu)_{79}B_6$ magnets are submitted to successive hydrogenation cycles, a modification of the hydrogenation behavior is observed (Fig.2-24a and Table 2-24b), as well as an evolution of the powder size distribution (Fig.2-25).

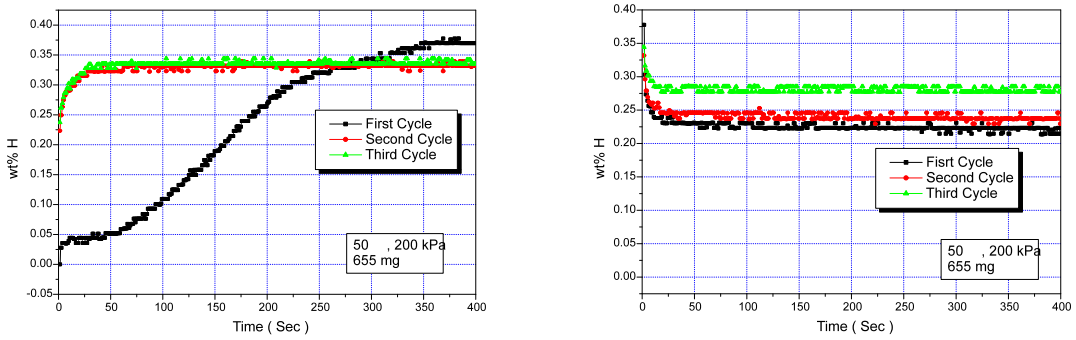

Fig.2-24 (a) Successive hydrogen absorptions performed at 50°C under 200 kPa of hydrogen pressure and (b) successive hydrogen desorptions performed at 300°C (first and second cycle) and 500°C (third cycle) on $(NdDy)_{15}(FeCoNbCu)_{79}B_6$ magnet scraps (sample weight 655mg).

During the first cycle, the sample absorbs a hydrogen content of as 0.378 % wt, with about 40 seconds incubation time. Then, the sample is heated at 300℃ in vacuum to release hydrogen. The sample reserves about 0.22 % wt of hydrogen after the desorption process.

During the second cycle, the sample absorbs hydrogen very rapidly to the content of 0.33 % wt. The amount of hydrogen absorbed remains lower that in the first hydrogen absorption, with dropping of about 10 % when compare with the first absorption. This was in fact expected, since the Nd-rich phase does not fully desorbed when treated at 300°C. The residual hydrogen content in the sample is about 0.23 % wt, which is comparable to the amount obtained after the first cycle.

The third desorption is performed at 500℃. Surprisingly, the residual hydrogen in the sample is 0.28 % wt, significantly higher than that of the first desorptions. This should be some part of $Nd_2Fe_{14}B$ grains have decomposed during this desorption procedure at such high temperature as following :

$$(Nd, Dy)_2(Fe, Co)_{14}B + (2\pm x)H_2 \quad \longleftrightarrow \quad 2(Nd, Dy)CoH_{2\pm x} + \alpha\text{-}(Fe, Co) + Fe_2B$$

The increase of residual hydrogen is due to the formation of (Nd, Dy)CoH. Then it appears very importance to control very accurately the desorption process following the decrepitation by applying low heating rates and / or desorption steps at lower temperature, in order to avoid disproportionation reaction.

As shown in Fig.2-25, when $(NdDy)_{15}(FeCoNbCu)_{79}B_6$ magnets scraps are submitted to hydrogen decrepitation for only once time, the decrepitated powders show great amount of large particles (80 % above 200µm). Then in order to minimize the powder size of the decrepitated powder, twice hydrogen decrepitation has been attempt. Furthermore, a desorption process has been applied between these two hydrogen decrepitations. Several hydrogen desorption temperatures have been tested in this experiment : 300°C, 500°C and 820°C respectively.

When $(NdDy)_{15}(FeCoNbCu)_{79}B_6$ magnets scraps are submitted to a second hydrogen decrepitation cycle, the decrepitated powder becomes finer and the amount of large particles is reduced down to 50 % (Fig.2-25). The decrepitated powders present more middle powder particles of 50 - 200µm and less large powder particles bigger than 200µm, when these decrepitated powders are desorbed at 300°C instead of 500°C or 820°C.

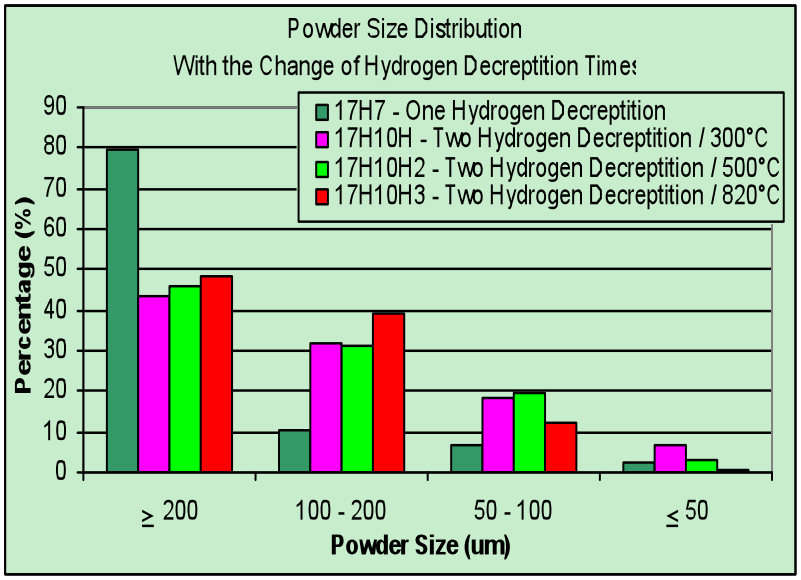

Fig.2-25 The powder size distribution of the decrepitated $(NdDy)_{15}(FeCoNbCu)_{79}B_6$ magnet scraps after twice hydrogen decrepitation.

Then, applying a twice hydrogen decrepitation process with an intermediate desorption step appears very efficient to reduce the amount of large particles in the final decrepitated powders.

2.3 Pressure-concentration-temperature relationship for the hydrogenation of sintered $(NdDy)_{15}(FeCoNbCu)_{79}B_6$ magnets

In the present work, sintered $(NdDy)_{15}(FeCoNbCu)_{79}B_6$ magnets absorb less hydrogen than in compositions $Nd_{15}Fe_{77}B_8$ and $Nd_{16}Fe_{76}B_8$, which was reported as $Nd_{15}Fe_{77}B_8H_{26}$ [CAD1986] and $Nd_{16}Fe_{76}B_8H_{27.8}$ [WIE1987], [POL1986], [HAR1987], [MCG1988] respectively. The gravimetric measurements give a total hydrogen content of 0.32 wt % and 0.42 ± 0.02wt% respectively.

The amount of hydrogen absorbed by $(NdDy)_{15}(FeCoNbCu)_{79}B_6$ magnets should be mainly correlated to the hydrogen absorption ability of $(NdDy)_2(FeCo)_{14}B$ phase. The elements substituted in $(NdDy)_2(FeCo)_{14}B$ lattice leads to a different hydrogen insertion scheme of $(NdDy)_2(FeCo)_{14}BH_x$ as in the case of $Nd_2Fe_{14}BH_x$ lattice. For the $(NdDy)_2(FeCo)_{14}B$ lattice, as a result of the replacement of Nd by Dy, the hydrogen atoms turn to occupy more 16k interstitial sites, while the hydrogen concentration in the 8j interstitial sites turns to be reduced when more hydrogen atoms occupy the 16k interstitial sites [FRU1997],[ISN1995],[FRU2004]. On the other side, the 16k interstitial sites themselves have less ability to absorb hydrogen than the 8j interstitial sites, due to their size difference and different chemical environments [FRU1997], [FRU2004]. Moreover, some particles are much larger than the grains of Φ phase after hydrogen absorption, the grains of Φ phase located in the center of the particles are surrounded well by Nd-rich phase then. Consequently, hydrogen atoms can be conveyed into these grains of Φ phase unless hydrogen atoms have enough energy to surpass the surface energy barrier between Nd-rich phase and Φ phase. This also makes the hydrogen diffusion in sintered $(NdDy)_{15}(FeCoNbCu)_{79}B_6$ magnets a little difficult, and results in relatively low concentration of hydrogen in it after hydrogen absorption.

The sintered $(NdDy)_{15}(FeCoNbCu)_{79}B_6$ magnets are mainly consist of two phases: Φ phase and Nd-rich phase. Both Φ phase and Nd-rich phase can absorb hydrogen simultaneously at 50℃ or 150℃ at a hydrogen pressure of 70 kPa during the hydrogenation kinetics measurement, which corresponds to the case which P. Liskzkowdki *et al.* have reported [TUR2000]. Moreover, the sintered $(NdDy)_{15}(FeCoNbCu)_{79}B_6$ magnets absorb more hydrogen at 50℃ than at 150℃ during the hydrogenation kinetics measurement. If we regard the Φ phase and Nd-rich phase as one "average phase", according to the ideal gas-solid solution hypothesis [SKO1993], [COE1996] and the calculation [TUR2000], [LIS2000], [COE1996], we can roughly describe hydrogen absorption characteristics of the sintered $(NdDy)_{15}(FeCoNbCu)_{79}B_6$ magnets at 50℃ and 150℃ by a pressure-concentration-temperature (*p*-*c*-T) diagram sketch as shown in Fig. 2-26. The hydrogen absorption curve at 50℃ is in right side of that at 150℃ along the hydrogen equilibrium concentration (C_{equ}) axis, so the sample will have higher hydrogen concentration at the same hydrogen pressure of 70 kPa when it absorbs hydrogen at 50℃.

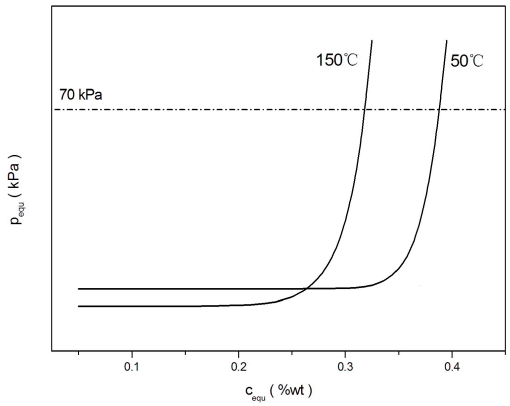

Fig. 2-26. The p-c diagram sketch for the hydrogen absorption by sintered $(NdDy)_{15}(FeCoNbCu)_{79}B_6$ magnet at 50°C and 150°C

Owing to the high stability of the Nd-rich hydride, we suggest that the sketch describe above should concern mainly with the 2-14-B phase.

2.4 Conclusions

The hydrogen absorption and desorption characteristics of $(NdDy)_{15}(FeCoNbCu)_{79}B_6$ sintered magnets by DSC measurement and hydrogenation kinetic measurement were studied in this part.

A previous heat-treatment under vacuum at the temperature above 150℃ is effective to promote hydrogen absorption of sintered $(NdDy)_{15}(FeCoNbCu)_{79}B_6$ magnets scraps at room temperature. Applying a twice hydrogen decrepitation process with an intermediate desorption step appears very efficient to reduce the amount of large particles in the final decrepitated powders.

The bulk magnets absorbed hydrogen mainly by Nd-rich phase in low temperature range of 40-185℃, and by Φ phase in the temperature range of 185-220℃ ; the decomposition of Φ phase occurred in a broad temperature range from around 500℃ to 800℃. At 300℃, hydrogen was desorbed mainly from Φ phase.

The hydrogenation kinetic measurements show a two-step process : the first one corresponds to an incubation period (activation – nucleation) and the second to a faster absorption period. Both these characteristic times decrease when the applied hydrogen pressure and temperature increase.

PART 3

Anisotropic powders prepared by hydrogen decrepitation, desorption and annealing treatments

3.1 Experimental procedure

3.1.1 Start materials

$(NdDy)_{15}(FeCoNbCu)_{79}B_6$ sintered magnets used in this test were manufactured by powder metallurgy. The magnetic properties are the following : H_{ci} = 31 kOe (2467.6 kA/m), B_r = 11.1 kGs (1.11 T) and $(BH)_{max}$ = 29.4 MGOe (234 kJ/m^3). As already presented in the Part 2 of this thesis, scanning electron microscopy (SEM), energy dispersive X-ray (EDX) and X-ray diffraction (XRD) analysis show that the magnets are composed of a tetragonal phase (Φ phase) $(NdDy)_2(FeCo)_{14}B$, and a intergranualr Nd-rich phase (NdDy)(FeCoCu).

3.1.1 Hydrogen decrepitation and desorption furnace

Three steps of treatment are included in the whole process : hydrogen decrepitation, hydrogen desorption, and annealing. These treatments were undertaken in a furnace built at CNRS, to work under controled atmosphere and high magnetic field (superconductor magnet) Fig. 3-1.

Fig.3-1 Furnace used for decrepitation and desorption treatments in CRETA / CNRS, Grenoble

The main characteristics are the following :

(a) Heating up to 1100℃,
(b) Supply magnetic field, up to 7 T,
(c) Hydrogen pressure up to 100 kPa,

(d) Vacuum, up to 5.0×10^{-4}Pa.

3.1.2 Bonded magnets preparing method for magnetic measurements

Bulk (NdDy)(FeCoNbCu)B sintered magnet were crushed into pieces by hand, and then about 60 g of these pieces were charged into the chamber of furnace (Fig.3-1) and vacuumed to 1.0×10^{-3} Pa. Then, the powders were prepared by following process, such as hydrogen decrepitation, hydrogen desorption, and annealing.

Hydrogen gas (purity of 99.999%) was introduced into the chamber to crumble the magnets pieces into powders, at certain temperatures during the hydrogen decrepitation process. These decrepitated powders were then submitted to the hydrogen desorption process at certain temperatures with a dwelling time of 1 hour, and finally to the annealing treatment. A magnetic field was applied during the hydrogen desorption process.

When the whole treatment procedure has completed, the HD-powders are crushed by hand for several seconds to disperse the large aggregates formed during the hydrogen desorption and annealing procedures. Then the HD-Powders are prepared as bonded magnets by mixing the powder with a bonder ARALDITE® in air, following by a polymerization under a magnetic field of 5 Tesla.

Magnetic properties of the powders were measured by extraction magnetometer in term of cylinder bonded magnets with 3 mm in diameter and 7 mm in length. With the help of the magnetic field, the powder particles in the bonded magnets rotated parallel to each other, and to their macroscopic texture axis. Values of magnetic properties of the powders were corrected to the density of 7.5×10^{3} kg/m^{3}.

The microstructure of the decrepitated or desorbed powders are observed by JEOL SEM JSM5600LV, and the phase constitute of these powders are analyzed by X-Ray diffraction analysis at PHILIPS PW 3830 X-Ray Generator.

3.1.3 Magnetic properties measurement

The magnetic properties of the bonded magnets are measured by extraction magnetometer equipped with a superconducting coil, in Néel Institut / CNRS Grenoble.

3.1.4 Thermo-Magnetic Analysis

Thermo-magnetic measurement are performed on powders sealed inside quartz tubes. These measurements are used to evidence the magnetic transitions, especially Curie

temperatures. This device has been very helpful to evaluate HDDR process of Nd-Fe-B alloys, due to its sensitive reflection to disproportionation and recombination reaction between $Nd_2Fe_{14}B$ and hydrogen [LIE1996]. In this thesis, we employed the thermo-magnetic measurements to reveal residual hydrogen content in the powders according to the disproportionation reaction between $Nd_2Fe_{14}B$ and hydrogen.

3.1.5 The main purpose of this part

Because most of bonded Nd-Fe-B magnets will be used in electric motor devices, it is important to obtain anisotropic powders with good thermal-properties. Among these, the Hcj of powders plays an important role. No reports have released on the anisotropic powders with the Hcj above 15 kOe. In present work, we try to start with sintered NdDyFeCoNbCuB magnets with a high Hcj above 30kOe, and attempt to prepare powders with high Hcj. NdDyFeCoNbCuB magnets have a good thermal stability due to a relatively large mount of Dy, Co elements, and also Nb, Cu doping elements.

Anisotropic Nd-Fe-B powders were made from sintered (NdDy)-(FeCoNbCu)-B bulk magnets by hydrogen decrepitation and desorption process. The hydrogen decrepitation temperature, the hydrogen desorption temperature, annealing temperature are investigated about their effective to the magnetic performance of the anisotropic powders.

3.2 Impact of the hydrogen decrepitation on the magnetic properties

3.2.1 The decrepitation temperature

To evaluate the impact of the decrepitation temperature on the magnetic performance of the HD/de-gas powders, about 60g of the sintered magnets scraps were hydrogen decrepitated at Room-Temperature, 50°C, and 150°C respectively in the furnace as described in the section 3.2.1 (Fig.3-2). The decrepitated powders were then submitted to hydrogen desorption and annealing treatments as described in Fig. 3-2.

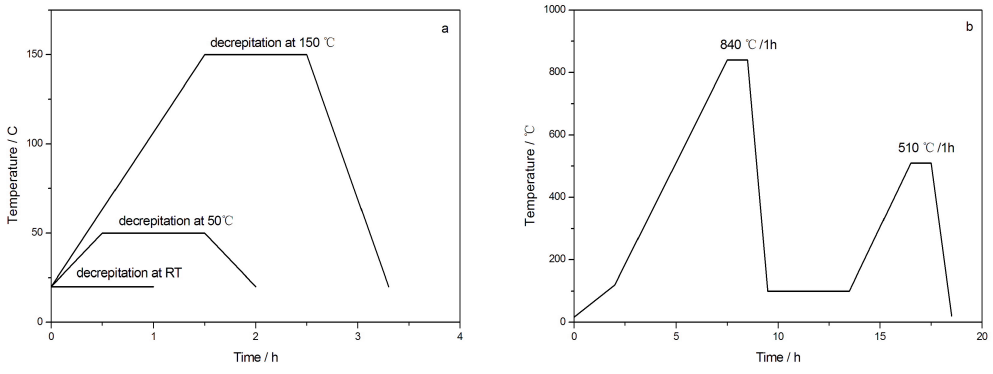

(a) (b)

Fig. 3-2. Technical process sketches used for hydrogen decrepitation (a), and subsequent desorption and annealing treatments (b).

Table 3-1 shows the magnetic performance of HD-powders decrepitated at different temperatures with the same desorption and annealing process. Fig. 3-3 shows the de-magnetization curves of these powders.

Table 3-1. Magnetic performances of HD-Powders decrepitated at different temperatures

Decrepitation*	Desorption	Annealing	Coercivity Hcj / kOe	Remanent Magnetization Br / kGs	Maximum Energy Product BH_{max} / MGOe
RT	400℃/2h, 840℃/1h	510℃/1h	10.4	9.09	13.98
50℃	400℃/2h, 840℃/1h	510℃/1h	12.6	9.70	16.87
150℃	400℃/2h, 840℃/1h	510℃/1h	9.7	9.76	16.67

* The hydrogen pressure was about 70 kPa during the decrepitation process.

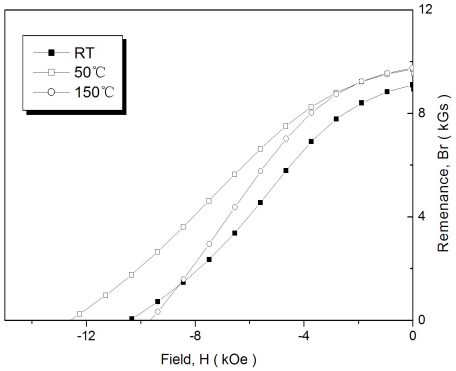

Fig.3-3 De-magnetization curves of HD-powders at different decrepitation temperatures

The decrepitation at 150℃ turns to have a lower coercivity of the powders. The decrepitation at room temperature does not benefit to obtain the powders with good magnetic performance either. Then, Hydrogen decrepitation at 50℃ appears to be preferable to obtain powders with good magnetic performances.

3.2.2 Twice hydrogen decrepitation cycles

Twice hydrogen decrepitation cycles were employed on the precursor (NdDy)-(FeCoNbCu)-B bulk magnets to prepare HD/Degas powders. Between the both hydrogenations, the samples were submitted to an intermediate hydrogen desorption step.

3.2.2.1 Technical process

Three different intermediate desorption treatments, in other words 300℃/3h, 500℃/3h, 820℃/1h, were applied between the twice decrepitation processes, as showing on the Fig3-4a. All these different desorbed powders were then submitted to the same hydrogen desorption and annealing treatment as shown in the Fig3-4b.

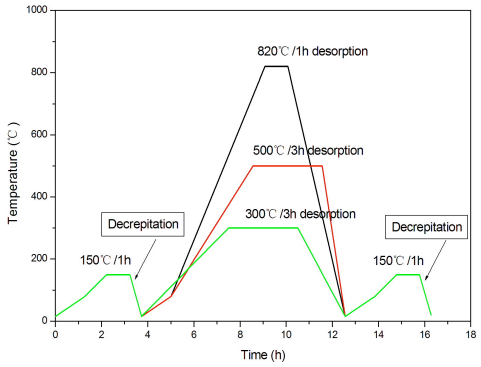

(a) The hydrogen decrepitation procedure

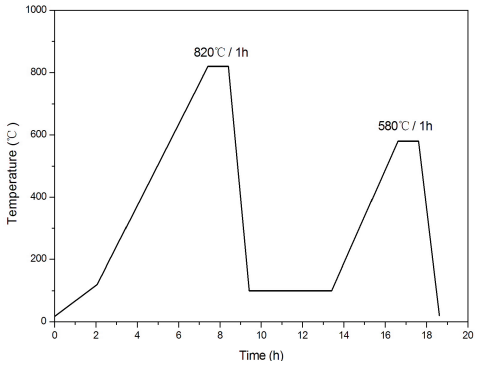

(b) The hydrogen desorption procedure

Fig. 3-4 Technical process sketch for the twice decrepitation cycles

3.2.2.2 Microstructure of the twice cycle decrepitated powders

Fig. 3-5 presents the SEM microstructure morphology of the twice hydrogen decrepitation (THD) powders which were prepared by a twice hydrogen decrepitation treatment.

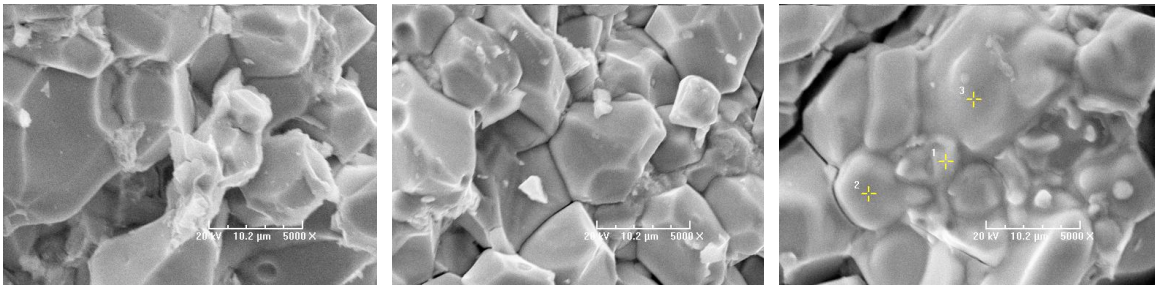

(a) 300℃/3h (b) 500℃/3h (c) 820℃/1h

Fig. 3-5 SEM morphology of the THD-powders for different intermediate desorption processes applied between the both decrepitations (a) for 300°C / 3h, (b) 500°C / 3h, (c) 800°C/1h

As shown in Fig.3-5, the powders turns to be smoother with the increase of the intermediate desorption temperature between the twice hydrogen decrepitations. At the temperature of 300°C and 500°C, some of fine particles can be seen on the surface of larger particles, meanwhile the fine particles are melted on the surface of larger particles at the high temperature of 820°C.

3.2.2.3 Size distribution of hydrogen decrepitated powders

After the twice hydrogen decrepitations process, the powder size distribution was identified by sieve-analysis. The analysis result is shown in Fig.3-6. As compared, the powders size distribution of once hydrogen decrepitation is also reported in Fig. 3-6.

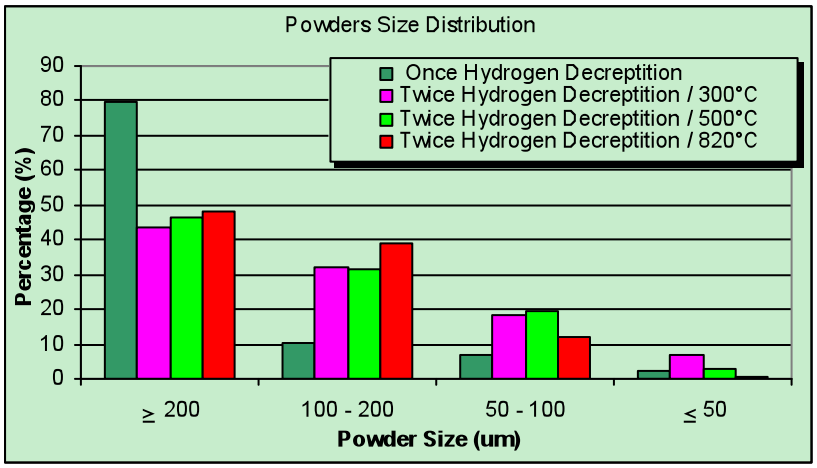

Fig. 3-6 Powders size distribution of the HD-powders prepared by different decrepitation treatments

As shown in Fig.3-6, when the magnets are submitted to a twice hydrogen decrepitation, the powder particles turn to be finer, with a larger part of the powders located in the range of 50-200 μm. The amount of powder particles larger than 200 μm reduces from 80% to less than 50%, meanwhile that of the powder particles smaller than 200μm are increased. Furthermore, the intermediate desorption temperature between the two decrepitation steps affects the powder size distribution too : the powders size distribution at higher desorption temperature (820℃) slightly increases the concentration in the range 100– 200μm.

3.2.2.4 Discussion

Hydrogen decrepitation of (NdDy)-(FeCoNbCu)-B magnets is a process of poly-phases reactions, in which Nd-rich phase is much easier to hydride than the $(NdDy)_2(FeCo)_{14}B$ main phase, and plays as a diffusion pass for hydrogen atoms into the magnets.

The layer near the surface of magnet scraps is easier to saturate with hydrogen atoms. The diffusion of hydrogen atoms inside the bulk magnets depends on the amount of Nd-rich phase, the distribution of this Nd-rich phase inside the magnets, and the ability of hydrogen atoms to move inside Nd-rich phases.

In fact, the distribution of Nd-rich phase inside samples is not homogenous as shown in Fig.2-9. As a result, when hydrogen atoms do not go much further into the center of the larger magnet pieces during the first decrepitation process, the material inside the particles is not fully hydrogenated. Then, the decrepitated particles turn to be larger. At the second decrepitation, thanks to the new fresh surfaces created during the first decrepitation, hydrogen atoms can reach more easily the centre of the powder particles, resulting in finer particles.

3.2.2.5 Magnetic Performance of THD-powders

The magnetic properties of the THD-powders have been measured after applying the

same desorption procedure (Fig. 3-4b). The results recorded for medium size (100–200μm) and large size (> 200 μm) are summarized in Table 3-2 and Fig. 3-9. For comparison, the magnetic properties of once decrepitated powders (HD-powders) are also reported. The de-magnetization curves of these powders are shown in Fig.3-7 and Fig.3-8.

Table 3-2 Magnetic properties of the HD-powders and THD-powders

Hydrogen Decrepitation*	Hydrogen Desorption	Powder Size	Remanence Br / kGs	Coercivity Hcj / kOe	Energy product (BH)m / MGOe
Twice at 150℃; 300℃ between	820℃/1h 580℃/1h	100-200 μm	10.36	4.5	9.89
		> 200 μm	10.63	9.8	14.61
Twice at 150℃; 500℃ between		100-200 μm	10.67	5.2	11.39
		> 200 μm	10.20	7.6	11.71
Twice at 150℃; 820℃ between		100-200 μm	11.02	3.1	7.95
		> 200 μm	10.05	4.5	9.54
Once at 150℃		100–200μm	10.19	7.4	16.4
		> 200 μm	10.95	7.1	18.5

* The hydrogen pressure is about 70kPa during the decrepitation process.

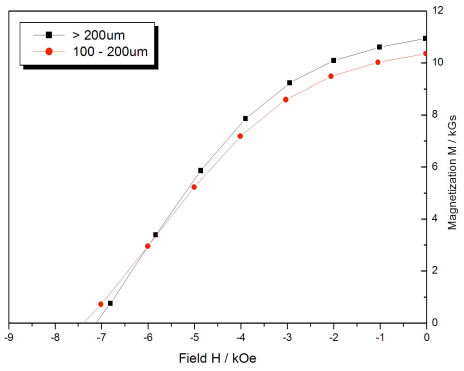

Fig. 3-7 Demagnetization curves of the once hydrogen decrepitated powders

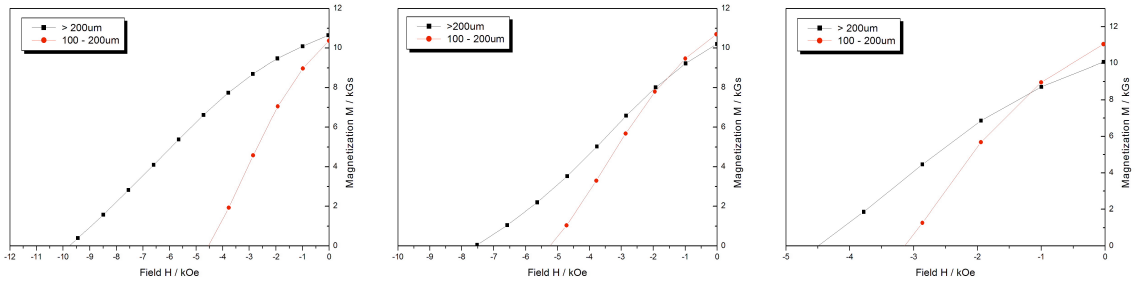

(a) 300℃/3h (b) 500℃/3h (c) 820℃/1h

Figure 3-8 Demagnetization curves of the THD-powders at the intermediate hydrogen desorption conditions of 300°C/3h (a), 500°C/3h (b), and 820°C/1h (c) respectively

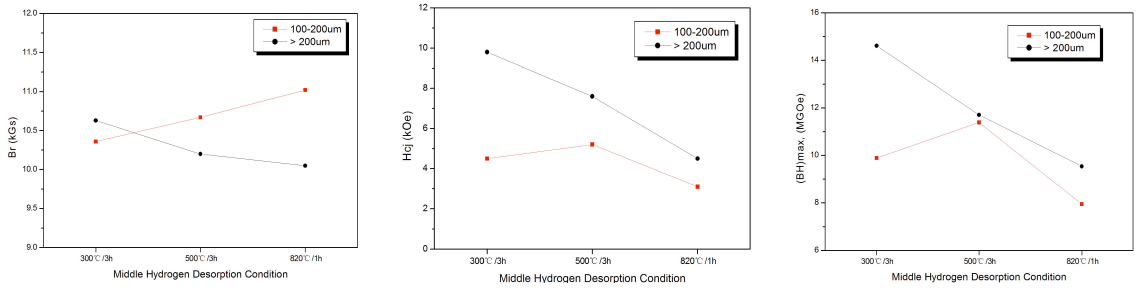

(a) B*r* (b) H*cj* (c) (BH)*max*

Figure 3-9 Magnetic properties of the THD-powders reported for the different intermediate desorption conditions : B*r* (a), H*cj* (b) and $(BH)_{max}$ (c)

Some results can be drawn from these tests :

(a) The twice hydrogen decrepitation cycles can make HD/Degas powders finer.

(b) The twice decrepitation cycles make the squareness of the de-magnetization curves of the HD/Degas powders worse, resulting in a lower $(BH)_{max}$.

The squareness of the de-magnetization curves of the THD-powders with desorption at 300℃ and 820℃ are better than that obtained at 500℃, both with large and medium powders.

(c) The larger powders have higher coercivity than that of the smaller one.

For the larger powders, the magnetic properties of THD-powders drop with the rising of the intermediate desorption temperature.

For the small powders, the B_r of the THD-powders increases with rising of the intermediate desorption temperature, while as Hcj and $(BH)_{max}$ are slightly modified at 500℃, but drop at 820℃.

(d) Intermediate desorption at low temperature, i.e. 300℃, during the twice hydrogen decrepitation treatment processes turns to achieve higher H*cj*.

3.3 Impact of the hydrogen desorption temperature on magnetic properties of the HD/Degas powders

To evaluate the impact of hydrogen desorption temperature on magnetic properties of the HD/Degas powders, the following procedure shown in Fig. 3-10 was applied. The tested parameters are listed in Table 3-3. The magnetic properties of HD-powders and their variation with the hydrogen desorption temperature are shown in Table 3-3, and in Fig. 3-11 respectively.

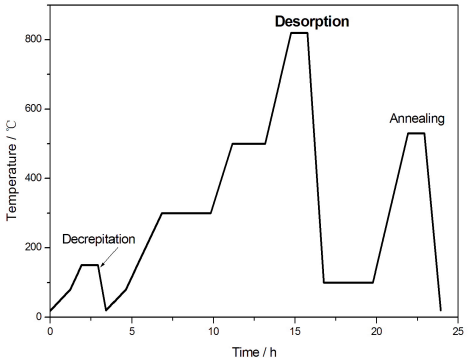

Fig.3-10 Sketch of the process applied for the hydrogen desorption of the HD-powders.

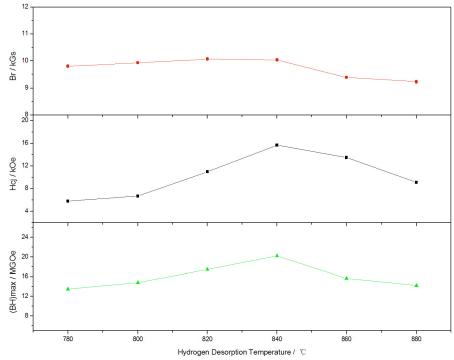

Fig. 3-11 Magnetic properties of the HD-powders versus the hydrogen desorption temperature

Table 3-3 Magnetic Properties of HD Powders treated at different desorption temperatures with the same decrepitation and annealing conditions

Decrepitation*	Desorption	Annealing	Coercivity Hcj / kOe	Remenance Br / kGs	Maximum Energy Product BH_{max} / MGOe
50℃	400℃/2h, 880℃/1h	530℃/1h	9.1	9.23	14.24
50℃	400℃/2h, 860℃/1h	530℃/1h	13.5	9.39	15.65
50℃	400℃/2h, 840℃/1h	530℃/1h	13.9	9.90	17.31
50℃	400℃/2h, 820℃/1h	530℃/1h	11.0	10.07	17.48

50℃	400℃/2h, 800℃/1h	530℃/1h	6.7	9.93	14.8
50℃	400℃/2h, 780℃/1h	530℃/1h	5.8	9.8	13.5

* The hydrogen pressure is about 70kPa during the decrepitation process.

From 780℃ to 840℃, the magnetic properties of the HD powders increase with the desorption temperature, but decrease from 840°C to 880°C. To recover B_r, the optimal hydrogen desorption temperature of the HD-powders is in the range of 820 – 840°C, while for H_{cj}, the optimal temperature is around 840°C. This is related with the slight melting of the Nd-rich phase, which makes the powder particles surface smooth (Fig.3-12a). However, at higher temperatures (above 840℃) the presence of a larger amount of melt leads to crystal growth, resulting in a decrease of coercivity.

The degradation of B_r above 820℃, is correlated to the melting of the Nd-rich phase which leads to reform the powder particles with disorientation grains (Fig. 3-12b).

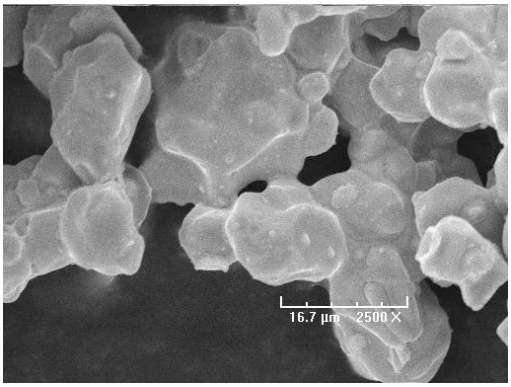

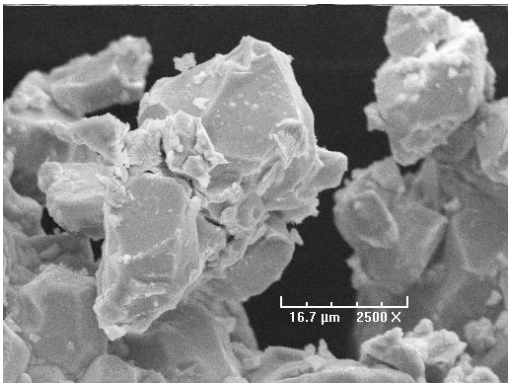

(a) (b)

Fig.3-12 SEM images of the powders desorbed at 840°C (a) and 820°C (b)

3.4 Impact of annealing temperature on the performance of HD powders

The annealing treatment of HD powders is shown in Fig.3-13. After decrepitation, the decrepitated powders were drawn out of the chamber of the furnace, and separated to several parts for the following different desorption and annealing treatments. The decrepitated powders were always contained in a green box full of argon atmosphere. After desorption, the de-gassed powders were directly annealed without taking out of the furnace. Then, the powders were prepared under the form of bonded magnets, according the method described in the part 3.1.

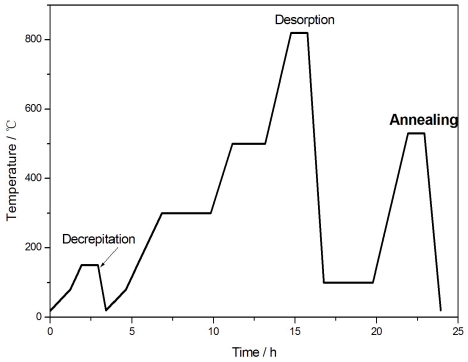

Figure 3-13 Technical process sketch for annealing treatment of the HD-powders

The magnetic performances were measured in terms of bonded magnets. The applied experimental conditions and the results obtained from the magnetic measurements are reported in table 3-4. The hysteretic curves of the HD-powders annealed at 490℃, 530°C, and 600°C respectively are shown in Fig. 3-14. The magnetic properties of the HD-powders as a function of the annealing temperature are reported on Fig. 3-15.

Table 3-4 Magnetic properties of HD-powders treated at different annealing temperatures with the same decrepitation and desorption conditions

Decrepitation*	Desorption	Annealing	Coercivity Hcj / kOe	Remenance Br / kGs	Maximum Energy Product BH_{max} / MGOe
50℃	400℃/1h, 840℃/1h	490℃/1h	7.1	9.86	16.17
50℃	400℃/1h, 840℃/1h	510℃/1h	12.6	9.70	16.87
50℃	400℃/2h, 840℃/1h	530℃/1h	13.9	9.90	17.31
50℃	400℃/2h, 840℃/1h	580℃/1h	11.0	9.81	16.52
50℃	400℃/2h, 840℃/1h	600℃/1h	6.0	9.37	11.9

* The hydrogen pressure is about 70kPa during the decrepitation process.

As observed on Fig 3-14, the annealing temperature plays an important role to modify the magnetic properties of the HD powders. Especially the corcivity H_{cj} increased obviously when the powders are annealed at around 530℃ (Table 3-4, Fig. 3-15). This temperature corresponds to that applied to achieve optimal magnetic properties for the sintered magnets.

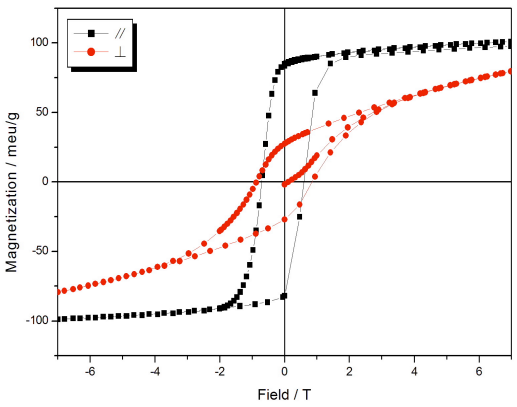

(a) 490℃

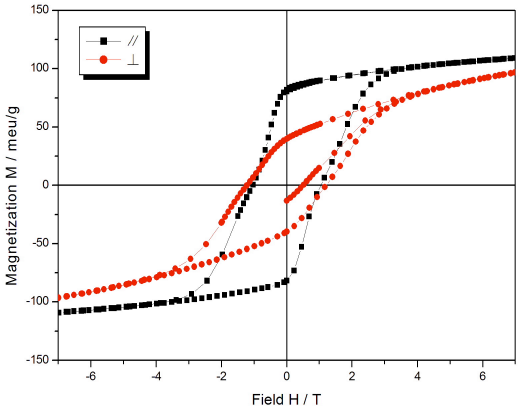

(b) 510°C

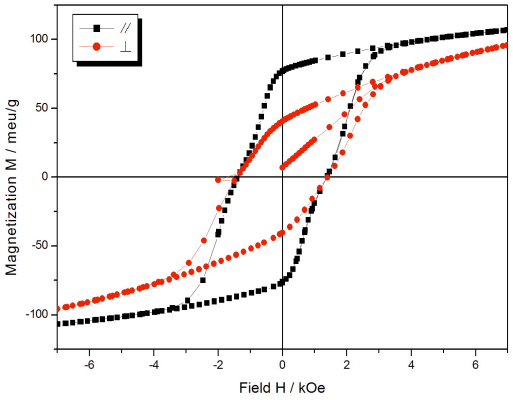

(c) 530°C

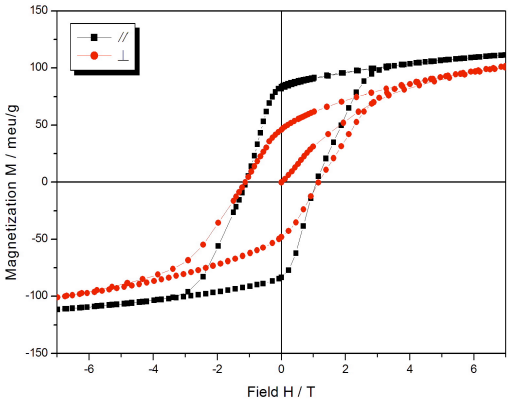

(d) 580°C

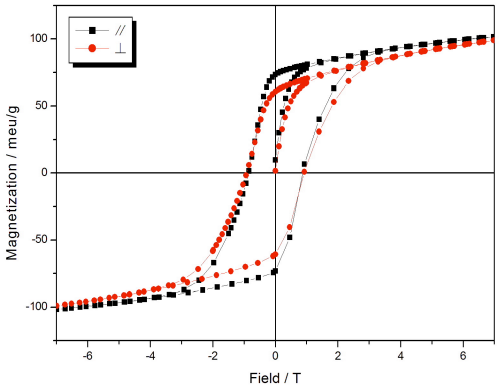

(e) 600°C

Fig. 3-14. Hysteresis curves of the HD-powders annealed at different temperatures

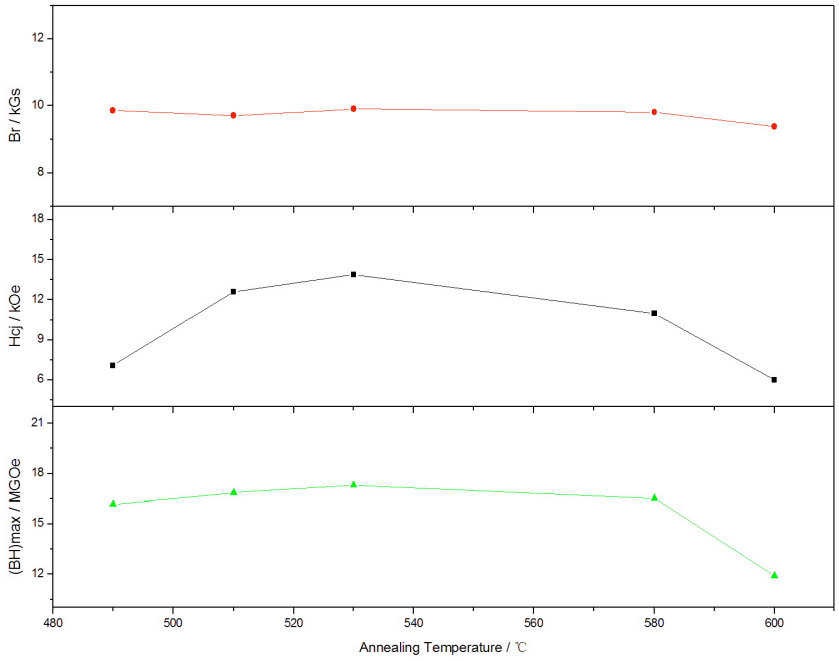

Fig. 3-15 Magnetic properties of HD-powders varying with the annealing temperature

Annealing at higher temperature, such as 600℃, results in a decrease of the anisotropy of the HD-powders as shown in Fig. 3-14c, while annealing at low temperature, such as 490℃, results in a better anisotropy of the HD-powders, but a lower coercivity (Fig. 3-14a).

3.5 Effect of a magnetic field applied during the hydrogen desorption on the magnetic properties of the powders

Yamaguchi *et al.* [YAM1989], [YAM1996] have observed remarkable effects of magnetic field on chemical equilibrium of systems containing ferromagnetic hydrides, such as $LaCo_5H_x$ systems. The applied magnetic field causes chemical equilibrium to shift towards the side that has greater magnetization so that magnetic energy is lowered. De Rango *et al.* [DAR2004] have presented similar results obtained on $NdFe_{10.5}V_{1.5}$ compound : the formation of nitrides is enhanced by applying a strong magnetic field, because $Nd(Fe,V)_{12}$ phase is paramagnetic whereas the nitride to be formed is ferromagnetic at the temperature of nitrogenation. S. Liesert *et al.* [LIE1996] have shown that high magnetic field was effective on $Nd_2Fe_{14}B$ nuclei around Curie temperature during Hydrogen Disproportionation Desorption Recrystallisation (HDDR) process.

In the present part, a high magnetic field has been applied during the hydrogen desorption process, intending to enhance magnetic properties of the powders.

3.5.1 Experimental procedure

Bulk (NdDy)(FeCoNbCu)B sintered magnets were crushed into pieces by hand, and then about 60g of these pieces were charged into the chamber of the furnace and vacuumed to 10^{-3} Pa. The powders were prepared by the following process as shown schematically in Fig 3-16. Hydrogen gas (purity of 99.999 %) was introduced into the chamber up to the pressure of 70 kPa at a temperature of 150°C to decrepit the magnets pieces into powders. These decrepitated powders were then submitted to a desorption process at the temperature of 820°C under magnetic field, in a superconducting magnet. A magnetic field of respectively 0, 1, 3, and 5 Tesla was applied above 450°C during the hydrogen desorption process. The following annealing treatment was then performed at 530°C for 1h.

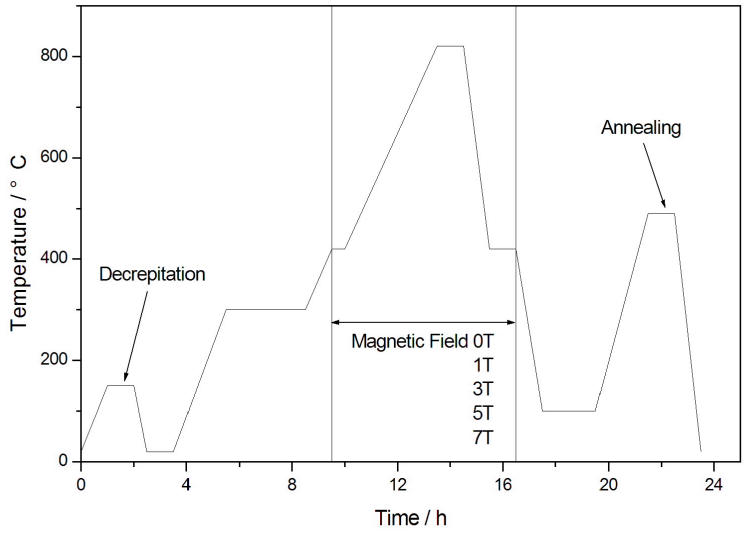

Fig.3-16 Process applied for hydrogen desorption under magnetic field

After that, the powders were sealed inside quartz tubes for thermo-magnetic measurement. We employed the thermo-magnetic measurement to reveal residual hydrogen content in the powders according to the disproportionation reaction between $Nd_2Fe_{14}B$ and hydrogen.

Magnetic properties of the powders were measured by extraction magnetometer on cylinder bonded magnets with 3 mm in diameter and 7 mm in length, polymerized under magnetic field of 5 T. Values of magnetic properties of the powders were corrected to the density of 7.5 10^3 kg/m^3.

3.5.2 Magnetic properties of the powders

Table 3-5 shows the magnetic properties of the HD-powders obtained by hydrogen desorption under magnetic field. Fig. 3-17 shows the variation of the magnetic properties

of the powders versus magnetic field during the desorption process. Fig. 3-18 shows the hysteretic loops of the powders desorbed under magnetic field.

Table 3-5 Magnetic properties of the HD-powders hydrogen desorbed under magnetic field

Decrepitation*	Desorption, Magnetic field	Annealing	Coercivity Hcj / kOe	Remenance Br / kGs	Maximum Energy Product BH_{max} / MGOe
50℃	400℃/2h, 840℃/1h, 0T	530℃/1h	13.9	9.90	17.31
50℃	400℃/2h, 840℃/1h, 1T	530℃/1h	14.0	10.05	17.34
50℃	400℃/2h, 840℃/1h, 3T	530℃/1h	14.3	10.29	21.67
50℃	400℃/2h, 840℃/1h, 5T	530℃/1h	13.5	10.32	17.99

* The hydrogen pressure is about 70kPa during the decrepitation process.

As shown in Table 3-5 and Fig. 3-17, high magnetic field, above 3T, help to increase the B*r*, but has less impact on the H_{cj} of the powders. $(BH)_{max}$ was not modified at 5 T because of the relative lower H_{cj}.

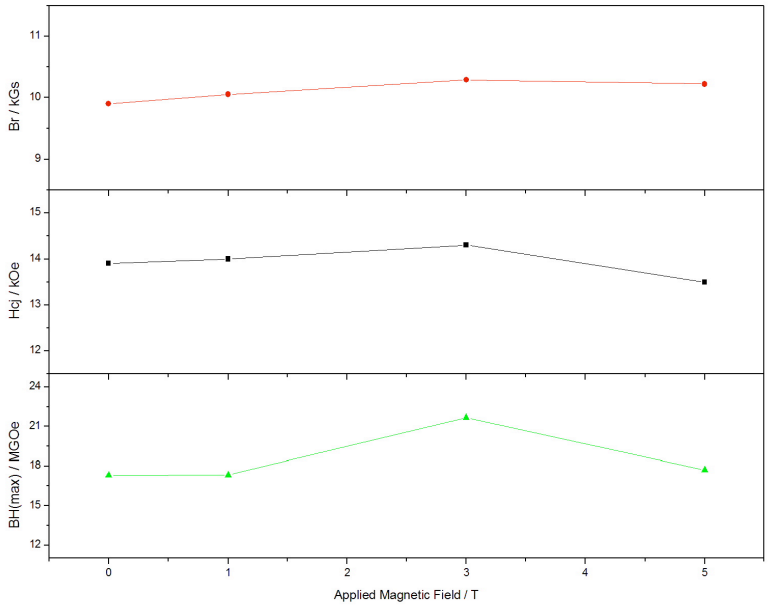

Fig.3-17 Magnetic properties of the powders desorbed under magnetic fields

Enhancement of the magnetic properties of anisotropic $(NdDy)_{15}(FeCoNbCu)_{79}B_6$ powders may comes from two possible mechanisms : one is the macroscopic magnetic effect contributed to a better orientation of the powder particles. The other is a less residual hydrogen content in the powders, as will be discussed in following sections.

3.5.3 Orientation of the powder particles

The ratio of $M_{r//}/M_{r\perp}$ has been employed to evaluate the orientation of powder particles, while $M_{r//}$ and $M_{r\perp}$ represent residual magnetization along and perpendicular to the magnetic direction, respectively. The larger the ratio of $M_{r//}/M_{r\perp}$ is, the better the

anisotropy of the powders is.

Calculated from Fig.3-18, the anisotropy ratio $M_{r//}/M_{r\perp}$ of the HD-powders desorbed under magnetic field was drawn in Fig. 3-19. The ratio of $M_{r//}/M_{r\perp}$ increased upon the magnetic field during the hydrogen desorption process : the increase is of about 175 % from 0 to 5 T.

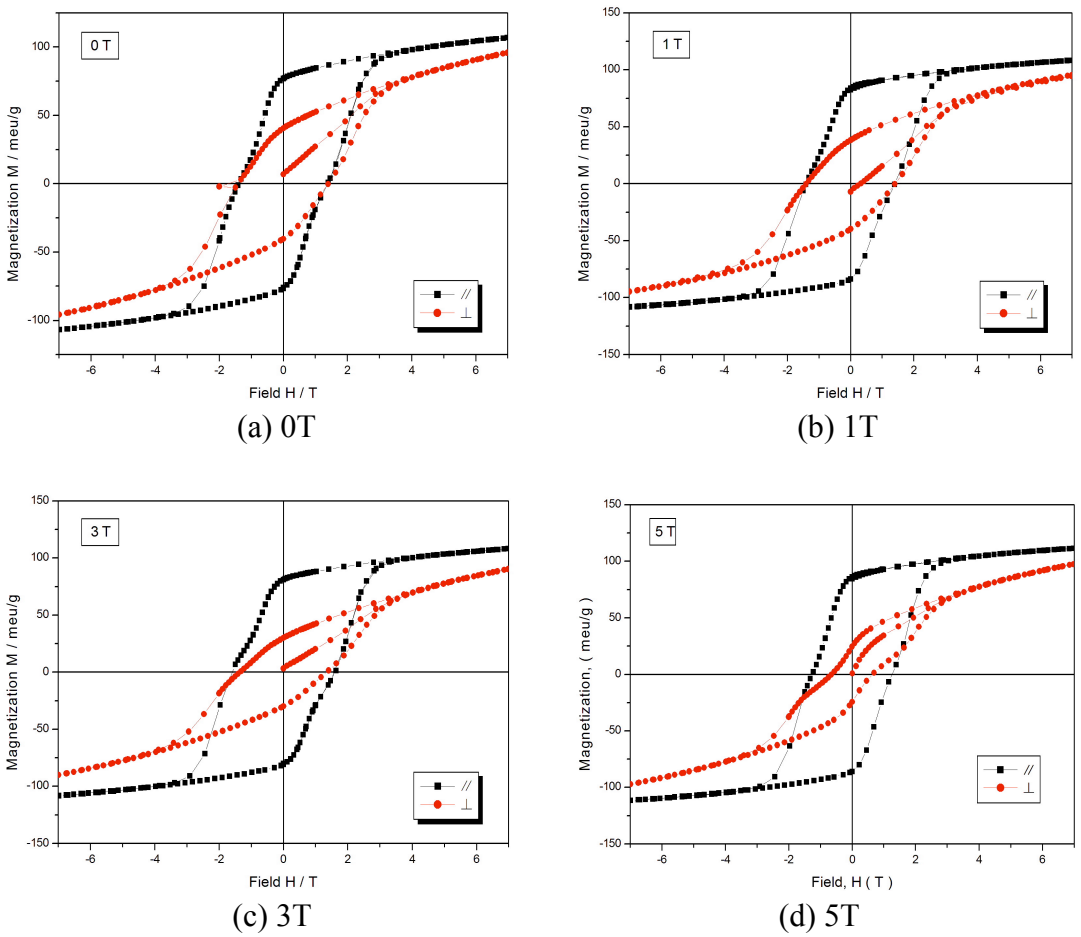

Fig. 3-18 Hysteresis loops of powders desorbed under different magnetic fields.

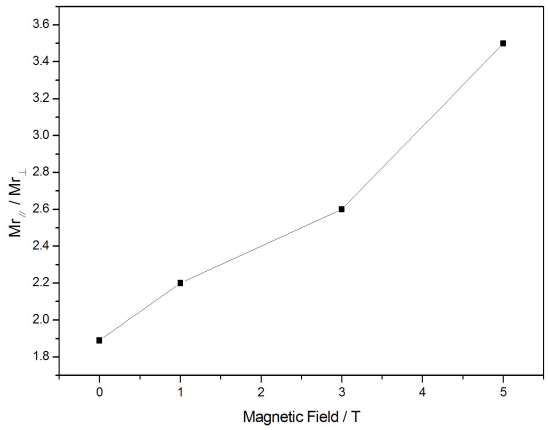

Fig.3-19 Anisotropy ratio $M_{r//}/M_{r\perp}$ of the powders prepared under a magnetic fields ranging from 0 to 5 Tesla

The orientation of particles during hydrogen desorption under magnetic field can be affected by the shape of these particles. P.J. McGuiness *et al.* [MCG1994], [YAR1996] have shown that hydrogen decrepitation of textured Nd-Fe-B sintered magnets happened preferentially along the direction perpendicular to the easy axis of magnets, resulting in flake-like pieces with the thinner direction along the easy axis. Fig. 3-20 shows the flake-like powder particles obtained in this test. This type of powder particles has large de-magnetization field. Then, this de-magnetization field tends to oppose to the applied magnetic field, when the powder particles were orientated under magnetic field during the hydrogen desorption, thus reducing the resulting anisotropy.

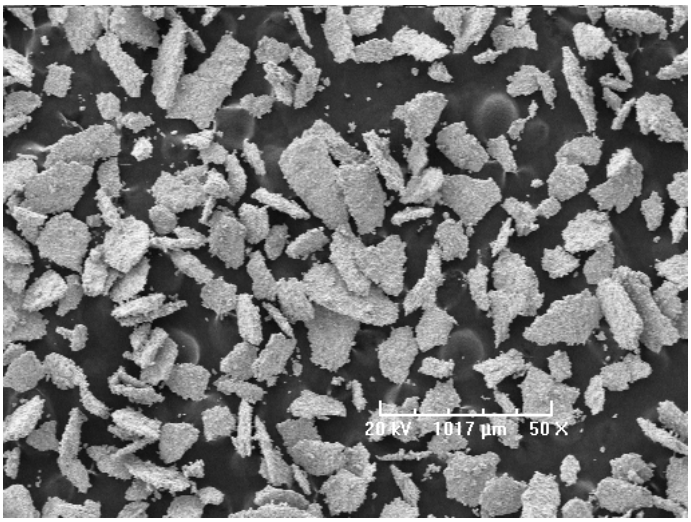

Fig.3-19 Flake-like morphology of the particles of the NdDyFeCoNbCuB HD powders

The enhancement of orientation of the powder particles comes from two aspects. Firstly, along the Hydrogen Decrepitation process, the individual decrepitated particles still hold the texture crystal structure originated from the bulk magnets [FRU1990], [FRU1997], [FRU2004]. Secondly, some of the powders particles are bonded by the liquid Nd-rich phase, which result from hydrogen desorption of hydride Nd-rich phase, and these particles evolved finally to form bigger powder particles during the hydrogen desorption and subsequent cooling process. These *reformed* powder particles keep the texture crystal structure of the original bulk magnets with the help of the magnetic field during the desorption process. This can be explained as following : without magnetic field, although keeping the textured crystal structure inside, the individual powder particles are distributed in random when they are desorbed and subsequent cooling, resulting in less macroscopic orientation of tetragonal phase grains in the *reformed* powder particles. Contrarily, with the help of the magnetic field, the powder particles are rotated along the direction of the applied magnetic field during the hydrogen desorption process, forming the *reformed* powder particles with the textured crystal structure as that of the original bulk magnets.

3.5.4 Thermo-magnetic analysis of the residual hydrogen content

Fig. 3-20 shows thermo-magnetic measurement performed on the powders. In the case of the powders desorbed without magnetic field, a transition occurs at around 600°C on heating, corresponding to the reaction between hydrogen and the tetragonal phase : $(NdDy)_2(FeCo)_{14}B + H_2 \rightarrow (NdDy)H_2 + \alpha\text{-}(FeCo) + FeB_2$ [LIE1998]. There was no obvious step found in the heating curves of the powders desorbed under a magnetic field ranging from 1 to 5 T, which indicates that no reaction occurred between hydrogen and the tetragonal phase. In other words, there should be no or less residual hydrogen remained in the powders. Therefore, it could be concluded that the application of a magnetic field during the hydrogen desorption process was helpful to release hydrogen from the powders.

The hydrogen desorption from the hydride (NdDy)-(FeCoNbCu)-B powders includes two processes upon heating in vacuum : hydrogen atoms are released from tetragonal hydride phase (Equation 1), and from Nd-rich hydride phase (Equation 2).

$$(NdDy)_2(FeCo)_{14}BH_x \rightarrow (NdDy)_2(FeCo)_{14}B + H_2 \quad (1)$$

$$(NdDyFeCoCu)H_{2.36} \rightarrow (NdDyFeCoCu) + H_2 \quad (2)$$

As mentioned above, (NdDyFeCoCu) is the Nd-rich phase of $(NdDy)_{15}(FeCoCu)_{79}B_6$ magnets.

It has been reported that applied magnetic field is expected to cause chemical equilibrium shift towards the side which has greater magnetization in the system including paramagnetic phase [YAM1989], [YAM1996], [DAR2004], [RIV2004]. Although magnetic properties of Nd-rich phase and Nd-rich hydride phase are not very clear until now, we may suppose that applied magnetic field is helpful to make the equation (2) to shift towards the right side, as will be benefit to lower the residual hydrogen contents of the powders. The applied magnetic field may not be helpful to release hydrogen atoms from the tetragonal hydride phase (Equation 1), because the tetragonal hydride has larger magnetization than that of the tetragonal phase [FRU2004].

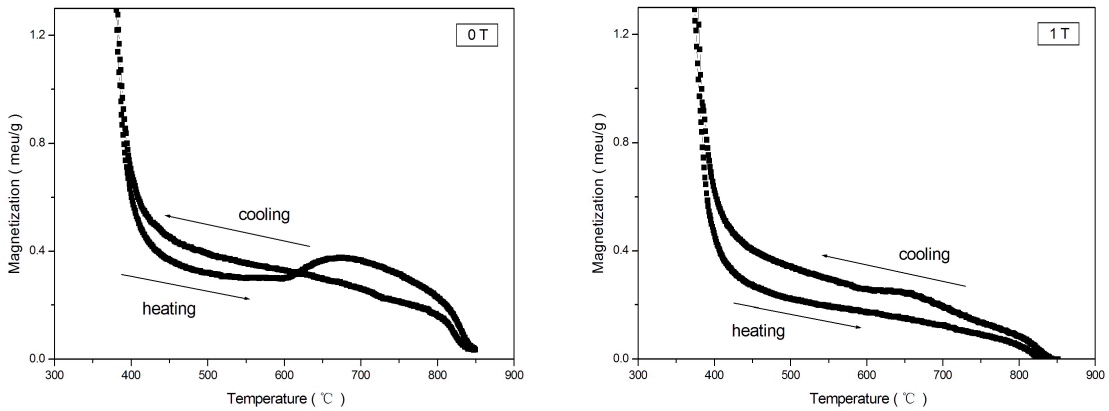

(a) 0 T (b) 1 T

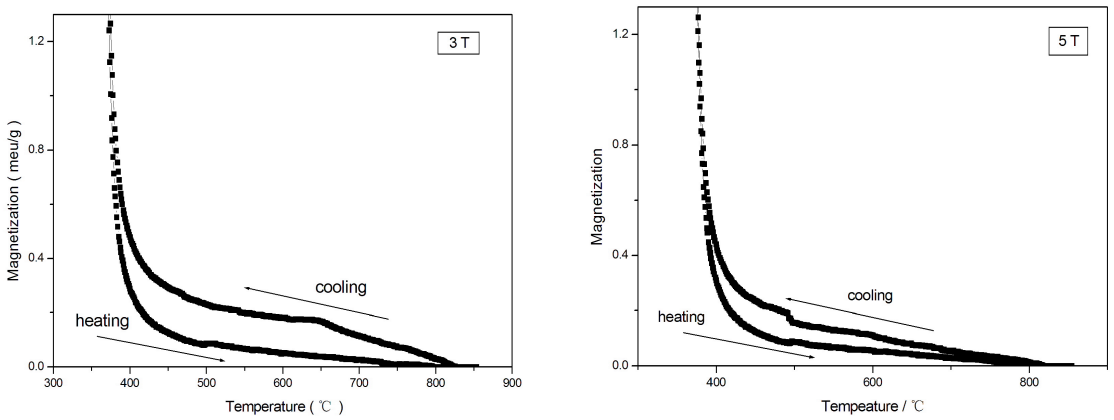

(c) 3 T (d) 5 T

Fig.3-20 Impact of the applied magnetic field on the residual hydrogen contain of the desorbed Nd-Fe-B powders.

3.5.5 Conclusions

Magnetic properties of anisotropic $(NdDy)_{15}(FeCoNbCu)_{79}B_6$ powders prepared by Hydrogen Decrepitation-Desorption-Annealing are enhanced when the powders are hydrogen desorbed in magnetic fields ranging from 1 to 5 T. The anisotropic powders with H_{ci}, B_r and $(BH)_{max}$ of 14.3 kOe (1138 kA/m), 10.29 kGs (1.029 T) and 21.67 MGOe (172.5 kJ/m^3) respectively, were achieved in this test. The enhancement of magnetic performances of the powders desorbed in magnetic field comes from two possible mechanisms : One is the macroscopic magnetic effect aroused from better orientation of the powder particles ; the other is less residual hydrogen content remained in the powders.

3.6 Impact of the bonded magnets preparing conditions on the magnetic properties of the powders

Fig. 3-21 shows the cross section morphology of bonded magnets prepared by the HD powders and ARALDITE® bonder. The surface in the figure is perpendicular to the orientation direction of bonded magnets. The grey part in Fig. 3-21 is the HD-powders, while the white part is ARALDITE® bonder. The shape of the HD powders is irregular, and with many defects around the surface. This is one of the reasons for the low coercivity of the powders, which is a microstructure sensitive factor.

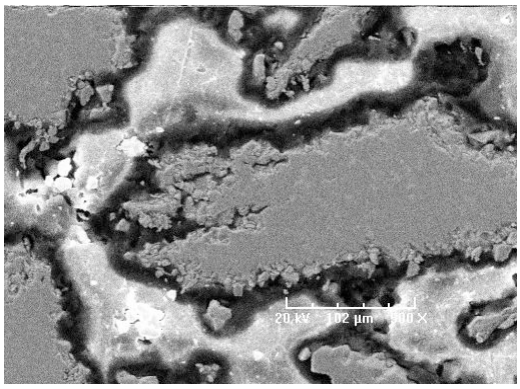

Fig. 3-21 Morphology SEM of the bonded magnets prepared by HD-powders

Some factors of the bonded magnets preparation procedure can affect the measured results of the HD-powders, such as the powders or bonder content, applied magnetic field, polymerization time, powders shape and size, etc… Among these factors, the bonder content and the applied magnetic field during the bonded magnets preparing process are the most sensitive parameters.

3.6.1 Impact of bonder content of Bonded Magnets on magnetic properties

To evaluate the impact of bonded magnets preparing method on the magnetic properties of the HD powders, a test on different bonder contents has been undertaken.

Fig. 3-22 shows the variation of the magnetic properties of the HD-powders with the powder mass ratio (mass of powder divided by the sum of powder and bonder mass). The Br slightly increases with the mass ratio, up to a value of about 0.75, then drops sharply for a mass ratio upper 0.8. This results from the fact that for low bonder content, the powder particles impede the rotation of each other during the orientation procedure under the magnetic field, leading to some extent of disorientation of the particles.

The H_{cj} increased continuously with the bonder content up to 0.85.

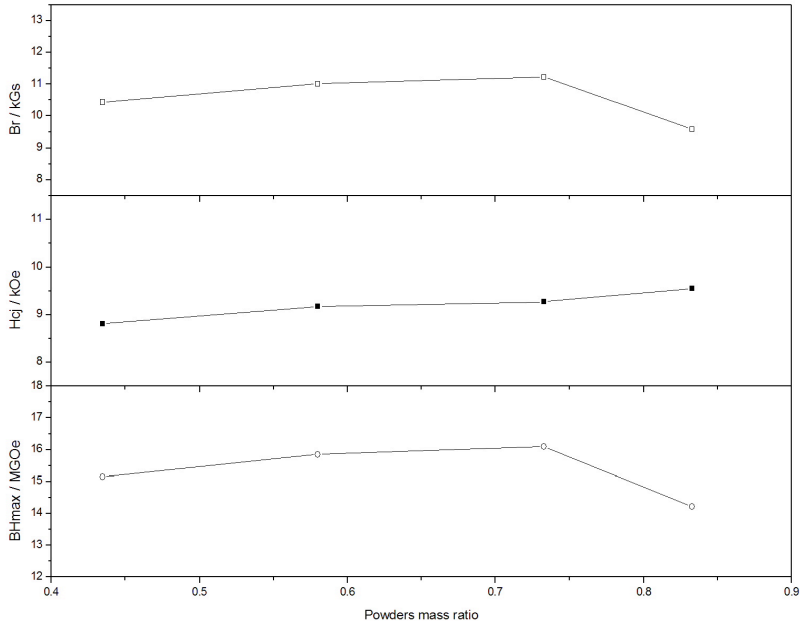

Fig. 3-22 Magnetic properties of HD-powders prepared with different bonder mass ratio.

3.6.2 The magnetic field for aligning HD powders

Magnetic field is applied during the bonder polymerization stage of the preparation of the bonded magnets. Fig. 3-23 shows the magnetic properties versus the applied magnetic field during the bonded magnets preparation procedure. B*r* is enhanced linearly upon the increase of the applied magnetic field, while H_{cj} increases only for a 7 Tesla magnetic.

With the increase of the magnetic field applied, the orientation of the powder particles is improved during the polymerization. The better orientation was then benefit to the enhancement of Br, and the very strong orientation benefit to the H_{cj} of the powders. Then, $(BH)_{max}$ is significantly improved by the application of a high magnetic field of about 7 Tesla.

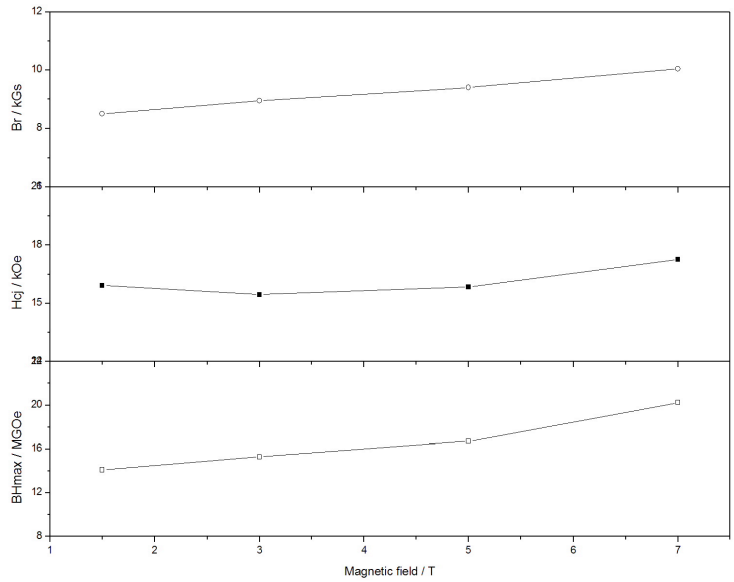

Fig. 3-23 Magnetic properties of the HD-powders vary with different applied magnetic fields during the bonded magnets preparation procedure.

3.7 Discussion on the recovery of intrinsic coercitivity of HD-Powders from bulk sintered magnets

The coercive forces that make the sintered Nd-Fe-B permanent magnets resistant to depolarization are correlated to the potential nucleation of reverse domains **[ZHO1999]**. If the tetragonal phase grains in Nd-Fe-B materials are textured, i.e. the crystallites being essentially oriented along a common direction, the resulting magnetization is multiplied by a factor 2 as compare to the isotropic situation **[FRU1997]**.

The coercivity is closely linked to the magnetic domains and domain walls **[SKO2004]**. Coercivity is due to energy barriers caused by magnetic anisotropy. However, even in optimized permanent magnets the coercivity is only 20-40 % of the anisotropy field. The main reason is imperfections, such as metallurgical in-homogeneities, grain boundaries, and surface irregularities. Imperfections tend to yield a local reduction of the anisotropy K_1 and a reduced coercivity. Combination of the thermal annealing and chemical modification of particle surface using the DyF_3 salt was found to be an effective processing technique for preparing a high-coercivity powder from the crushed sintered Nd-Fe-B magnets **[JAN2004], [KWO2004]**.

As in the case of sintered Nd-Fe-B magnetic materials, L.J. Eshelman et al. **[ESH1988]** sugested that the exposed layer of crystallites of the Nd-Fe-B materials is magnetically soft owing to oxidation of the $Nd_{70}Fe_{30}$ eutectic phase. While in rapidly

solidified Nd-Fe-B material the exposed layer constitutes only a small fraction of the total volume, in the sintered materials this layer would constitute a large majority, if not all, of an individual grain.

Some grains of the HD-powders in this test present low coercivity. Especially, grains located in the surface regions of the powders, reverse their magnetization in a magnetic field significantly smaller than the coercivity of the bulk magnet. These grains create stray fields H_s on adjacent grains, and trespassing of the domain walls across the grain boundary occurs when effective field acting on the adjacent grains reaches a critical value H_n:

$$H_n = H_{cj} + H_s \qquad (3\text{-}1)$$

For two grains with opposite flat poles facing each other, H_s may be equated with M_s, then :

$$H_n = H_{cj} + M_s \qquad (3\text{-}2)$$

In sintered Nd-Fe-B magnets, it is suggested that the grain boundary region contains bcc micro-crystallites and is a soft magnet with a Curie temperature in the 400-450K range. Thus, the grain boundary region of the Nd-Fe-B sintered magnets may be considered as a planar substance with an appreciably smaller anisotropy than the matrix. Thus, it may be proposed that the domain walls are trapped at the boundary between the bcc phase and matrix and that the magnetization reversal in the Nd-Fe-B sintered magnets takes place as a collective trespassing of the domain walls across the grain boundaries. The process proceeds along the direction of magnetization with the aid of the stray fields. Contrarily, in the Nd-Fe-B magnets the boundary bcc phase is always magnetically softer than the matrix phase because of its negligible anisotropy and low T_c. It appears that the existence of the bcc boundary phase in the grain boundary region of the sintered Nd-Fe-B magnets is an essential factor in the magnetic hardening mechanism in this type of magnet. It has been suggested that magnetic hardening in the Nd-Fe-B sintered magnets is due to the existence of the bcc boundary phase which acts as a planar pinning substance **[HIR1986]**.

It is suggested that in the sintered Nd-Fe-B magnet, Hci can be denoted as **[HIR1986]**:

$$H_{cj} = c\ \frac{2K_1}{M_S}\frac{W}{\delta} \qquad (3\text{-}3)$$

Where K_1 is the anisotropy constant, M_s is the saturation magnetization, W and δ are the thickness of the planar substance and the domain wall width, respectively.

When considered the shape and the size of the particles of powders, we should also pay attention to the de-magnetization field. Then the effect field will describe as:

$$H_n = H_{cj} + M_s + \alpha H_d \qquad (3\text{-}4)$$

Herein, α is a coefficient, which is correlatted closely with the condition and size of powders.

Hydrogen absorbed in Nd-Fe-B type magnets can substantially reduces their H_A,

result in low coercivity of the hydrogen contained powders **[FRU2004]**. So one more coefficient β should be considered as following:

$$H_n = \beta H_{cj} + M_s + \alpha H_d \qquad (3\text{-}5)$$

Herein, β is a coefficient less than 1, and is connected with low H_A due to residual hydrogen content in the HD-powders.

Then, the factual coercivity force for HD-powders can be described as equation 3-5.

CONCLUSION

Anisotropic Nd-Fe-B powders have been achieved by applying HD process to sintered Nd-Fe-B magnets. After optimization of the successive steps of the process, anisotropic powders with good properties have been achieved : B*r* = 10.29 kGs (1.029 T), H_{cj} = 14.3 kOe (1138 kA/m), $(BH)_{max}$ = 21.67 MGOe (172.5 kJ/m^3). It corresponds respectively to 93%, 46% and 74% of the magnetic properties of the precursor sintered (NdDy)-(FeCoNbCu)-B permanent magnets.

The intrinsic coercivity of these anisotropic Nd-Fe-B powders is mostly dependent on the decrepitation temperature, desorption temperature, and annealing temperature. The preparation conditions of the bonded magnets, such as bonder content and polymerization magnetic field, also affect the measured magnetic properties. Coercive force of HD-powders is varied with the size of the HD-powders: a larger particles size leads to higher coercive force.

Twice hydrogen decrepitation cycles is efficient to make HD-powder finer, but deteriorate the magnetic properties. The application of a high magnetic field during the hydrogen desorption process reduces the residual hydrogen contain in HD-powders, then allowing to recover higher magnetic properties of HD-powders.

The partial recovery of the initial coercivity has been attributed to the poor morphology of the shape of the powders, and less Nd-rich phase around outer surfaces of the powders.

REFERENCE

[ASA2001] K. Asabe, A. Saguchi, W. Takahashi, R.O. Suzuki, K. Ono. Recycling of Rare Earth Magnet Scraps: Part I Carbon Removal by High Temperature Oxidation. Mater. Trans. 42 (12) (2001): 2487-2491

[BOO1995] D. Book, I.R. Harris. Hydrogen absorption/desorption and HDDR studies on $Nd_{16}Fe_{76}B_8$ and $Nd_{11.8}Fe_{82.3}B_{5.9}$. Journal of Alloys and Compounds 221 (1995): 187-192

[BRA1993] J. H. V. J. Brabers, G. F. Zhou, F. R. de Boer, K. H. J. Buschow. Magnetic properties of $ThMn_{12}$-type $RCo_{12-x}V_x$ compounds with R = Y, Gd, Tb, Dy, Ho, Er. Journal of Magnetism and Magnetic Materials, 118(1993): 339-346

[BUS1988] K.H.J. Buschow. Structure and properties of some novel ternary Fe-rich rare-earth intermetallics. J. Appl. Phys. 63(1988): 3130-3135

[BUR2000] V.S.J. Burns, A.J. Williams, I.R. Harris. Production of anisotropic powder from hot deformed RE-Fe-B-Cu Alloys. Proceedings of the 16th International Workshop on Rare-Earth Magnets and their Applications, Sendai, Japan, (2000): 355-364

[CAD1986] J.M. Cadogan, J.M.D. Coey. Hydrogen absorption and desorption in $Nd_2Fe_{14}B$. Appl. Phys. Lett. 48(6) (1986): 442-444

[COE1996] J.M.D Coey. Interstitial intermetallics, *J. Magn. Magn. Mater.* 159(1996): 80-89

[CRO1984] J.J. Croat, J.F. Herbst, R.W. Lee, F.E. Pinkerton, Pr-Fe and Nd-Fe-based materials: A new class of high-performance permanent magnets. J. Appl. Phys. 55 (1984): 2078-2081

[CRO1988] J.J. Croat. Neodymium-iron-boron permanent magnets prepared by rapid solidification. J. Mater. Eng. 10 (1988): 7-13

[CRO1997] J.J. Croat. Current status and future outlook for bonded neodymium permanent magnets. J. Appl. Phys. 81(8), (1997): 4804-4809

[DAL1987] P. Dalmas de Réotier, D. Fruchart, L. Pontonnier, F. Vaillant, P. Wolfers, A. Yaouanc, J.M.D. Coey, R. Fruchart, P. l'Héritier. Structural and magnetic properties of $RE_2Fe_{14}BH(D)_x$ RE≡Y, Ce, Er. J. Less-Common Met. 129 (1987) 133-144.

[DAR2004] P. De Rango, I. Popa, S. Rivoirard, D. Fruchart. Nitrogenation of $Nd(Fe,V)_{12}$ compounds under magnetic field, Proceeding of the 18th Int. Workshop on High Performance Magnets and their Applications (HPMA04) (Annecy, France) (September 2004): 257-260.

[DID2003] V.A. Didus, S.B. Rybalka, D. Fruchart, V.A. Goltsov. Influence of hydrogen pressure on the kinetics of hydrogen-induced diffusive phase transformations in the $Nd_2Fe_{14}B$ alloy. Journal of Alloys and Compounds 356–357 (2003): 386–389

[DOS1991] M. Doser, FL W. Ribitch, J. J. Croat, V. Panchanathan. Bonded anisotropic Nd-Fe-B magnets from rapidly solidified powders. J. Appl. Phys. 69 (8) (1991): 5835-5837

[DOS1991B] M. Doser, V. Panchanathan, R.K. Mishra, Pulverizing anisotropic rapidly

solidified Nd-Fe-B materials for bonded magnets. J. Appl. Phys. 70 (10-11) (1991): 6603-6605

[ESH1988] L.J. Eshelman, K.A. Young, V. Panchanathan, J.J. Croat. Properties of Nd-Fe-B anisotropic powder prepared from rapidly solidified materials. J. Appl. Phys. 64(10), (1988): 5293-5295

[FAS1996] Rob H.J. Fastenau, Evert J. van Loenen. Applications of rare earth permanent magnets. Journal of Magnetism and Magnetic Materials 157/158 (1996): 1-6

[FID1995] J. Fidler, J. Bernardi, T. Schrefl. Permanent magnets – new microstructural aspects. Scripta Metallurgica et Materialia, Vol. 33 (1995): 1781-1791

[FRU1984] D. Fruchart, P. Wolfers, P. Vulliet, A. Yaouanc, R. Fruchart, P. L'Héritier, in: I.V. Mitchell (Ed.), Nd–Fe Permanent Magnets-Their Present and Future Applications, C.E.C. Bruxelles, 1984.

[FRU1990] D. Fruchart, S.Miraglia, R. Perrier de la Bathie, R. Fruchart, P. Mollard. Patent EP 90 06-206

[FRU1991] D. Fruchart, S.Miraglia. Hydrogenated hard magnetic alloys from fundamental to applications. J. Appl. Phys. 69 (1991): 5578-5583

[FRU1992] D. Fruchart, S. Miraglia, S. Obbade, R. Verhoef, and P. Wolfers, Physica B 180 & 181 (1992): 5878-5882

[FRU1997] D. Fruchart, M. Bacmann, P. de Rango, O. Isnard, S. Liesert, S. Miraglia, S. Obbade, J.-L. Soubeyroux, E. Tomey, P. Wolfers. Hydrogen in hard magnetic materials. Journal of Alloys and Compounds 253-254 (1997): 121-127

[FRU2003] D. Fruchart, R. Perrier De La Bâthie, S. Rivoirard, P. De Rango. Method for preparing a magnetic material by forging and magnetic material in powder form. United States Patent 6592682 (2003)

[FRU2004] D. Fruchart, S. Miraglia, P. de Rango, P. Wolfers. Hydrogen location in hard magnet materials: scheme, fundamental aspects, processes. Journal of Alloys and Compounds 383 (2004): 17–22

[GOL1999] V.A. Goltsov, S.B. Rybalka, A.F. Volkov. Kinetics of the hydrogen-induced diffusive phase transformation in Nd-Fe-B industrial alloy. International Journal of Hydrogen Energy, Vol.24 (1999): 913-917

[GOO1986] E. Goo, G. Thomas, R. Ramesh, M. Okada, M. Homma, K.M. Krishnan. Microstructure of Fe-didymium-B magnets. J. Magn. Magn. Mater. 54-57(1986): 563-566

[HAN1996] A. Handstein, J. Wecker, K. Schnitzke, D. Hinz, L. Schultz. Mechanically alloyed anisotropic Nd-Fe-B powder. Journal of Magnetism and Magnetic Materials 157/158 (1996):15-16

[HAR1985] I.R. Harris, C. Noble, T. Bailey. Hydrogen decrepitation of an $Nd_{15}Fe_{77}B_8$ magnetic alloy. Jouranl of the less-common Metals, 106(1) (1985): L1-L4.

[HAR1987] I.R. Harris, P.J. McGuiness, D.G.R. Jones, J.S. Abell. Absorption/Desorption Studies (HADS) on $Nd_{16}Fe_{76}B_8$ and $Nd_2Fe_{14}B$. Phys.Scr. T19B (1987): 435-440

[HIN1994] D. Hinz, A. Handstein, I.R. Harris. Microstructure and magnetic properties of anisotropic Nd-Fe-B powders from hot rolled ingots by HD process. IEEE Transactions on Magnetics 30(1994): 601-603

[HON2004] Y. Honkura. HDDR magnets and their potential use for automotive applications. 18th International workshop on high performance magnets and their applications, (Annecy, France) (2004): 559-565

[HOR2004] T. Horikawa, M. Itoh, S. Suzuki, K. Machida. Magnetic properties of the Nd–Fe–B sintered magnet powders recovered by Yb metal vapor sorption. Journal of Magnetism and Magnetic Materials 271 (2004): 369-380

[HOR2006] T. Horikawa, K. Miura, M. Itoh, K. Machida. Effective recycling for Nd-Fe-B sintered magnet scraps. Journal of Alloys and Compounds, 408-412 (2006): 1386-1390

[ISN1994] O. Isnard, D. Fruchart. Magnetism in Fe-based intermetallics: relationships between local environments and local magnetic moments. Journal of Alloys and Compounds, 205(1994): 1-15

[ISN1995] O. Isnarda, W. B. Yelon, S. Miraglia, D. Fruchart. Neutron-diffraction study of the insertion scheme of hydrogen in $Nd_2Fe_{14}B$. J. Appl. Phys. 78 (3) (1995): 1892-1898

[JAN2004] T. S. Jang, D. H. Lee, A. S. Kim, S. Namgung, H. W. Kwon, D. H. Hwang. Recovery of high coercivity of the powders obtained by crushing Nd-Fe-B sintered magnet scraps. Physica status solidi(a), 201(8), (2004): 1794-1797

[JIA2003] J.R. Jia, W.J. Qiang, C.H. You. Preparation of anisotropic Nd-Fe-B powders by crushing sintered magnet at high temperatures (I). Journal of University of Science and Technology Beijing Vol.25 (2003): 46-49 (*in chinese*)

[KIA1985] A. Kiabvasg, I.R. Harris. Hydrogen decrepitation as a method of powder preparation of a 2:17-type, Sm(Co,Cu,Fe,Zr)8.92 magnetic alloy. Journal of Materials Science, 20(2) (1985): 682-688

[KIM2004] A.S. Kim, D.H. Kim, S. Namkung, T.S. Jang, D.H. Lee, H.W. Kwon, D.H. Hwang. Development of high coercive powder from the Nd-Fe-B sintered magnet scrap. IEEE Transactions on Magnetics, Volume 40(4), (2004): 2877-2879

[KNO1989] K.G. Knock, E. Bischoff, E. Th. Henig, J. Fidler. Analytical TEM study of cast Nd80Fe15B5 alloys. Materials Letters 8(1989): 301-304

[KWO2004] H.W. Kwon, D.H. Hwang, I.C. Jeong, A.S. Kim, D.H. Kim, S. Namkung, T.S. Jang, D.H. Lee. Coercivity enhancement in Nd-Fe-B powder obtained from crushed sintered magnets, *HPMA'04, 18th International Workshop on High Performance Magnets and their Applications*, Annecy, France, 2004

[KWO2006] H.W. Kwon, I.C. Jeong, A.S. Kim, D.H. Kim, S. Namkung, T.S. Jang, D.H.Lee. Restoration of coercivity in crushed Nd-Fe-B magnetic powder. J. Magn. Magn. Mater. 304 (2006): e219-e221

[LHE1984] P. l'Héretier, P. Chaudouét, R. Madar, A. Rouault, J. Sénateur, R. Fruchart. A new serie of ferromagnetic metallic hydrides of $Nd_2Fe_{14}BH_x$-type ($0<x<5$). C.R. Acad. Sci., 299 II (13) (1984): 849-852. (*in French*)

[LIE1996] S. Liesert, P. de Rango, J.L. Soubeyroux, D. Fruchart, R. Perrier de la Bâthie. Anisotropic and coercive HDDR Nd-Fe-B powders prepared under magnetic field. J. Magn. Magn. Mat. 157(1996): 57-58

[LIE1997] S. Liesert, D. Fruchart, P. de Rango, S. Rivoirard, J.L. Soubeyroux, R. Perrier de la Bathier. HDDR process of Nd-Fe-B with an excess of intergranular Nd-rich phase under magnetic field. Journal of alloys and compounds 262-3(1997): 366-371

[LIE1998] S. Liesert, PhD these of UJF, 1998.

[LIS2000] P. Liszkowski, K. Turek, H. Figiel. The influence of decrepitation on the diffusion kinetics of hydrogen in Nd–Fe–B. Journal of Alloys and Compounds 307 (2000): 297–303

[LUOY2007] Y. LUO. The development and difficulties of bonded magnets industry. Journal of Magnetic Materials and Devices. Vol.38(5) (2007): 1-7 (*in Chinese*)

[LOT2003] M.V. Lototsky, V.A. Yartys, V.S. Marinin, N.M. Lototsky. Modelling of phase equilibria in metal–hydrogen systems. Journal of Alloys and Compounds 356-357 (2003): 27-31

[MA2002] B.M. Ma, J.W. Herchenroeder, B.Smith, M. Suda, D.N. Brown, Z. Chen. Recent development in bonded NdFeB magnets. Journal of magnetism and magnetic materials, Vol.239, No.1-3 (2002): 418-423

[MAC2003] K. Machida, M. Masuda, S. Suzuki, M. Itoh, T. Horikawa. Effective recovery of Nd-Fe-B sintered magnet scrap powders as isotropic bonded magnets. Chemistry Letters Vol. 32(7) (2003): 628-629

[MAC2003-2] K. Machida, M. Masuda, M. Itoh, T. Horikawa. Effective recovery of Nd-Fe-B sintered magnet scrap powders as microwave absorbing materials. Chemistry Letters, Vol. 32(7) (2003): 658-659

[MCG1986] P.J. McGuiness, I.R. Harris, E. Rozendaal, J. Ormerod, M. Ward. The production of a Nd-Fe-B permanent magnet by a hydrogen decrepitation/attritor milling route. J. Mater. Sci. 21(1986): 4107-4110

[MCG1988] P.J. McGuiness, I.R. Harris. The use of the hydrogen in the production and characterization of NdFeB magnets. J. Appl. Phys. 64(10) (1988): 5308-5310

[MCG1989] P.J. McGuiness, E. Devlin, I.R. Harris, E. Rozendaal, J. Ormerod. A study of Nd-Fe-B magnets produced using a combination of hydrogen decrepitation and jet milling. Journal of Materials Science Vol.24(7) (1989): 2541-2548

[MCG1990] P.J. McGuiness, A. Ahmed, D.G.R. Jones, I.R. Harris, S. Burns, E. Rozendaal. The hydrogen decrepitation behavior of alloys and magnets based on $Nd_{16}Fe_{76}B_8$. J. Appl. Phys. 67(9) (1990): 4626-4628

[MCG1990B] P.J. McGuiness, X.J. Zhang, X.J. Yin, I.R. Harris, Hydrogenation, disproportionation and desorption (HDD): An effective processing route for Nd-Fe-B type magnets. J. Less-Common Met., 158 (1990) 379-387.

[MCG1990C] P.J. McGuiness, X.J. Zhang, H. Forsyth, I.R. Harris, Disproportionation in $Nd_{16}Fe_{76}B_8$-type hydrides. J. Less-Common Met., 162 (1990) 359-365

[MCG1994] P.J. McGuiness, L. Fitzpatrick, V.A. Yartys, LR. Harris, Anisotropic hydrogen decrepitation and corrosion behaviour in NdFeB magnets, J. Alloys

and Comp. 206 (1994): L7-L11

[MIU2006] K. Miura, M. Masuda, M. Itoh, T. Horikawa, K. Machida. Microwave absorption properties of the nano-composite powders recovered from Nd-Fe-B bonded magnet scraps. Journal of Alloys and Compounds 408-412 (2006): 1391-1395

[MOO1988] I.S. Moosa, J. Nutting. Hydrogen decrepitation of a permanent magnet Nd-Fe-B alloy. Journal of the Less Common Metals. Vol.144(2) (1988): 221-225

[NAK1991] R. Nakayama, T. Takeshita, M. Itakura, N. Kuwano, K. Oki. Magnetic properties and microstructures of the Nd-Fe-B magnet powder produced by hydrogen treatment. J. Appl. Phys. 70(1991): 3770-3774

[NAK1993] R. Nakayama, T. Takeshita. Nd-Fe-B anisotropic magnet powders produced by the HDDR process. Journal of alloys and compounds, 193(1993): 259-261

[NAM2004] S. Namkung, A.S. Kim, D.H. Kim, T.S. Jang, D.H. Lee, H.W. Kwon, D.H. Hwang. Coercivity of anisotropic magnet powder obtained from the Nd-Fe-B sintered magnet scrap, *HPMA'04, 18th International Workshop on High Performance Magnets and their Applications*, Annecy, France (2004): 108-112

[NOZ1988] Y. Nozawa, K.Iwasaki, S. Tanigawa, M. ToKunaga, H. Harada. Nd-Fe-B die-upset and anisotropic bonded magnets. J. Appl. Phys. 64(10) (1988): 5285-5289

[OHA1988] K. Ohashi, Y. Tawara, R. Osugi, J. Sakurai, Y. Komura. Identification of the intermetallic compound consisting of Sm, Ti, Fe.Journal of the Less Common Metals, 139(1988): L1-L5

[POL1986] R.J. Pollard, H. Oesterreicher. Novel recording media: $Fe_{14}R_2B$ particles. IEEE Trans. Magn. MAG22(1986): 735-737

[RAM1987] R. Ramesh, J. K. Chen, G. Thomas. On the grain-boundary phase in iron rare-earth boron magnets. J. Appl. Phys. 61(1987): 2993-2998

[RIV2000] S. Rivoirard, J.G. Noudem, P. de Rango, D.Fruchart, S. Liesert, J.L. Soubeyroux. Anisotropic and coercive Nd-Fe-B powder for bonded magnets. *Proceedings of the 16th Int. Workshop on Rare-Earth Magnets and Their Applications* (Sendai Japan) (2000): 347-350

[RIV2004] S. Rivoirard, D. Givord, V.M.T.S. Barthem, E. Beaugnon, P.E.V. De Miranda. Preparation of NdFeB anisotropic alloys by ribbon crystallization under high magnetic field, *Proceeding of the 18th Int. Workshop on High Performance Magnets and their Applications (HPMA04)*, (Annecy, France) (September 2004): 250-256.

[RUN1984] S. Rundqvist, R. Tellgren, Y. Andersson, Hydrogen and deuterium in transition metal-p element compounds: Crystal chemical aspects of interstitial solid solubility and hydride phase formation, J. Less-Comm. Met. 101 (1984) :145-168.

[RUP1988] B. Rupp, A. Resnik, D. Shaltiel, P. Rogl. Phase relations and hydrogen absorption of neodymium-iron-(boron) alloys. L Mater. Sci., 23 (1988): 2133-2141

[SAG1984] M. Sagawa, S.Fujimura, N. Togawa, H. Yamamoto, Y. Matsuura, New material for permanent magnets on a base of Nd and Fe. J. Appl. Phys. 55, (1984) :2083-20

[SAG2006] A. Saguchi, K. Asabe, T. Fukuda, W. Takahashi, R.O. Suzuki. Recycling of rare earth magnet scraps: Carbon and oxygen removal from Nd magnet scraps. Journal of Alloys and Compounds, 408-412(2006): 1377-1381

[SHI2004] Y. Shinba, K. Ishikawa, K. Hiraga, T.J. Konno, M. Sagawa. TEM observations on the Nd-rich phase and grain boundary structure of Nd-Fe-B sintered magnets. *HPMA'04, 18th International Workshop on High Performance Magnets and their Applications*, Annecy, France (2004): 419-428

[SHI2005] Y. Shinba, K. Ishikawa, K. Hiraga, T.J. Konno, M. Sagawa. Transmission electron microscopy study on Nd-rich phase and grain boundary structure of Nd–Fe–B sintered magnets. J. Appl. Phys. 97, 053504(2005)

[SKO1993] R. Skomski, J.M.D. Coey. Nitrogen diffusion in Sm_2Fe_{17} and local elastic and magnetic properties. J. Appl. Phys.73 (11) (1993): 7602-7611

[STA1986] H.H. Stadelmaier, N.C. Liu. Effect of mechanical comminution on the intrinsic coercivity of Fe-Nd-B sintered magnets. Materials Letters Vol.4 (1986): 304-306

[SUG2004] S. Sugimoto, D. Book, Recent developments in the HDDR processing of Nd–Fe–B magnets, Metal Mater. Proc. 15 (1–2) (2004): 149-166

[SUZ2001] R.O. Suzuki, A. Saguchi, W. Takahashi, R.O. Suzuki, K. Ono, Recycling of Rare Earth Magnet Scraps: Part II Oxygen Removal by Calcium. Mater. Trans.42 (12) (2001): 2492-2498

[SWI1978] A.C. Switendick, in: G. Alefeld (Ed.), Hydrogen in Metals I, Springer Verlag, Berlin, 1978 (Chapter 5).

[TAK1989] T. Takeshita, R. Nakayama. Magnetic properties and microstructures of the Nd-Fe-B magnet powder produced by hydrogen treatment. [A]. *Proceedings of the 10th International Workshop on Rare Earth Magnets and Their Applications*. Kyoto: (1989): 551-554.

[TAK1995] T. Takeshita, Some applications of hydrogenation -decomposition -desorption -recombination (HDDR) and hydrogen-decrepitation (HD) in metals processing. J. Alloys Comp. 231 (1995): 51-59

[TAK1996] T. Takeshita, K. Morimoto. Anisotropic Nd-Fe-B bonded magnets made from HDDR powders. J. Appl. Phys. 79 (8) (1996): 5040-5044

[TAK2006] O. Takeda, T.H. Okabe, Y. Umetsu. Recovery of neodymium from a mixture of magnet scrap and other scrap. Journal of Alloys and Compounds, 408-412 (2006): 387-390

[TAN1988] W.Z. Tang, S.Z. Zhou, R. Wang. On the neodymium-rich phases in Nd-Fe-B magnets. J. Less-Common Met. 141(2) (1988): 217-223

[TUR2000] K. Turek, P. Liszkowski, H. Figiel. The influence of the kinetics of the hydrogenation of Nd–Fe–B alloys on hydrogen distribution in the alloy phases. Journal of Alloys and Compounds 309 (2000): 239–243

[TUR2001] K. Turek, P. Liszkowski, H. Figiel. Corrigendum to 'The influence of the kinetics of the hydrogenation of Nd–Fe–B alloys on hydrogen distribution in

the alloy phases'. Journal of Alloys and Compounds 315 (2001): 284
[VER1994] M. Verdier, J. Morros, D. Pere, I.R. Harris, Stability of Nd-Fe-B powders obtained by hydrogen decrepitation. IEEE Trans. Magnetics 30(2) (1994): 657-659
[VON1995] F. Von Staa. Investigation of the magnetization processes of Nd-Fe-B permanent magnets using a torsion pendulum magnetometer. J. Appl. Phys. **77**(1995): 1194-1200
[VON1996] F. von Staa, K.A. Hempel, H. Artz. On the magnetization processes of Nd-Fe-B powders prepared by HDDR. Journal of Magnetism and Magnetic Materials 157/158 (1996): 25-26
[VON1996-2] F. von Staa, K.A. Hempel, H. Artz, Y. Wang, J. Schneider. Magnetic properties of anisotropic Nd-Fe-B powder and magnets. Journal of Magnetism and Magnetic Materials 157/158 (1996): 23-24
[WEC1994] J. Wecker, H. Cerva, C. Kuhrt, K. Schnitzke, L. Schultz. Microstructure and magnetic properties of mechanically alloyed anisotropic Nd-Fe-B. J. Appl. Phys. 76(1994): 6238-6240
[WIE1987] G. Wiesinger, G. Hilscher, R. Grossinger. Effect of hydrogen absorption on the magnetic properties of $Nd_{15}Fe_{77}B_8$. J. Less-Common Met. 131(1987): 409-417
[WIL1990] A.J. Williams, P.J. McGuiness and I.R. Harris, Mass spectrometer studies of hydrogen desorption from hydrided NdFeB. IEEE Trans.Magn., 26 (5) (1990) 1945-1947.
[WIL1991] A.J. Williams, P.J. McGuiness. I.R. Harris, Mass spectrometer hydrogen desorption studies on some hydrided NdFeB-type alloys. J. Less-Common Met., 171 (1991): 149-155.
[WOL2001] P. Wolfers, M. Bacmann, D. Fruchart. Single crystal neutron diffraction investigations of the crystal and magnetic structures of $R_2Fe_{14}B$ (R=Y, Nd, Ho, Er), *J. Alloys and Comp*., 317-318(1) (2001): 39-43
[YAM1989] M. Yamaguchi, I. Yamamoto, T. Goto, S. Miura. Shift in the chemical equilibrium of the LaCo5-H system by strong magnetic fields. Physics Letters A, 134, 8-9 (1989): 504-506.
[YAM1996] I. Yamamoto, M. Yamaguchi, M. Fujino, F. Ishikawa, T. Goto, S. Miura. Magnetic field effects on the chemical equilibrium between metals and hydrogen. Physica B 216 (1996): 399 402
[YAN1999] G. Yan, A.J. Wiliams, J.P.G. Farr, I.R. Harris. The effect of density on the corrosion of NdFeB magnets. J. Alloys Comp. 292(1999): 266-174.
[YAR1996] V.A. Yartys, A.J. Williams, K.G. Knoch, P.J. McGuiness, I.R. Harris. Further studies of anisotropic hydrogen decrepitation in $Nd_{16}Fe_{76}B_8$ sintered magnets. Journal of Alloys and Compounds 239 (1996): 50-54
[YAR1997] V.A. Yartys, O. Gutfleisch, V.V. Panasyuk, I.R. Harris. Desorption characteristics of rare earth (R) hydrides (R=Y, Ce, Pr, Nd, Sm, Gd and Tb) in relation to the HDDR behaviour of R-Fe-based-compounds. Journal of Alloys and Compounds 253-254(1997):128-133
[YIN1993] X.J. Yin, M.G. Hall, I.P. Jones, R.N. Faria, I.R. Harris. The microstructural

characterization of NdFeB alloys. J. Magn. Magn. Mater. 125(1993): 78-90
[ZAK2006] M. Zakotnik, E. Devlin, I.R. Harris, A.J. Williams. Hydrogen decrepitation and recycling of NdFeB-type sintered magnets. Journal of Iron and Steel Research, International. Vol 13, Supplement 1. (2006): 289-295
[ZAK2008] M. Zakotnik, I.R. Harris, A.J. Williams. Possible methods of recycling NdFeB-type sintered magnets using the HD/degassing process. Journal of Alloys and Compounds 450 (2008): 525–531
[ZHO1999] S.Z. Zhou, Q.F. Dong. Super Permanent Magnets – Rare Earth Ferrous permanent materials. Metallurgical Industry Press, Beijing, 1999 (*in Chinese*)

Abstract

The purpose of this thesis was to study the Hydrogen Decrepitation (HD) process as a way to recycle waste scraps of Nd-Fe-B sintered magnets into highly coercitive and anisotropic powders, for the industry of bonded magnets. The process consists in a first hydrogenation, the bulk material being reduced into powder, as a result of the large volume expansion of the lattice. Then Hydrogen Desorption and annealing treatments are requested to restore the initial characteristics of the precursor (coercivity and anisotropy). Starting with sintered $(NdDy)_2$-$(FeCoNbCu)_{14}$-B magnets as a precursor, the different steps of the HD process have been studied.

Differential Scanning Calorimetry (DSC) and Hydrogenation Kinetics measurements were used to investigate the hydrogen absorption and desorption characteristics. Thermal-magnetization measurement was used to investigate the effect of the residual hydrogen content on magnetic properties of the anisotropic (NdDy)-(FeCoNbCu)-B powders.

The thesis focuses on the effect of the applied experimental conditions such as hydrogen decrepitation temperature, twice hydrogen decrepitation cycle, hydrogen desorption temperature, magnetic field during hydrogen desorption, annealing temperature etc… on magnetic properties of (NdDy)-(FeCoNbCu)-B powders. Among these factors, hydrogen absorption temperature, hydrogen desorption temperature and annealing temperature play important roles on the magnetic properties. Twice hydrogen decrepitation improves the size distribution of the powders. Hydrogen desorption under magnetic field reduces the residual hydrogen content of the anisotropic powders, resulting in raising their remanence (B_r).

After optimization of the successive steps of the process, anisotropic powders with good properties have been achieved : B_r = 10.29 kGs (1.029 T), H_{cj} = 14.3 kOe (1138 kA/m), $(BH)_{max}$ = 21.67 MGOe (172.5 kJ/m^3). It corresponds respectively to 93%, 46% and 74% of the magnetic properties of the precursor sintered (NdDy)-(FeCoNbCu)-B permanent magnets.

Résumé

L’objectif de la thèse était d'étudier le procédé de Décrepitation à l'Hydrogène (HD) en tant que moyen de recycler les rebus d’aimants frittés Nd-Fe-B en poudres fortement coercitives et anisotropes, pour l'industrie d'aimants liés. Le procédé consiste à appliquer une première hydruration, afin de réduire le matériau massif en poudre, grâce à l’expansion du volume de la maille. Des traitements de désorption de l’hydrogène et de recuit sont ensuite nécessaires pour rétablir les caractéristiques initiales du précurseur (coercivité et anisotropie). Les différentes étapes du procédé HD ont été étudiées à partir d’aimants frittés $(NdDy)_2(FeCoNbCu)_{14}B$ utilisés comme précurseurs.

Les caractéristiques d'absorption et de désorption de l’hydrogène ont été étudiées par Calorimétrie Différentielles (DSC) et par des mesures de cinétique d'hydruration. Des mesures magnétothermiques ont permis d’analyser l'effet de la présence d’hydrogène résiduel sur les propriétés magnétiques des poudres (NdDy)-(FeCoNbCu)-B.

La thèse porte plus particulièrement sur l'impact des conditions expérimentales appliquées, telles que la température de décrepitation, l’application d’un double cycle de décrépitation, la température de désorption, l’application d’un champ magnétique pendant la désorption de l’hydrogène, la température de recuit, etc… sur les propriétés magnétiques des poudres (NdDy)-(FeCoNbCu)-B. Parmi ces facteurs, les températures d’absorption et de désorption, et la température de recuit jouent un rôle prépondérant sur les propriétés magnétiques. La double décrépitation améliore la distribution de taille des poudres. La désorption de l’hydrogène sous le champ magnétique réduit le contenu d’hydrogène résiduel des poudres anisotropes, et conduit ainsi à une augmentation de la rémanence (Br).

Après l'optimisation des étapes successives du procédé, des poudres anisotropes présentant des propriétés satisfaisantes ont été obtenues : Br = 10.29 kGs (1.029 T), Hcj = 14.3 kOe (1138 kA/m), $(BH)_{Max}$ = 21.67 MGOe (172.5 kJ/m3). Les propriétés magnétiques initiales des aimants frittés (NdDy)-(FeCoNbCu)-B ont été restaurées respectivement à 93 %, 46 % et 74 %.